Lars Zenke Hansen

Stability of Masonry Columns

BYG·DTU

DANMARKS
TEKNISKE
UNIVERSITET

DTU

Stability of Masonry Columns

Lars Zenke Hansen

$$M = M_0 + N \cdot \frac{1}{\alpha} \cdot \kappa \cdot l^2$$
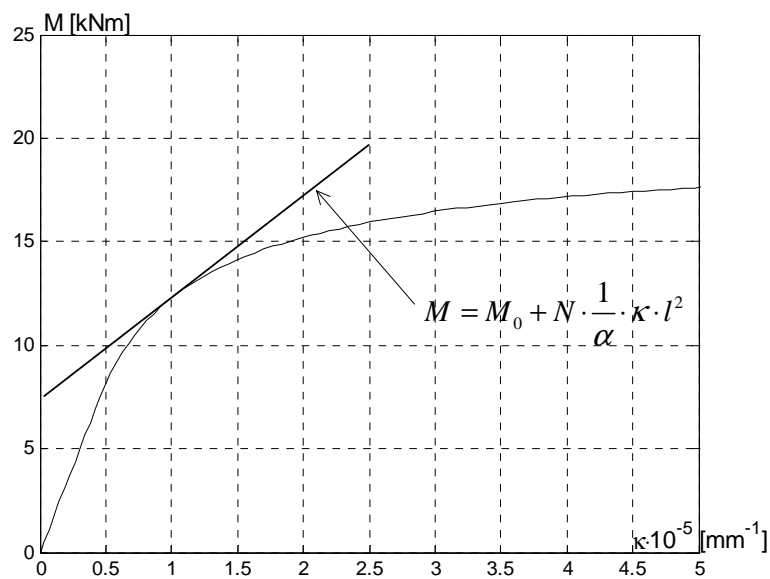
1 Preface

This report is prepared as a partial fulfilment of the requirements for obtaining the Ph.D. degree at the Technical University of Denmark.

The work has been carried out at the Department of Structural Engineering and Materials, Technical University of Denmark (BYG•DTU) under the supervision of Professor, Dr. techn. M. P. Nielsen.

I would like to thank my supervisor for giving valuable advice and inspiration as well as valuable criticism to the present work.

Lyngby, June 2003

Lars Zenke Hansen

2 Summary

In this report, unreinforced and reinforced masonry columns and beam columns have been treated by different constitutive models for masonry. The models have been compared individually and with experiments. The tensile strength has been set at zero. To provide tensile strength to masonry reinforcement must be used.

Unreinforced masonry

In the report, expressions have been derived for the load carrying capacity of columns and beam-columns with and without membrane action and for laterally loaded masonry one-way walls without axial load. Comparison with experiments shows that columns may be calculated by Ritter's equation without the correction factor suggested in the Danish Code of Practice, DS414. Results for unreinforced masonry beam-columns have been compared with experiments and the comparison shows that calculations made by using a modified linear elastic model overall provide the best results. The method developed is iterative. Simple conservative calculations may be made by using a linear elastic model, and in this case the calculations may be made analytically. All together 307 experiments have been collected and used for the comparison.

Furthermore, it has been shown that masonry made by Danish bricks has an initial stiffness of around $375 f_{cm}$, where f_{cm} is the compressive strength of the masonry in MPa. This value is much smaller than the initial stiffness met in other countries in Europe. Thus, an investigation of the behaviour of Danish masonry in compression has been undertaken.

Regarding masonry members with membrane action, it has been shown that a small pressure perpendicular to the bed joint increases the lateral strength notably.

Furthermore, it has been shown how the lateral strength of masonry walls without external axial compression may be calculated by taken the weight of the masonry into account.

Reinforced masonry

In the report reinforced masonry has been treated by the same methods as unreinforced masonry. Experiments collected from the literature are very limited in number so a thorough comparison has not been possible. Only 24 experiments have been found. However, it seems fair to conclude that reinforced masonry beam-columns may be calculated by using the method given in DS414.

In the report, practical calculation methods have been derived to simplify calculations of an interaction diagram between the axial load and the bending moment.

3 Resumé

Formålet med nærværende rapport er at undersøge opførslen af murværkssøjler, bjælkesøjler og enkeltspændte vægge. Disse kan være armeret eller uarmeret. Rapporten er inddelt i tre dele, hvor den første del koncentrerer sig om opførslen af uarmeret murværk, den anden del handler om armeret murværk og den tredje del sammenligner de fundne teorier med forsøg fundet i litteraturen.

Uarmerede og armerede murværkssøjler og bjælkesøjler er blevet behandlet ved at antage forskellige materialemodeller for murværk. Modellerne er blevet sammenlignet individuelt og med forsøg. Fælles for modellerne er at de ikke medtager trækstyrken af murværk parallelt med liggefugen. Den eneste trækstyrke, som tages i regning, er den, der skyldes evt. armering.

Uarmeret murværk

I rapporten er der udledt udtryk til beregning af bæreevnen af søjler og bjælkesøjler med og uden buevirkning. Ydermere er der fortaget gennemregning af enkeltspændte vægge uden normaltryk. Sammenligninger med forsøg viser at søjler kan beregnes efter Ritters formel uden medtagelse af den korrektionsfaktor som er foreskrevet i den danske norm for murværkskonstruktioner, DS414. Beregningsmetoder for uarmerede bjælkesøjler er blevet sammenlignet med forsøg, og det har vist sig, at hvis opførslen modelleres som i den danske norm for betonkonstruktioner (DS411), får man generelt den bedste overensstemmelse med forsøg. Beregninger på den sikre side kan foretages analytisk ved at bruge den lineærelastiske model beskrevet i rapporten. I alt er der samlet 307 forsøg til sammenligning med teorien.

Endvidere er det vist, at murværk med danske sten og mørtler har et begyndelses-elasticitetsmodul på omkring $375f_{cm}$, hvor f_{cm} er trykstyrken af murværk i MPa. Dette er meget mindre end man finder i andre europæiske lande. Trykarbejdslinien for dansk murværk er derfor behandlet nøjere.

Murværkskonstruktioner med buevirkning er også undersøgt og det er blevet vist at små tryk vinkelret på liggefugen øger bæreevnen ved tværlast markant.

Det er også blevet vist hvorledes bæreevnen af tværbelastet murværk kan bestemmes ved at tage massen af murværket i regning.

Armeret murværk

Armeret murværk behandles efter samme retningslinier som uarmeret murværk. I litteraturen er der desværre kun publiceret et meget begrænset antal forsøg, kun 24 forsøg er fundet. Det har derfor ikke været muligt at foretage en dybtgående sammenligning mellem teori og forsøg. Men det synes rimeligt at konkludere at beregninger udført efter DS414 giver den bedste overensstemmelse med forsøg.

Rapporten indeholder også praktiske metoder til bestemmelse af interaktions-diagrammer mellem normalkraft og ydre moment.

4 Contents

5 Notation

The most commonly used symbols are listed below. Exceptions from the list may appear. They will be commented upon in the text.

Geometry

h	:Depth of a cross-section
b	:Width of a cross-section
A	:Area of a cross-section
A_c	:Area of a masonry cross-section
A_s	:Area of reinforcement at the bottom face
A_s'	:Area of reinforcement at the top face
I	:Moment of inertia
i	:Radius of inertia
h_c	:Distance from the bottom face to the centre of the bottom reinforcement
h_c'	:Distance from the top face to the centre of the top reinforcement
y_0	:Distance from the top face to the neutral axis
l	:Length of a beam
e	:Eccentricity
u	:Deflection
κ	:Curvature
α	:Parameter of shape
x, y, z	:Cartesian coordinates

Physics

ε	:Strain
ε_{cm}	:Masonry strain
ε_{cmy}	:Strain of masonry at f_{cm}
ε_{cmu}	:Strain of masonry at failure
ε_s	:Strain in reinforcement
ε_{sy}	:Yield strain of reinforcement
σ	:Stress
σ_c	:Compressive stress in masonry
σ_s	:Stress in reinforcement
σ_{cr}	:Critical stress
f_{cm}	:Compressive strength of masonry
f_{cmo}	:Compressive strength of mortar
f_{cb}	:Compressive strength of brick
f_{tlk}	:Flexural strength of bed joints according to DS414
$f_{mor,tlk}$	:Strength of the interface use to determine the tensile flexural strength according to DS414
f_y	:Yield strength of steel
E_s	:Modulus of elasticity of steel
E_0	:Initial modulus of elasticity of masonry
$E_0{}^*$	:Secant modulus of elasticity at ε_{cmy}
E_σ	:Tangent modulus of masonry
n	:Ratio between the stiffness of steel and masonry
φ	:Reinforcement ratio
Φ_0	:Reinforcement degree
C_{cm}	:Resulting compressive force in masonry
C_s	:Resulting compressive force in compressive steel
T	:Resulting tensile force in tensile steel
N	:Axial load
N_p	:Maximum compressive load
N_{cm}	:Maximum compressive force in masonry

N_{cr} :Critical load

M_{cm} :Moment from stresses in masonry in compression

M :Moment

M_0 :Simple moment

M_p :Pure bending yield moment

M_f :Bending yield moment

P :Point force

q :Line load

6 Introduction

This report treats the behaviour of reinforced and unreinforced masonry columns, beam columns and one-way slabs. The report is subdivided into a section dealing with unreinforced masonry and a section dealing with reinforced masonry. Each section will be subdivided into sections dealing with the type of members mentioned above. Emphasis is put on unreinforced masonry since masonry often is unreinforced. The purpose is to establish theories for the load carrying capacity of masonry with and without axial load. If the axial load is small, masonry members may be treated by simple membrane action. Simple methods for including membrane action based on the yield hinge method are proposed.

At the end of the report, the theories are compared with experiments collected from the literature.

7 Masonry

7.1 Properties of Masonry

Masonry is a composite material of bricks and mortar. When these are joint together, a third "material" appears. This "material" is the interface between brick and mortar. The bond properties of the interface are very dependent on the properties of the brick and the mortar. For a detailed description, see [51]. The mechanism of developing bond is that the brick sucks water from the mortar leaving an area between the brick and the mortar with other material properties than the mortar. It is believed that the bond is a crystalline zone, which develops an interlock with the rough surface of the brick. Depending on the suction from the brick and the mortars ability to retain water the bond might be strong or weak. In general, it might be said that masonry made with high suction bricks and a mortar with a low ability to retain water[1] provides a weak bond. Thus, masonry made with low suction bricks and a mortar with a reasonable ability to retain water provides a strong bond.

Masonry from different parts of the world might have different properties dependent on the techniques used to fabricate the bricks. Therefore, a national expression for the strength properties often has to be established.

In this report, masonry will be modelled as a homogeneous material with a uniaxial compressive strength and no tensile strength.

---

[1] The mortars ability to retain water is influenced to a high degree by the amount of lime in the mix.

7.2 Material behaviour of masonry in compression

7.2.1 Stress-strain relation

The failure mode of masonry in pure compression depends on the properties of the mortar and the brick. Stiffness as well as strength play a role. A combination of low mortar stiffness (equal to low compressive strength) and high brick stiffness (equal to high compressive strength) leads to a splitting failure of the masonry specimen. If the stiffness' are similar, the failure will be a shear failure. The different types of failure are investigated in [45] and [35]. They are shown in Figure 7.1.

$$f_{cb} \sim f_{cmo} \qquad\qquad f_{cb} > f_{cmo}$$
Shear   Splitting
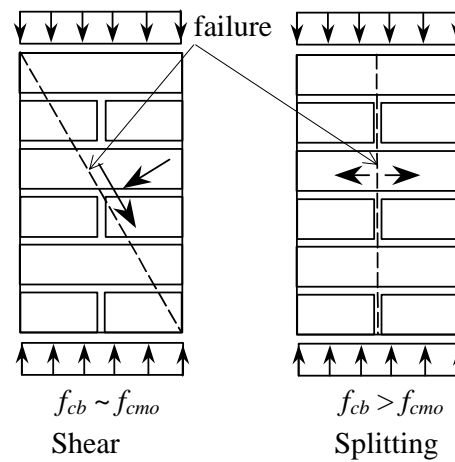
Figure 7.1 Different compressive failure modes of masonry

The splitting failure arises because the deformation of the mortar pulls the bricks apart, which again are caused by the lower deformation capacity of the bricks, combined with the low tensile strength, see Figure 7.2.
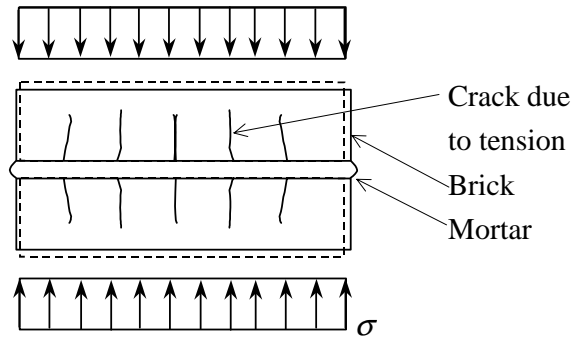
Figure 7.2 Sketch of the splitting failure mechanism

From this it is seen that failure of masonry in compression is a rather complex problem. This might also be said regarding deformation up to failure and during failure.

The stress-strain relationship of masonry in compression is non-linear. It is very dependent on the brick and mortar used. Some measured stress-strain relationships are shown in Figure 7.3. They have been taken from [36].
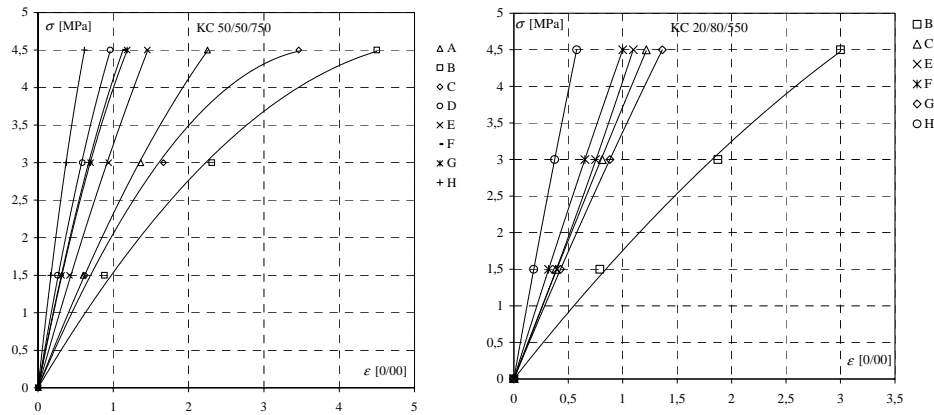
Figure 7.3 Stress-strain relationships for masonry in compression

In Figure 7.3, tests results with eight different bricks combined with two mortars (K ~ Lime and C ~ Cement measured by weight) are shown. The bricks are referred to by a letter, which is explained in Table 7.1 (f_{cb} ~ compressive strength of the bricks and IRA ~ initial rate of absorption).

Brick type	Comments	f_{cb} [MPa]	IRA [kg/m^2/min]
A	Red, soft stroked	12.6	2.45
B	Red, soft stroked	9.3	4.28
C	Yellow, soft stroked	9.7	4.05
D	Red, soft stroked	28.7	1.48
E	Red, soft stroked	29.2	2.22
F	Yellow, soft stroked	28.1	2.99
G	Yellow, soft stroked	27.7	2.73
H	Yellow, soft stroked	57.7	2.99

Table 7.1 The properties of the bricks

The stress-strain relation may be modelled by a parabolic function. One example is shown in Figure 7.4. The equation is:
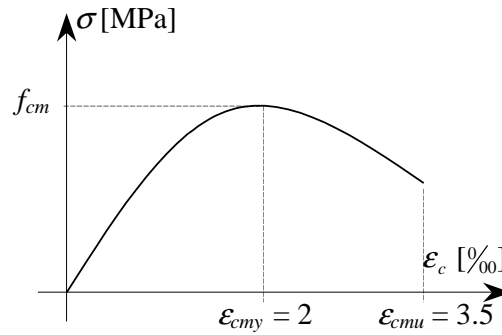
Figure 7.4 Stress-strain relationship for masonry

$$\sigma = f_{cm} \frac{\varepsilon}{\varepsilon_{cmy}} \left(2 - \frac{\varepsilon}{\varepsilon_{cmy}} \right) \qquad (7.1)$$

The figure has been drawn for the special case where the compressive strength is reached at a strain $\varepsilon_{cmy} = 2$ $^o/_{oo}$.

If the tests in Figure 7.3 are plotted in a diagram with the ordinate axis σ / f_{cm} and the abscissa axis $\varepsilon / \varepsilon_{cmy}$, Figure 7.5 is obtained.
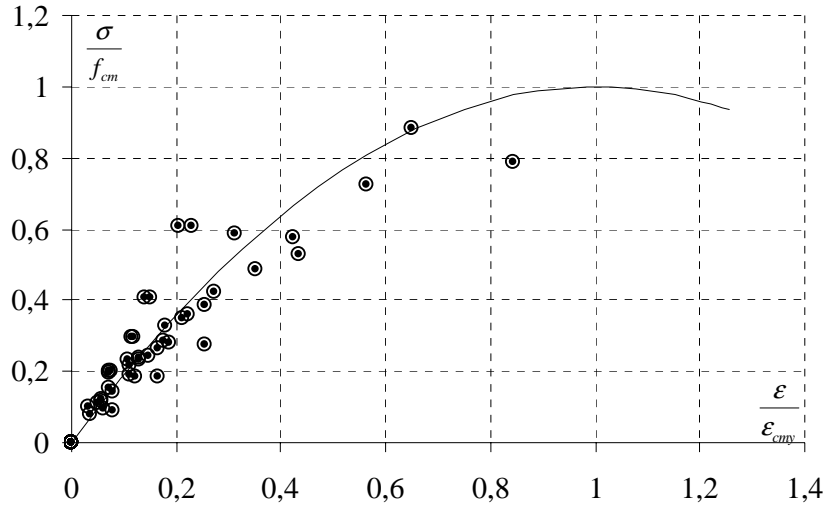
Figure 7.5 Stress-strain relationship for masonry for various bricks and mortars

The initial stiffness E_0 obtained from (7.1) is $2f_{cm}/\varepsilon_{cmy}$. If E_0 is set equal to $375f_{cm}$, see section 7.2.2, we get the equation

$$E_0 = 2\frac{f_{cm}}{\varepsilon_{cmy}} = 375f_{cm} \qquad (7.2)$$

which solved for ε_{cmy} gives $\varepsilon_{cmy} = 5.33\ °/_{oo}$. Thus, ε_{cmy} may be set to the constant value $5.33\ °/_{oo}$. This is the value used in Figure 7.5.

7.2.2 Stiffness

For the stress-strain relations shown in Figure 7.3, the initial stiffness E_0 may be calculated by fitting the parabolic function (7.1) to the test points, see Figure 7.3. Then the fully drawn lines in Figure 7.3 appear.

The calculated initial stiffness' are listed in Table 7.2 together with the compressive strengths of the masonry.

Brick type	Mortar	E_0	f_{cm}	f_{cb}	f_{cmo}
		[MPa]	[MPa]	[MPa]	[MPa]
A	KC50/50/750	2582.4	7.8	12.6	6,16
	KC20/80/550				
B	KC50/50/750	1691.4	5.7	9.3	4.86
	KC20/80/550	1887.7	6.2	9.3	20.82
C	KC50/50/750	2365.8	5.1	9.7	6.29
	KC20/80/550	3587.6	7.4	9.7	24.09
D	KC50/50/750	5943.4	13.7	28.7	5.86
	KC20/80/550				
E	KC50/50/750	3584.4	10.6	29.2	6.04
	KC20/80/550	3855.1	15.8	29.2	20.82
F	KC50/50/750	5164.9	12.9	28.1	6.04
	KC20/80/550	3695.6	16	28.1	20
G	KC50/50/750	5075.9	12.5	27.7	5.68
	KC20/80/550	4790.7	16.4	27.7	20
H	KC50/50/750	9269.1	15.2	57.7	6.16
	KC20/80/550	8378.8	19.5	57.7	20.26

Table 7.2 Values of the initial stiffness E_0 and the compressive strength f_{cm} taken from [36]

In Figure 7.6 the initial stiffness is plotted versus the compressive strength of masonry. The points referred to as Piers KC50/50/750 and Piers KC20/80/550 are the results listed in Table 7.2.

Furthermore, measurements on walls have been reported in [36]. Besides measuring the ultimate compressive strength, the compressive strains during loading was measured as well, making it possible to calculate the initial stiffness of the wall. These results are also plotted in Figure 7.6 (referred to as Wall KC50/50/750 and Wall KC20/80/550). The values from the wall tests are listed in Table 7.3.

Mortar	E_0	f_{cm}
	[MPa]	[MPa]
KC50/50/750	6697,7	13,7
KC20/80/550	6506,1	16,2

Table 7.3 Initial stiffness of walls taken from [36]

A simple equation for the initial stiffness is proposed in equation (7.3).

$$E_0 = 375 f_{cm} \quad (f_{cm} \text{ in MPa}) \tag{7.3}$$
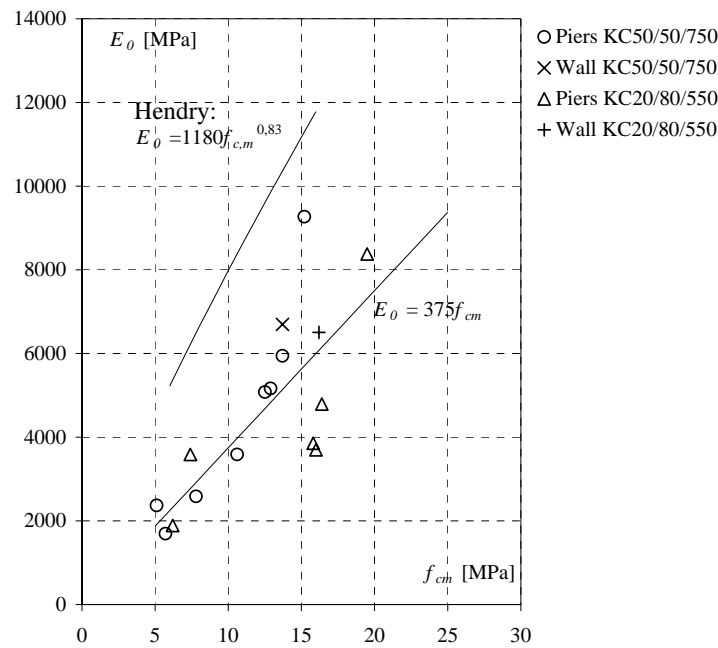
Figure 7.6 Initial stiffness versus the compressive strength of masonry

Figure 7.6 also shows an equation taken from Hendry ([38]), which he supposes to be a general value. This indicates that the stiffness of Danish masonry is very different from the stiffness of masonry in other countries.

The initial stiffness used in the Danish Code of Practice is illustrated in Figure 7.7 as the 5 % fractile. Furthermore, DS414 gives values for the 95% fractile, which is plotted as well.
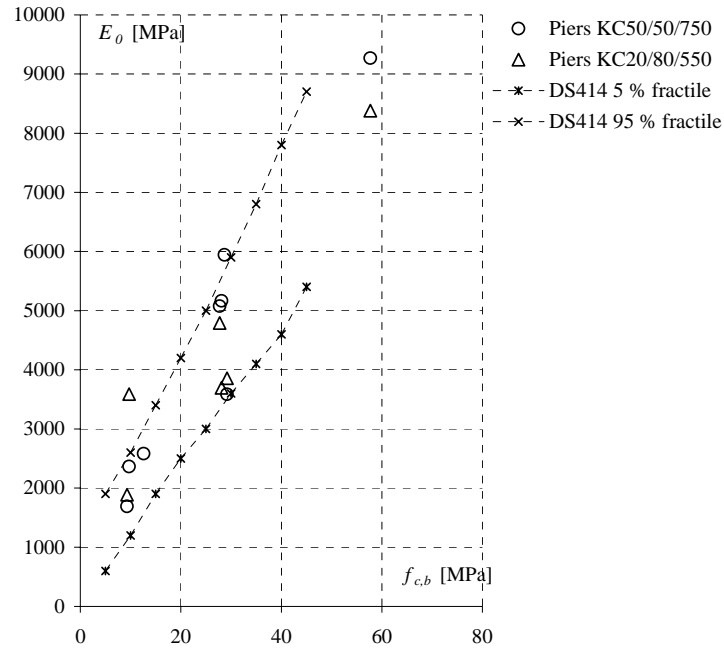
Figure 7.7 Initial stiffness according to DS414 for the same mortars as in Figure 7.6

In [37] an equation (7.4) for the initial stiffness is proposed, which is based only on the strength of the brick.

$$E_0 = 120 f_{cb} \quad (f_{cb} \text{ in MPa}) \tag{7.4}$$
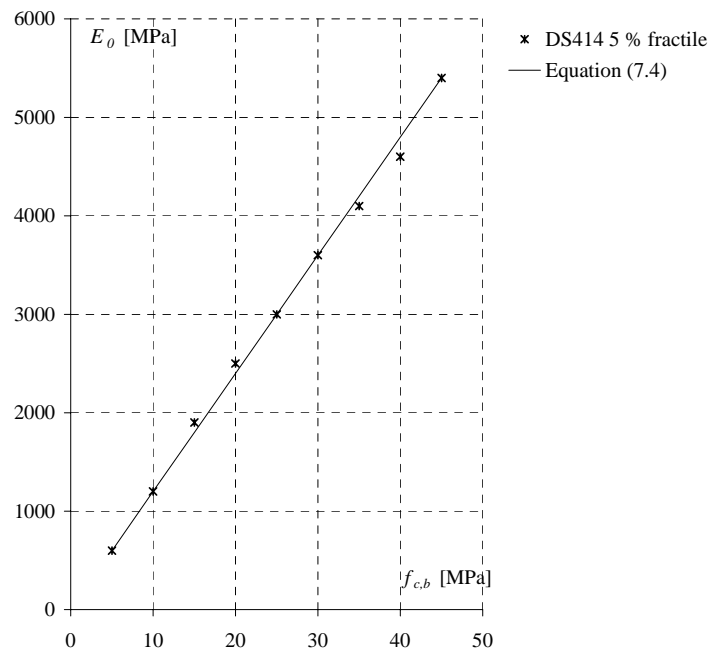
Figure 7.8 Equation (7.4) compared with the 5 % fractile given in DS414

This value is compared with the 5 % fractile in DS414 in Figure 7.8.

Since the stiffness of masonry depends on the properties of the mortar as well as the properties of the bricks, an equation based on the compressive strength of the masonry must be preferred.

Initial stiffness' have also been measured by Suenson and Dührkop, [16].

In earlier time, it was common to have two different types of bricks, a brick for the facade and a brick for the rest of the masonry. The reason was that the burning temperature and the clay properties were not controlled as well as to day leading to bricks with different colours within the same production. This also gave variation in strength and stiffness. The best bricks were used in the facade and the remaining masonry was built with bricks having errors from the burning.

The mortars used were the same as known today. However, a mortar referred to as a KD-mortar is no longer in production. The mortar consisted of lime, wind sieved clay (diatomol) and sand. It was normally used for high suction bricks because the diatomol was better in retaining the water than the lime itself. The mix of the mortar was KD10/15/100, meaning that the mortar consisted of 10 units of lime, 15 units of diatomol and 100 units of sand measured by weight.

The bricks normally used were "moler" stones and "flamme" stones. "Moler" stones had a very low stiffness and compressive strength, because the density was low, about 800 kg/m^3. "Flamme" stones were as the bricks we know today with similar density (1800 kg/m^3) and strength properties.

In [16], results of stiffness' measurements of masonry piers have been given. They are listed in Table 7.4 and illustrated in Figure 7.9.

Stones	"Moler" stone				"Flamme" stone			
	Water cured		Air cured		Water cured		Air cured	
	E_0	f_{cm}	E_0	f_{cm}	E_0	f_{cm}	E_0	f_{cm}
Mortar	[MPa]	[MPa]	[MPa]	[MPa]	[MPa]	[MPa]	[MPa]	[MPa]
KD	854.9	3.8	1266.9	3.9	1442.0	6.5	2255.7	7.0
K	1205.1	3.8	1586.2	3.3	3100.3	7.2	3357.8	5.4
KC	1637.7	5.0	2399.9	6.1	4181.8	9.5	6705.3	12.7
C	2399.9	7.4	2441.1	6.9	7591.1	17.7	6705.3	15.1

Table 7.4 Measured stiffness' and compressive strengths
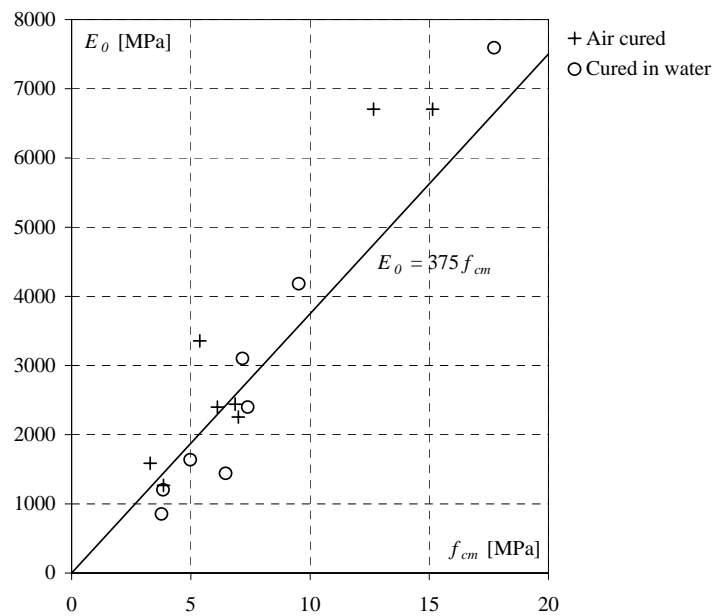

Figure 7.9 Initial stiffness plotted together with the proposed equation (7.3)

The measured initial stiffness' are compared with the proposed equation (see (7.3)) and the agreement seems to be good. However, the scatter is rather large, which probably is due to, among other things, that two types of curing conditions were used.

8 Basic assumptions

The columns[2] and beam-columns[3] considered in this report are Bernoulli beams, meaning that plane sections remain plane and perpendicular to the curve of deflection. Further, deformations due to shear are neglected.

Regarding the calculations of masonry beam-columns, some further remarks are made. For simply supported beam columns with a deflection symmetrical about the midpoint, the maximum deflection in the midpoint may be calculated as

$$u = \frac{1}{\alpha} \kappa l^2 \tag{8.1}$$

where κ is the curvature in the midpoint, α a parameter depending on the form of the curvature curve and l the length.

We have $\alpha = 9,6$ for a parabolic curvature form and $\alpha = \pi^2$ for a sine curve. Often $\alpha = 10$ is a good estimate.

Formula (8.1) may be used for a column fixed in one end and free in the other one if l is inserted as the free length, i.e. twice the length.

The simply supported beam-column and the column fixed in one end and free in the other one are called simple columns.

In the case of statically indeterminate beams, formula (8.1) may be used to calculate the maximum deflection along the free length measured relative to a line through zero moment points.

---

[2] A column will normally be a one-way wall loaded by a concentrical axial load

[3] A beam-column will normally be a one-way wall loaded by an eccentrical axial load or a concentrical axial load and a transverse load

The basic procedure in the calculation of simple beam-columns is to determine the moment-curvature relationship and then solve for the point where the line corresponding to the midpoint moment $M_0 + Nu = M_0 + N\frac{1}{\alpha}\kappa l^2$ is a tangent to the moment-curvature relationship. Here M_0 is the simple moment and N the axial load. The condition is illustrated in Figure 8.1. Any line $M_0 + N\frac{1}{\alpha}\kappa l^2$ crossing the moment-curvature curve gives rise to equilibrium solutions. When the tangent condition mentioned is satisfied, the corresponding value of M_0 will be at a maximum M_0^{max}, see Figure 8.1.
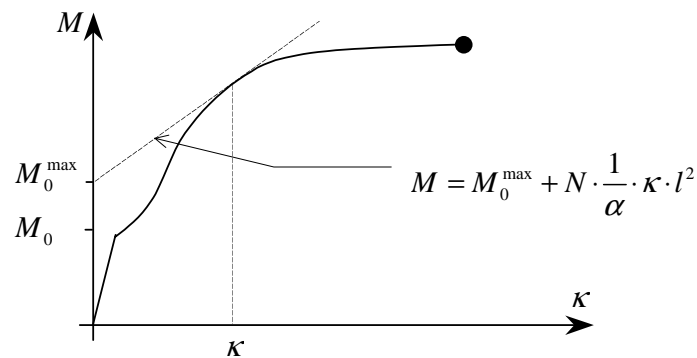
Figure 8.1 The moment-curvature relationship

This procedure was proposed in [4] by Jørgen Nielsen and further developed in [5] by Ervin Poulsen.

9 Unreinforced masonry

9.1 Introduction

In this section buckling loads for columns and beam-columns are analysed. The moment-curvature relation is obtained by expressing statical equivalence between the sectional forces and the internal stresses. The tensile strength of masonry is assumed equal to zero.

Masonry will be modelled by different stress-strain relations for compression, namely linear elastic behaviour, non-linear behaviour using a parabolic stress-strain relation and finally rigid plastic behaviour.

At the end of this chapter, membrane-action will be dealt with.

9.2 Instability of masonry columns

9.2.1 Linear elastic material behaviour

If the material is linear elastic, the critical load may be calculated from the Euler equation. The Euler equation for a simply supported column with constant normal force, N, may be derived from equilibrium conditions and the constitutive equation, relating bending moment to bending stiffness. The differential equation governing this problem is outlined in equation (9.1)

$$EI\frac{d^2u}{dx^2} + N \cdot u = 0 \qquad (9.1)$$

where EI is the bending stiffness.

By solving this homogeneous ordinary differential equation and using the boundary conditions the well-known Euler equation is obtained.

$$N_{cr} = N_E = \frac{\pi^2 EI}{l^2} \tag{9.2}$$

For other end conditions, the length, l, has to be replaced by the free length.

9.2.2 Non-linear material behaviour

If the stress-strain relationship is parabolic, cf. section 7.2.1, the critical load may be calculated by Engesser's first theory. The tangential stiffness E_σ as a function of the initial stiffness E_0 is given by

$$E_\sigma = E_0 \sqrt{1 - \frac{\sigma}{f_{cm}}} \tag{9.3}$$

If E in (9.2) is replaced by E_σ and the equation is solved for $\sigma = \sigma_{cr}$ one finds by introducing the Euler stress

$$\sigma_E = \frac{\pi^2 E_0}{\left(\dfrac{l}{i}\right)^2} \tag{9.4}$$

the critical stress

$$\frac{\sigma_{cr}}{f_{cm}} = \frac{1}{2} \frac{\sigma_E}{f_{cm}} \left(\sqrt{\left(\frac{\sigma_E}{f_{cm}}\right)^2 + 4} - \frac{\sigma_E}{f_{cm}} \right) \tag{9.5}$$

Here $i^2 = I/A$ is the radius of inertia. Equation (9.5) renders the critical stress according to Engesser's first theory.

If instead of (9.3) the tangential stiffness is assumed linear in σ, we have

$$E_\sigma = E_0 \cdot \left(1 - \frac{\sigma}{f_{cm}}\right) \tag{9.6}$$

Equation (9.6) is conservative compared with equation (9.3). The equation (9.6) was first proposed by Ritter and leads to the following equation for the critical stress

$$\frac{\sigma_{cr}}{f_{cm}} = \frac{1}{1 + \dfrac{f_{cm}}{\pi^2 \cdot E_0}\left(\dfrac{l}{i}\right)^2} \tag{9.7}$$

The equation is called Ritter's equation.

The Danish code of practice DS414 employs Ritter's equation. However, the critical stress is multiplied by a factor k_t given in equation (9.8).

$$k_t = \begin{cases} 0.7 \text{ for massive masonry with thickness } t \leq 90 \text{ mm} \\ 0.9 \text{ for massive masonry with thickness } t \geq 90 \text{ mm} \end{cases} \qquad (9.8)$$

Such factor was proposed by Knutson in 1991, see [40]. He suggested to use $k_t = 0.8$ for $90 \text{ mm} \leq t \leq 125 \text{ mm}$ and $k_t = 0.9$ for $125 \text{ mm} \leq t \leq 175 \text{ mm}$. For $t > 175 \text{ mm}$ he suggested $k_t = 1$. Knutson gave the following reason for introducing k_t: "*In masonry, the mortar will be confined and compressed during the bricklaying process, but there will be no confinement of the mortar at the surface of the masonry. Thus, the joints near the surface may be weaker. This may affect the strength of thin walls so it is suggested that the assessed carrying capacity is reduced for thin walls, by multiplying by a factor k_t*".

The formulas by Euler, Engesser and Ritter are shown for a wall with thickness t and a height l in Figure 9.1 (same $E_0/f_{cm} = 375$ is used).
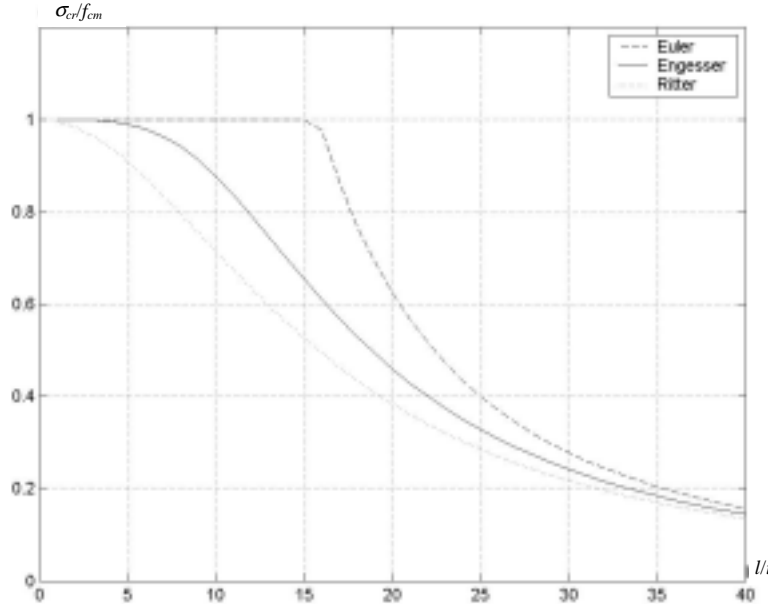
Figure 9.1 Ritter's, Engesser's and Euler's equations verses the slenderness ratio

9.3 Instability of beam columns and one-way walls

In this section, three different methods of calculating the load carrying capacity of beam-columns will be presented. The only difference in the methods is the assumed constitutive relationship.

9.3.1 Linear elastic material behaviour

If the material is linear elastic without any tensile capacity, the stress-strain relationship is as shown in Figure 9.2.
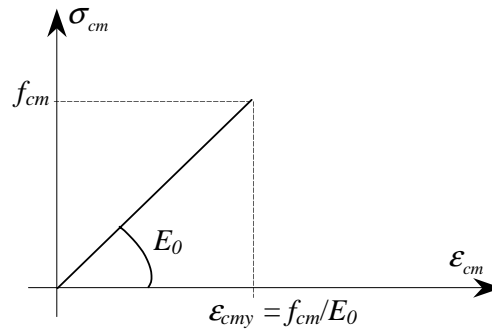
Figure 9.2 Linear elastic material

The relationship between the stresses and the strains may be written as

$$\sigma_{cm} = \frac{f_{cm}}{\varepsilon_{cmy}} \varepsilon \tag{9.9}$$

Measuring y' from the neutral axis as shown in Figure 9.3, the strains in the cross section are

$$\varepsilon = \frac{\varepsilon_{cm}}{\varepsilon_{cmy}} y' \tag{9.10}$$
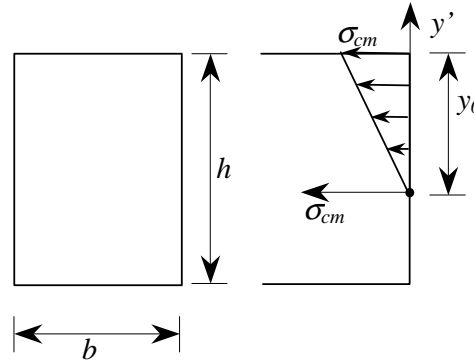
Figure 9.3 Definition of *y'*

Combining equation (9.9) and equation (9.10) the stresses in the masonry becomes the following function of *y'*.

$$\sigma_{cm} = \frac{f_{cm}}{y_0} \frac{\varepsilon_{cm}}{\varepsilon_{cmy}} y' \tag{9.11}$$
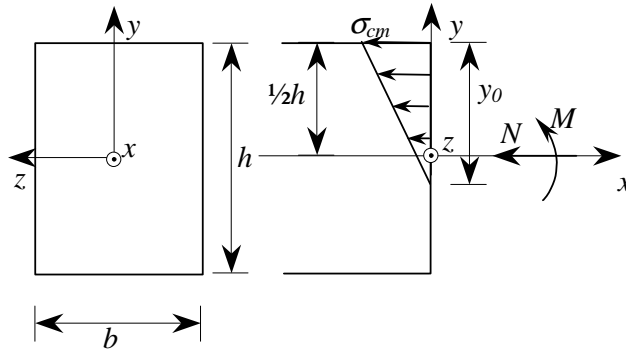
Figure 9.4 Cross section of unreinforced masonry (the bricks and joints are not shown)

In what follows *M* and *N* are referred to the midpoint of the section.

The projection equation becomes when $y_0 \leq h$

$$N = C_{cm} \tag{9.12}$$

where

$$C_{cm} = \int_{A_{cm}} \sigma_{cm} dA_{cm}$$

$$C_{cm} = \int_0^{y_0} \frac{f_{cm}}{y_0} \cdot \frac{\varepsilon_{cm}}{\varepsilon_{cmy}} \cdot y' dy' = \frac{1}{2} \cdot b \cdot f_{cm} \cdot \frac{\varepsilon_{cm}}{\varepsilon_{cmy}} \cdot y_0 \tag{9.13}$$

If a dimensionless parameter $\beta = \dfrac{y_0}{h}$ is introduced and equation (9.12) is solved for β by inserting equation (9.13), we find

$$\beta = \frac{2 \cdot N}{b \cdot h \cdot f_{cm} \cdot \dfrac{\varepsilon_{cm}}{\varepsilon_{cmy}}} \tag{9.14}$$

The moment equation around the point $y' = 0$ gives for $y_0 \le h$

$$M - N\left(\frac{h}{2} - y_0\right) = M_{cm}$$

where

$$M_{cm} = \int_0^{y_0} \frac{f_{cm}}{y_0} \cdot \frac{\varepsilon_{cm}}{\varepsilon_{cmy}} \cdot \left(y'\right)^2 dy' = \frac{1}{3} \cdot b \cdot f_{cm} \cdot \frac{\varepsilon_{cm}}{\varepsilon_{cmy}} \cdot y_0^2$$

If β is introduced into the moment equation, the moment, M, may be calculated by

$$M = \frac{1}{3} \cdot b \cdot h^2 \cdot f_{cm} \cdot \frac{\varepsilon_{cm}}{\varepsilon_{cmy}} \beta^2 + \frac{1}{2} \cdot N \cdot h \cdot \left(1 - 2 \cdot \beta\right) \tag{9.15}$$

The curvature is

$$\kappa = \frac{\varepsilon_{cm}}{y_0} = \frac{\dfrac{\varepsilon_{cm}}{h}}{\beta} = \frac{M - \dfrac{1}{2} \cdot N \cdot h \cdot \left(1 - 2 \cdot \beta\right)}{\dfrac{1}{3} \cdot b \cdot h^3 \cdot \beta^3 \cdot E_0} \tag{9.16}$$

When y_0 is larger than h, normal theory of elasticity for homogeneous sections may be used.

The moment-curvature relationship and the relationship between the simple moment M_0 and the curvature can now be found. The result is shown in Figure 9.5 and Figure 9.6. The data used in these calculations are listed in Table 9.1. The maximum strain is set equal to 2 ‰ as in Eurocode 6, [44].

b	h	l	f_{cm}	ε_{cmy}
[mm]	[mm]	[mm]	[MPa]	[‰]
1000	108	$20 \cdot h$	15	2

Table 9.1 Data used for calculating the moment-curvature relationship

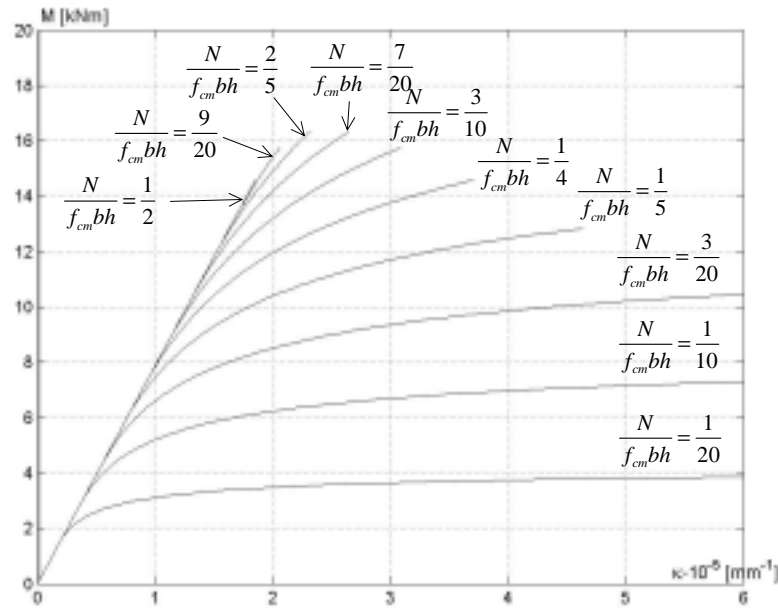**Figure 9.5 Moment-curvature relationship for different normal forces**
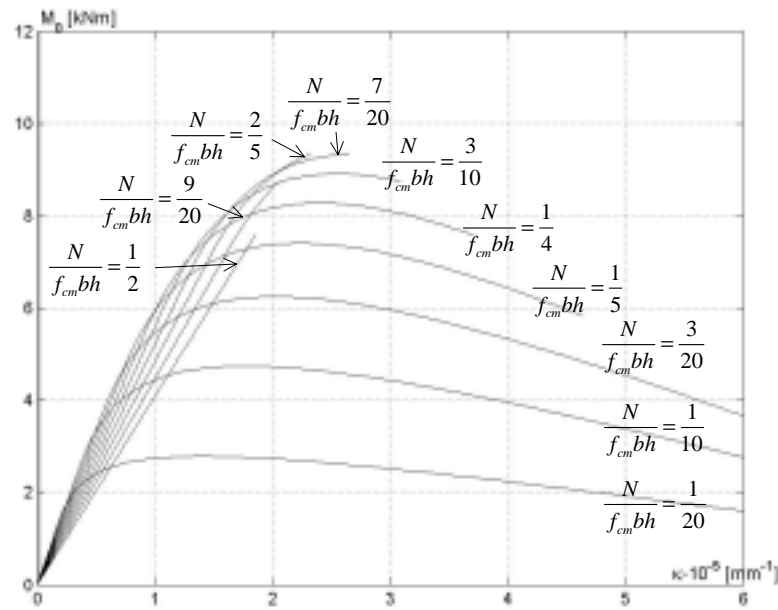
Figure 9.6 Simple moment-curvature relationship for different normal forces

Equations (9.14) to (9.16) do not provide a closed form solution, but the calculations are easy to carry out on a computer.

To find a closed form solution the moment equation is taken about the resulting compressive force of the masonry in compression.

The projection equation becomes, using the same symbols as in Figure 9.4

$$N = \frac{1}{2} \cdot \sigma_{cm} \cdot b \cdot y_0 \tag{9.17}$$

The moment equation becomes

$$M - N \cdot \left(\frac{1}{2} \cdot h - \frac{1}{3} \cdot y_0 \right) = 0 \tag{9.18}$$

By inserting the projection equation into the moment equation and introducing the curvature,

$$\kappa = \frac{\sigma_{cm}}{E_0 \cdot y_0} \tag{9.19}$$

equation (9.20) can be established

$$E_0 \cdot \kappa \cdot \left(\frac{1}{2} \cdot h - \frac{M}{N} \right) \cdot 3 = \frac{2 \cdot N}{3 \cdot \left(\frac{1}{2} \cdot h - \frac{M}{N} \right)} \Leftrightarrow$$

$$\kappa \cdot \left(\frac{1}{2} - \frac{M}{N \cdot h} \right)^2 = \frac{2}{9} \cdot \frac{N}{h^2 \cdot b \cdot E_0} \tag{9.20}$$

If $\kappa_{cm} = \dfrac{f_{cm}}{E_0 \cdot h}$ and $N_{cm} = b \cdot h \cdot f_{cm}$ are introduced into equation (9.20) the moment-curvature relationship may be written as

$$\frac{M}{N \cdot h} = \frac{1}{2} - \frac{\sqrt{2}}{3} \sqrt{\frac{N}{N_{cm}} \cdot \frac{\kappa_{cm}}{\kappa}} \tag{9.21}$$

The derivative of the moment with respect to the curvature may be calculated from equation (9.20)

$$\frac{d}{d\kappa} \left(\kappa \cdot \left(\frac{1}{2} - \frac{M}{N \cdot h} \right)^2 \right) = \frac{d}{d\kappa} \left(\frac{2}{9} \cdot \frac{N}{h^2 \cdot b \cdot E_0} \right) = 0 \Leftrightarrow$$

$$-\left(\frac{1}{2} - \frac{M}{N \cdot h} \right)^2 + 2 \cdot \kappa \cdot \left(\frac{1}{2} - \frac{M}{N \cdot h} \right) \frac{\dfrac{dM}{d\kappa}}{N \cdot h} = 0 \tag{9.22}$$

Equation (9.22) can be rewritten by use of equation (9.20) and the derivative is then determined by equation (9.23).

$$\frac{dM}{d\kappa} = 27 \cdot \left(\frac{1}{2} - \frac{M}{N \cdot h} \right)^3 E_0 I \tag{9.23}$$

where $I = \frac{1}{12} \cdot b \cdot h^3$

From the equilibrium equation we get

$$M = M_0 + \frac{1}{\alpha} \cdot \kappa \cdot l^2 \cdot N \Rightarrow$$

$$\frac{dM}{d\kappa} = \frac{N \cdot l^2}{\alpha}$$

Then the maximum moment may be found inserting this value of dM/dx into (9.23). The result is

$$\frac{M}{N \cdot h} = \frac{1}{2} - \frac{1}{3} \sqrt[3]{\frac{N}{N_{E\alpha}}} \tag{9.24}$$

where $N_{E\alpha} = \frac{\alpha \cdot E_0 I}{l^2}$ is the critical load obtained by replacing in the Euler equation π^2

with α.

The curvature becomes

$$\kappa = \left(\frac{1}{2} - \frac{M_0}{N \cdot h} - \frac{1}{3} \sqrt[3]{\frac{N}{N_{E\alpha}}} \right) \cdot \frac{h \cdot \alpha}{l^2} \tag{9.25}$$

Thus, the maximum deflection may be calculated by using this κ-value in the formula

$$u = \frac{1}{\alpha} \kappa \cdot l^2 \tag{9.26}$$

By inserting (9.24) and (9.25) into (9.21) an equation for the simple moment as a function of N is found to be

$$\frac{M_0}{N \cdot h} = \frac{1}{2} - \frac{1}{3} \sqrt[3]{\frac{N}{N_{cm}}} - 2 \cdot \frac{N}{N_{cm}} \frac{\kappa_{cm}}{\frac{\alpha \cdot h}{l^2} \cdot \left(\frac{N}{N_{E\alpha}} \right)^{\frac{2}{3}}} \tag{9.27}$$

The equations are only valid as long as $y_0 \leq h$ and $\sigma_{cm} < f_{cm}$. When $y_0 > h$, the stresses may be determined by Navier's equation. In this case $\kappa = M/EI$ and a simple equation may be established to find M_{0max} as a function of N.

Results using equation (9.25) and (9.27) are plotted in Figure 9.8 showing the simple moment-curvature relationship. The values of M_0 are shown by circles.

These expressions only cover the cases when σ_{cm} is smaller than the compressive strength. To cover the case of compressive failure a new cross-section analysis has to be made.
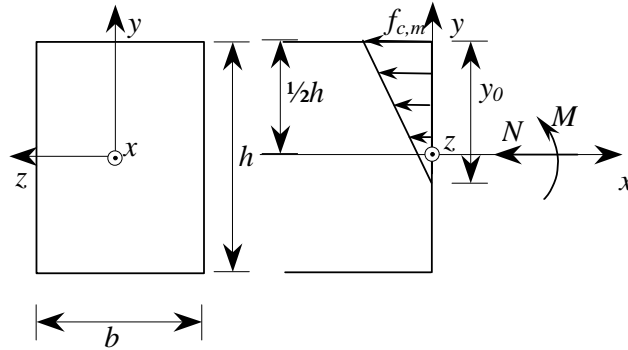
Figure 9.7 Cross section of unreinforced masonry (the bricks and joints are not shown)

The projection equation now becomes

$$N = \frac{1}{2} \cdot b \cdot f_{cm} \cdot y_0 \tag{9.28}$$

The moment equation becomes

$$M = N \cdot \left(\frac{1}{2} \cdot h - \frac{1}{3} \cdot y_0 \right) \tag{9.29}$$

The depth of the compressive zone y_0 is found from equation (9.28) and inserted into the moment equation, which again is inserted into the equilibrium equation $M = M_0 + N \frac{1}{\alpha} \kappa l^2$. Thereby equation (9.30) is obtained.

$$N \cdot \left(\frac{1}{2} \cdot h - \frac{1}{3} \cdot \frac{2 \cdot N}{b \cdot f_{cm}} \right) = M_0 + \frac{1}{\alpha} \cdot \frac{f_{cm}}{E_m \dfrac{2 \cdot N}{b \cdot f_{cm}}} \cdot l^2 \cdot N \Leftrightarrow$$

$$\frac{M_0}{N \cdot h} = \frac{1}{2} - \frac{2}{3} \cdot \frac{N}{N_{cm}} - \frac{1}{6} \frac{N_{cm}^2}{N_{E\alpha} \cdot N} \tag{9.30}$$

The curvature is calculated as $\kappa = f_{cm} / (E_0 y_0)$. In Figure 9.8 the points determined by equation (9.30) (represented by a plus), are plotted together with the previous results (the slenderness (l/h) ratio is 20).
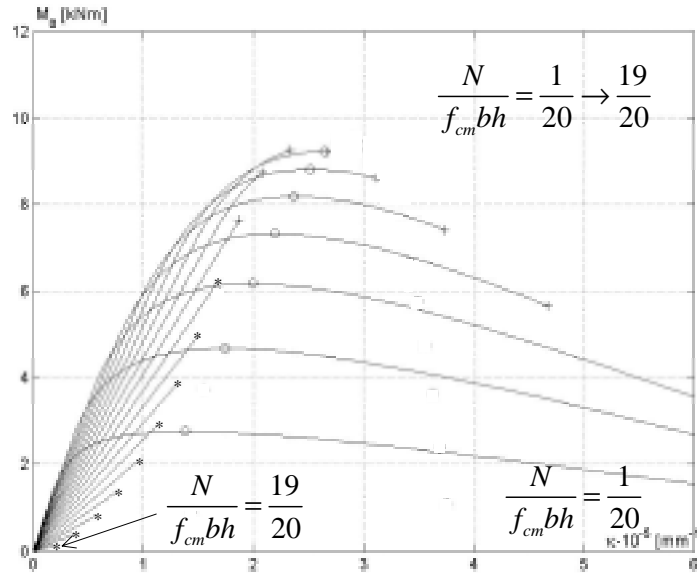
Figure 9.8 Simple moment-curvature relationship

Figure 9.8 shows that equation (9.27) and (9.30) provides the maximum values of M_0 until the entire cross section is in compression, where the usual theory of linear elasticity is used (these points are marked with a *).

This means that the interaction diagram may be found as shown in Figure 9.9. A simplified interaction diagram is shown in the figure. It consists of straight lines through points corresponding to some characteristic stress conditions and the Ritter value.
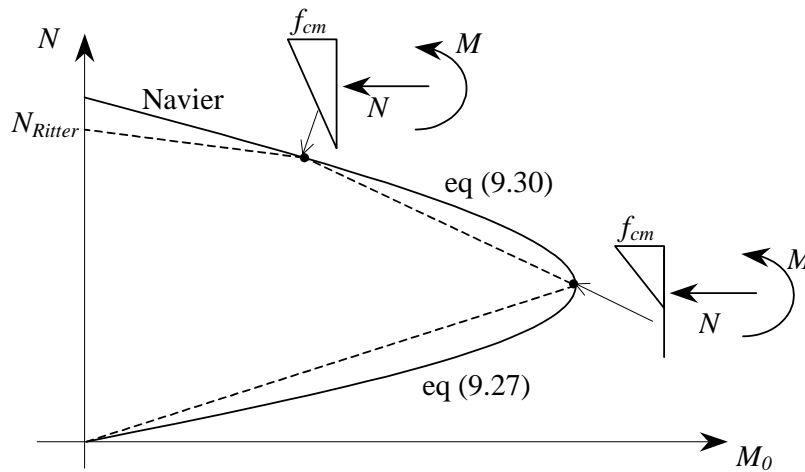
Figure 9.9 Interaction diagram

9.3.1.1 Instability of beam-columns and one-way walls according to DS414 and a modified linear elastic model

DS414

The Danish Code of Practice, DS414, provides an equation for eccentrically loaded masonry columns and one-way slabs. In this equation, an effective cross-section is used. The method may only be used for very simple columns where a line of compression may be drawn.
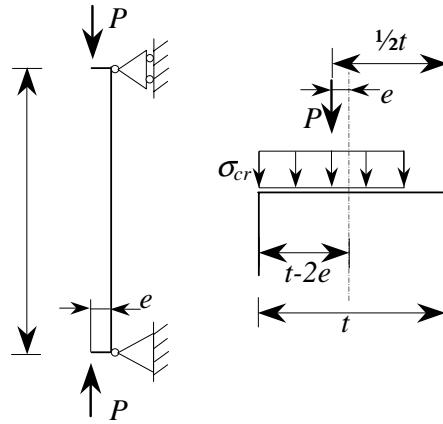
Figure 9.10 Eccentrically loaded column, Danish code of practice (DS414)

As shown in Figure 9.10 the effective cross-section is defined as the total thickness minus two times the eccentricity. The load carrying capacity is then calculated from the Ritter equation:

$$\sigma_{cr} = k_t \frac{f_{cm}}{1 + \dfrac{f_{cm}}{E_0 \pi^2} \lambda^2} \tag{9.31}$$

where λ is determined by

$$\lambda = \frac{l}{i} = 12 \left(\frac{l}{t - 2e} \right)^2 \tag{9.32}$$

The parameter k_t is defined in section 9.2.2. Thereby the critical load can be determined as

$$N_{cr} = A_{cm} \sigma_{cr} = b(t - 2e) \sigma_{cr} \tag{9.33}$$

Modified linear elastic model

In the Danish concrete code, DS411, laterally loaded or eccentrically loaded columns may be calculated by means of a modified linear elastic model. It is natural to try to extend this method to cover masonry columns, which turn out to be possible. However, some parameters have to be changed.

The stress-strain relation for masonry is assumed parabolic as given by equation (9.34), i.e.

$$\sigma = f_{cm} \frac{\varepsilon}{\varepsilon_{cmy}} \left(2 - \frac{\varepsilon}{\varepsilon_{cmy}} \right) \tag{9.34}$$

It is recalled that when $E_0 = 375 f_{cm}$, the strain at the stress f_{cm} is 5.33 $^0/_{00}$. In the moment-curvature relations, the maximum moment will occur for a larger strain in the compressive face than ε_{cmy}. In Figure 9.11 the moment as a function of the strain ε_{cm} for different levels of axial load is shown. It turns out, that maximum moment for pure bending is obtained at a maximum strain equal to 6.8 $^0/_{00}$. Larger *N*-levels lead to somewhat lower values.
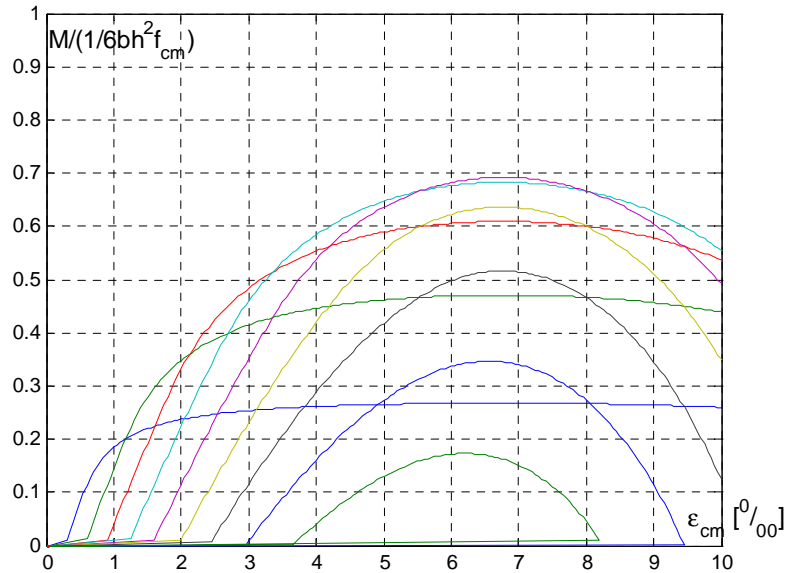
Figure 9.11 Moment as a function of the strain in masonry for different *N*-levels

$\dfrac{N}{hbf_{cm}}$	$\dfrac{M}{\frac{1}{6}bh^2 f_{cm}}$	$\varepsilon_{c\max}$ [‰]
0,10	0,27	6,75
0,20	0,47	6,75
0,30	0,61	6,75
0,40	0,68	6,75
0,50	0,69	6,75
0,60	0,64	6,75
0,70	0,52	6,75
0,80	0,35	6,55
0,90	0,17	6,20

Table 9.2 The maximum strain for different *N*-levels

The strain values leading to maximum moment are shown in Table 9.2.

A linear elastic model to calculate the load carrying capacity is obtained by setting the area under the parabolic stress-strain relation equal to a area under the linear stress-strain relation. Further, it is assumed that in the linear elastic model the modulus of elasticity is set to the secant modulus.

$$E_0^* = \frac{f_{cm}}{\varepsilon_{cmy}} = 188 f_{cm} \tag{9.35}$$

The area *A* under the parabolic stress-strain curve is obtained by integration from zero to the maximum strain, i.e.

$$A = \int_0^{\varepsilon_{cmu}} \sigma(\varepsilon)\, d\varepsilon = E_0 \int_0^{\varepsilon_{cmu}} \left(\varepsilon - \frac{1}{2}\frac{\varepsilon^2}{\varepsilon_{cmy}} \right) d\varepsilon = \frac{1}{2} E_0 \varepsilon_{cmu}^2 \left(1 - \frac{1}{3}\frac{\varepsilon_{cmu}}{\varepsilon_{cmy}} \right) \tag{9.36}$$

The area given by equation (9.36) is set equal to the area of a rectangle with the lengths $k\varepsilon_{cmu}$ and f_{cm}. Then $k = 0.73$. The area of the rectangle is then set equal to the area under the linear elastic stress-strain curve with the inclination E_0^* given by (9.35). Thus, equation (9.37) is obtained:

$$\frac{1}{2} E_0^* \varepsilon^2 = 0.73 f_{cm} \varepsilon_{cmu} \tag{9.37}$$

This gives a maximum strain $\varepsilon = \varepsilon_{cmu} = 7{,}2$ ‰, corresponding to $f_{cm}^* = 1{,}35\, f_{cm}$. If, as for concrete, $f_{cm}^* = 1{,}25 f_{cm}$ is chosen as the maximum stress, this is achieved at the strain

$\varepsilon = 6.6\ ^0/_{00} \cong \varepsilon_{cmu}$. This is a conservative value of f_{cm}^* since it provides a smaller strain energy than corresponding to equal areas. Thus in the calculations the following linear elastic model is suggested.

$$E_0^* = 188 f_{cm} \qquad f_{cm}^* = 1,25 f_{cm} \qquad \varepsilon_{cmu} = 6,7\ ^0/_{00}$$

To include the non-linear behaviour a modified modulus of elasticity has to be introduced in the calculations of the deflections. The modulus must vary with the stresses in the section and fulfil three conditions:

1. When the stress is zero in the entire cross-section the modulus of elasticity has to be equal to the initial stiffness E_0.
2. For a uniform stress distribution, the modulus of elasticity has to be equal to E_σ, the tangential stiffness used in the Ritter equation.
3. When the cross-section is cracked and the zone of compression is completely utilized the modulus of elasticity must be equal to $E_0^* = 188 f_{cm}$.

The maximum stress in compression is defined as

$$f_{cm}^* = \begin{cases} 1,25 f_{cm} \\ 1,25 f_{cm} \left(1 - 0,2 \dfrac{\sigma_{cm,\min}}{f_{cm}} \right) \end{cases} \tag{9.38}$$

To fulfil the first two conditions above the modulus of elasticity has to vary as

$$E_{cr} = E_0 \left(1 - k \frac{\sigma_{c,\max}}{f_{cm}} - (1-k) \frac{\sigma_{c,\min}}{f_{cm}} \right) \tag{9.39}$$

The third condition determines the value of k as

$$k = 0,8 \left(1 - \frac{E_0^*}{E_0} \right) = 0,8 \left(1 - \frac{188}{375} \right) = 0,3989 = 0,4 \tag{9.40}$$

When the stresses are known the deflection at a certain stress level may be determined as

$$u = \frac{1}{\alpha} \frac{\sigma_{cm,\max} - \sigma_{cm,\min}}{E_{cr} \Delta h} l^2 \tag{9.41}$$

where Δh is the distance between the fibres with the stresses $\sigma_{cm,\max}$ and $\sigma_{cm,\min}$, respectively, α is a parameter of shape and l is the length of the column.

The calculation procedure is to estimate the deflection, calculate the stresses and determine the deflection by using equation (9.41), compare it with the estimated deflection and when a sufficient correlation is achieved, the calculation is finished.

If the parabolic[4] and the modified elastic model are compared in the case of a short beam column and a slender beam column, the result is as shown in Figure 9.12.
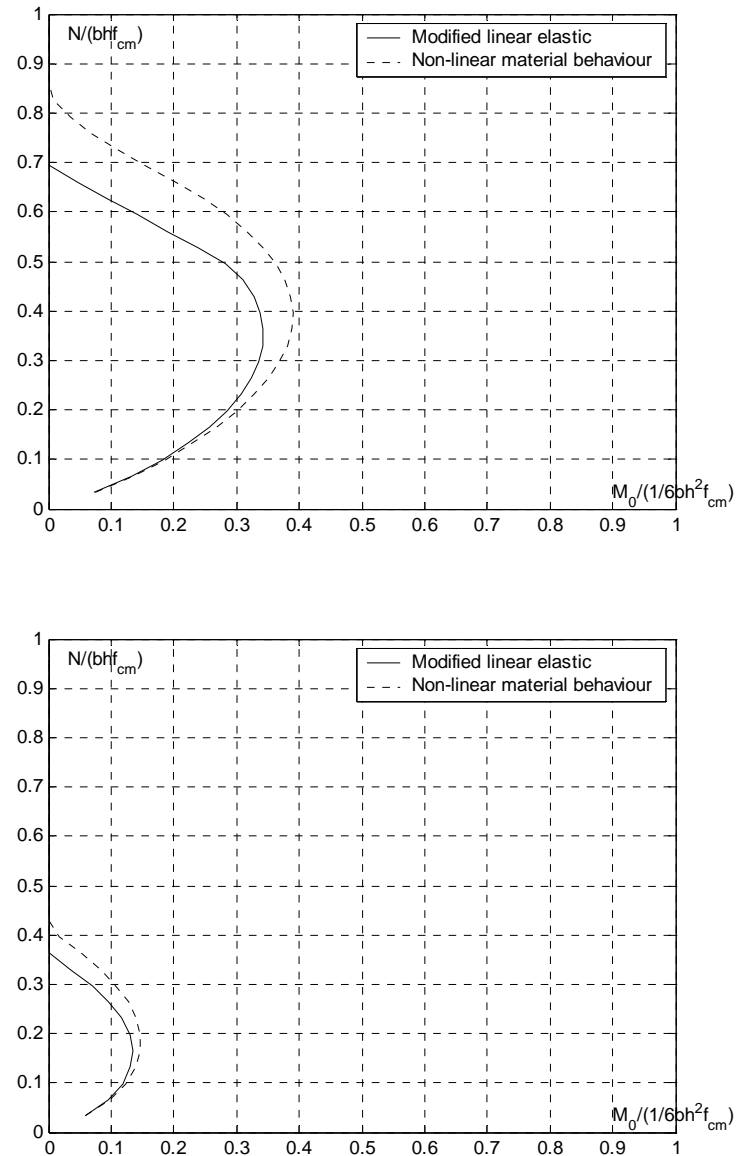
Figure 9.12 Interaction diagram for l/h=12 in the top figure and 24 in the bottom figure

---

[4] The interaction diagram for a parabolic material is described thoroughly in section 9.3.2

In Figure 9.13 the maximum axial load as a function of the curvature is shown for, $l/h=12$.
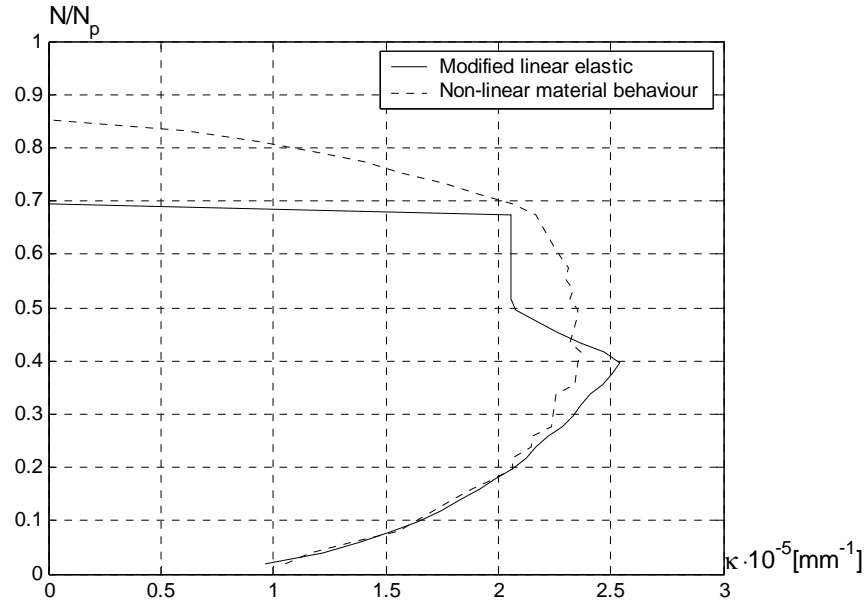
Figure 9.13 Maximum axial load as function of the curvature for two models

9.3.2 Non-linear material behaviour

In this section, the constitutive equation is the parabolic relation treated previously.
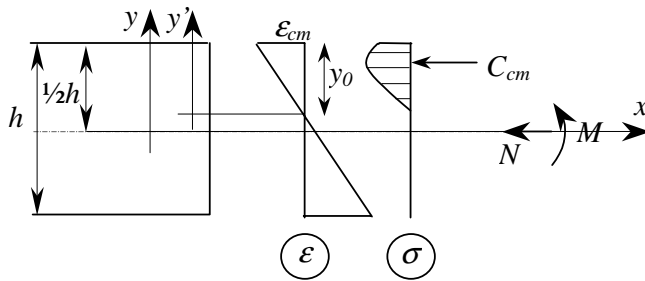
Figure 9.14 Cross section with a parabolic stress distribution

Projection equation, when $y_0 \leq h$:

$$N = C_{cm}$$

where

$$C_{cm} = b \int_0^{y_0} \sigma_{cm} dy'$$

$$C_{cm} = b \int_0^{y_0} f_{cm} \frac{\varepsilon_{cm} \frac{y'}{y_0}}{\varepsilon_{cmy}} \left(2 - \frac{\varepsilon_{cm} \frac{y'}{y_0}}{\varepsilon_{cmy}} \right) dy' = \frac{f_{cm} b}{\varepsilon_{cmy}} \varepsilon_{cm} \left(1 - \frac{\varepsilon_{cm}}{3\varepsilon_{cmy}} \right) y_0$$

Moment equation, when $y_0 \leq h$:

$$M = M_{cm} + N \left(\frac{h}{2} - y_0 \right)$$

where

$$M_{cm} = b \int_0^{y_0} \sigma_{cm} y' dy'$$

$$M_{cm} = b \int_0^{y_0} f_{cm} \frac{\varepsilon_{cm} \frac{y'}{y_0}}{\varepsilon_{cmy}} \left(2 - \frac{\varepsilon_{cm} \frac{y'}{y_0}}{\varepsilon_{cmy}} \right) y' dy' = \frac{f_{cm} b}{\varepsilon_{cmy}} \varepsilon_{cm} \left(\frac{2}{3} - \frac{\varepsilon_{cm}}{4\varepsilon_{cmy}} \right) y_0^2$$

From these equations the moment-curvature relationship may be determined, see Figure 9.15. Then the load carrying capacity is determined as before. For the data given in Table 9.1 results are shown in Figure 9.16. Distinction must be made between the cases where the depth of the compression zone is smaller or larger than the depth of the cross section, respectively.
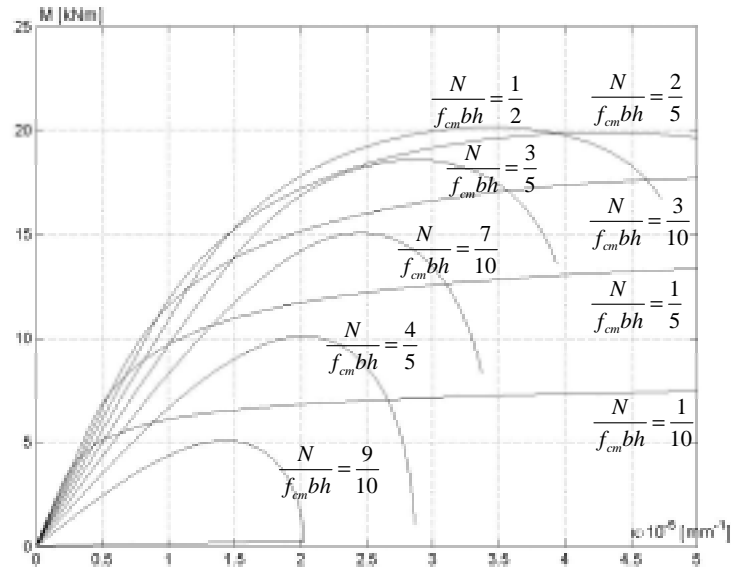
Figure 9.15 The moment-curvature relationship
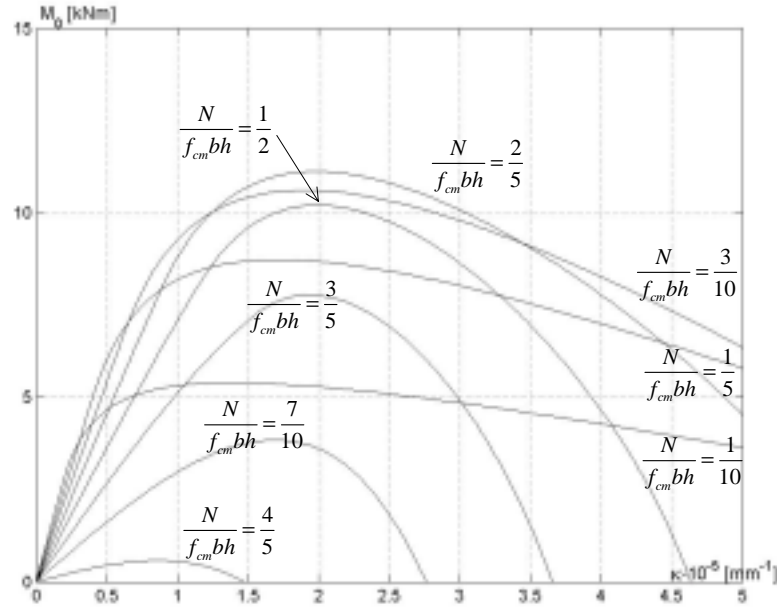
Figure 9.16 The simple moment-curvature relationship

The maximum strain, ε_{cmu}, is in this calculation set equal to $3.5^0/_{00}$ as in Eurocode 6, [44].

9.3.3 Rigid plastic material behaviour

The ultimate moment as a function of the axial load is calculated on the basis of the stress distribution shown in Figure 9.17 where the material is rigid plastic.
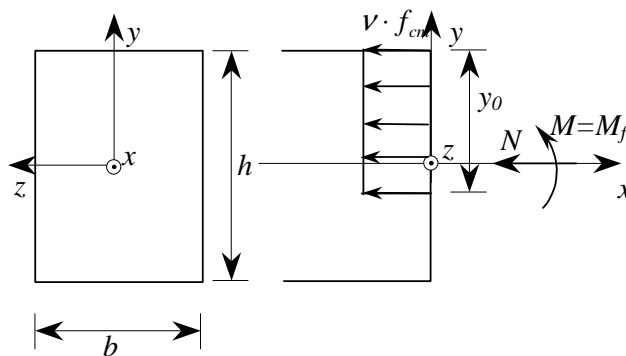
Figure 9.17 Cross-section of unreinforced masonry with rigid plastic stress block

The projection equation becomes, ν being the effectiveness factor on f_{cm}.

$$N = b \cdot v f_{cm} \cdot y_0 \tag{9.42}$$

The moment equation becomes, M_f being the ultimate moment.

$$M_f = N \cdot \left(\frac{1}{2} \cdot h - \frac{1}{2} \cdot y_0 \right) \Leftrightarrow$$

$$\frac{M_f}{N \cdot h} = \frac{1}{2} \cdot \left(1 - \frac{N}{N_{cm}} \right) \tag{9.43}$$

where $N_{cm} = b \cdot h \cdot v f_{cm}$. The simple moment may be calculated by using the equilibrium equation:

$$M_f = M_0 + \frac{1}{\alpha} \cdot \kappa \cdot l^2 \cdot N \tag{9.44}$$

In this case, the curvature must be estimated. The following estimate is suggested:

$$\kappa = \frac{f_{cm}}{E_0^* h} \tag{9.45}$$

where in the case of Danish masonry $E_0^* = 188 f_{cm}$.

The relation between the simple moment and the axial load may be expressed as done in (9.46)

$$\frac{M_0}{N_{cm} h} = \frac{N}{N_{cm}} \left(\frac{1}{2} - \frac{\kappa \cdot l^2}{h \cdot \alpha} - \frac{1}{2} \frac{N}{N_{cm}} \right) \tag{9.46}$$

which may be rewritten into

$$\frac{N}{N_{cm}} = \frac{1}{2} \left(1 - 2 \frac{\kappa \cdot l^2}{\alpha \cdot h} \pm \sqrt{1 - 4 \frac{\kappa \cdot l^2}{\alpha \cdot h} \left(\frac{\kappa \cdot l^2}{\alpha \cdot h} - 1 \right) + 8 \frac{M_0}{N_{cm} h}} \right) \tag{9.47}$$

The maximum value of M_0 corresponding to equation (9.46) is easily found by differentiation with respect to N:

$$\frac{dM_0}{dN} = \frac{1}{2} h - \frac{N \cdot h}{N_{cm}} - \frac{1}{\alpha} \cdot \kappa \cdot l^2 = 0 \Leftrightarrow$$

$$\frac{N}{N_{cm}} = \frac{1}{2} - \frac{\kappa \cdot l^2}{\alpha \cdot h} \tag{9.48}$$

Equation (9.46) renders $M_0 = 0$ when $N = 0$ and when N has the value given by equation (9.49), which is easily found by requiring $M_0 = 0$ and introducing equation (9.45).

$$\frac{N}{f_{cm}b \cdot h} = \frac{\sigma_{cr}}{f_{cm}} = \frac{\alpha - 2\frac{f_{cm}}{E_0}\left(\frac{l}{h}\right)^2}{\alpha} \tag{9.49}$$

Results for the rigid plastic model with $\nu = 1$ are shown in Figure 9.18. The curvature has been estimated according to (9.45) in the curve to the right. In the curve to the left E_0^* in (9.45) is replaced by E_0.

The rigid plastic model severely underestimates the load carrying capacity. To render good results the estimate of the curvature must be refined. As a minimum it must depend on the slenderness ratio.
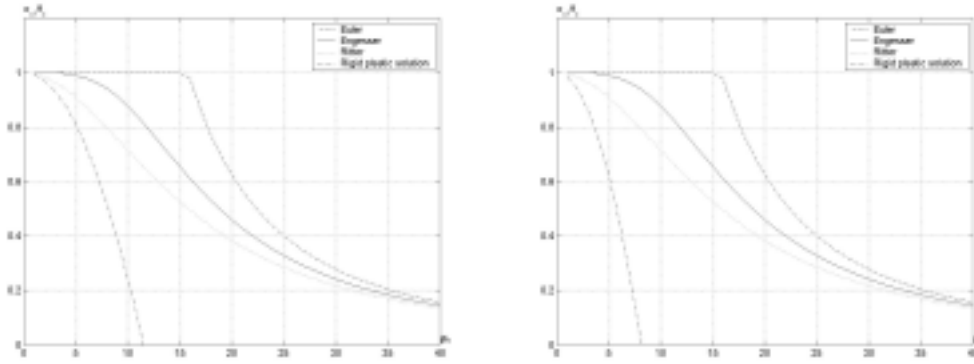
Figure 9.18 Critical load for estimated curvature $\kappa = \frac{f_{cm}}{E_0 h}$ to the left and $\kappa = \frac{f_{cm}}{E_0^* h}$ to the right

9.3.4 Comparison of calculation methods

The three calculation methods are compared in Figure 9.19 in the case of Danish masonry. For the rigid plastic material, the effectiveness factor ν is set equal to one.
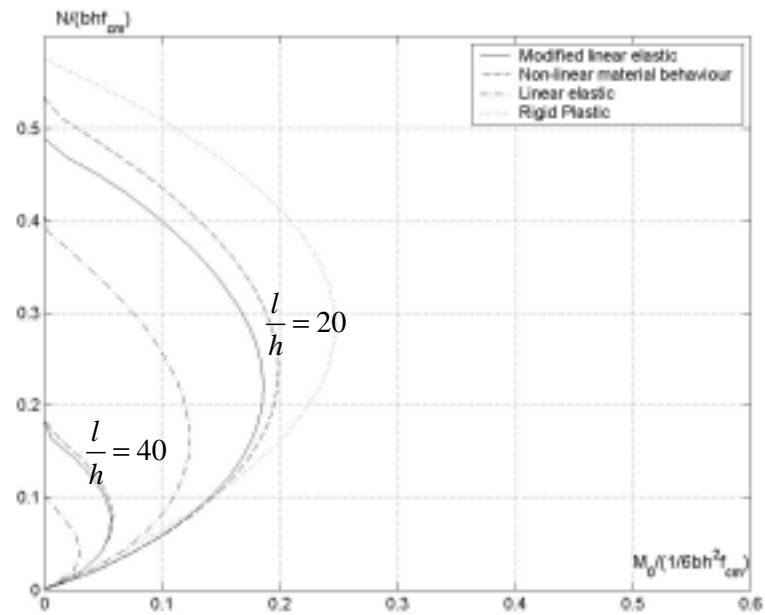
Figure 9.19 Interaction curves for the different models

Figure 9.19 shows that the non-linear, the modified linear elastic and the rigid-plastic material behaviour render higher load carrying capacity than the linear elastic model. Figure 9.20 is similar to Figure 9.19, the only difference being, that the effectiveness factor suggested in [11] for concrete is used, i.e.

$$v = 0.85 - \frac{f_{cm}}{300} \tag{9.50}$$

This is done because concrete and masonry has similar behaviour in compression, which means that a similar reduction of the compressive strength of masonry may be expected when using a rigid-plastic material model.
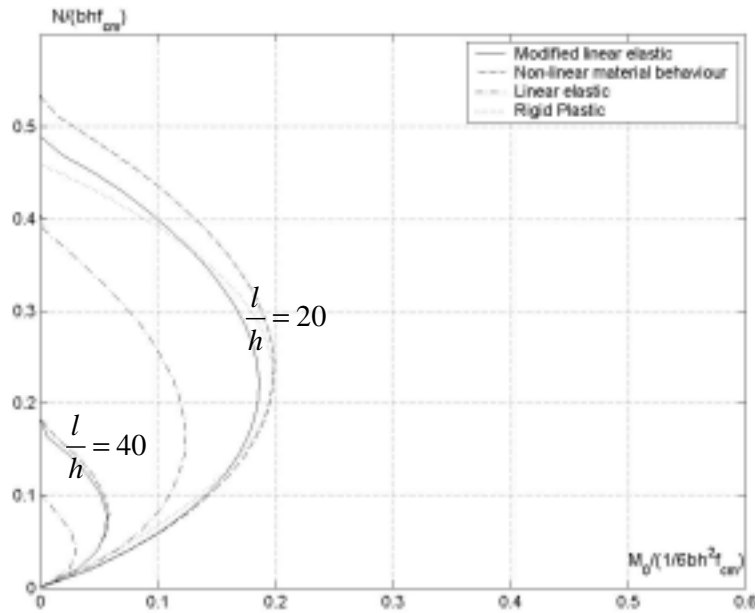
Figure 9.20 Interaction curves for the different models

It appears that for short beam-columns three of the models (modified linear elastic model, non-linear model and the rigid plastic model with reduced compressive strength) produce similar results. It also appears that the linear elastic model is conservative compared with the other models.

9.3.5 Load carrying capacity of beam-columns with small axial load

In this section, simple upper bound solutions will be used to calculate the load carrying capacity of masonry beam-columns. It is assumed that the axial load is small so the additional moment from the axial load multiplied with the deflection can be disregarded.

First we consider the case shown in Figure 9.21 where the failure mechanism is illustrated. It is assumed that the relative rotation point in the midpoint is at the right face. This assumption implies that the internal work becomes equal to zero when the tensile strength of the bed joint is set equal to zero.
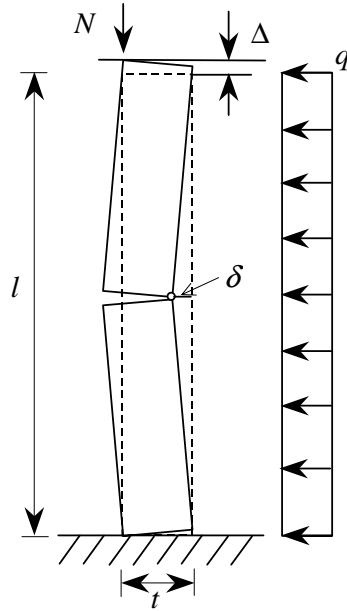
Figure 9.21 Failure mechanism of masonry with small axial load

The external work becomes

$$W_E = -N \cdot \Delta + \frac{1}{2} \cdot q \cdot b \cdot l \cdot \delta \qquad (9.51)$$

where

$$\frac{\frac{1}{2}\Delta}{t} = \frac{\delta}{\frac{1}{2}l} \Leftrightarrow \Delta = 4 \cdot \delta \cdot \frac{t}{l}$$

N is the normal force acting in the left top corner, q is the transverse load per unit area and b is the width.

Setting $W_E = 0$ provides a relation between the axial load and the transverse load:

$$N = \frac{1}{8} \cdot q \cdot b \cdot \frac{l^2}{t} \qquad (9.52)$$

Equation (9.52) is plotted in a (q,N) diagram in Figure 9.22

In the above calculation, the resultant normal force acts in the outermost position possible, i.e. at the left face. This position leads to maximum work of the normal force. If the position of the resultant normal force is statically determined this assumption may not apply, and the calculation may be on the unsafe side. An upper bound solution corresponding to another position of the resultant normal force may easily be obtained in the same way.
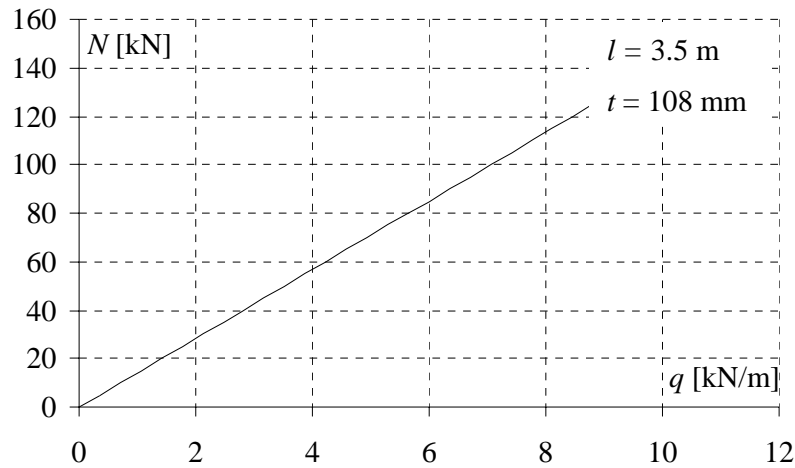
Figure 9.22 Interaction curve with membrane actions

The method is compared with experiments in [38], section 7.3, from where Figure 9.23 is taken.
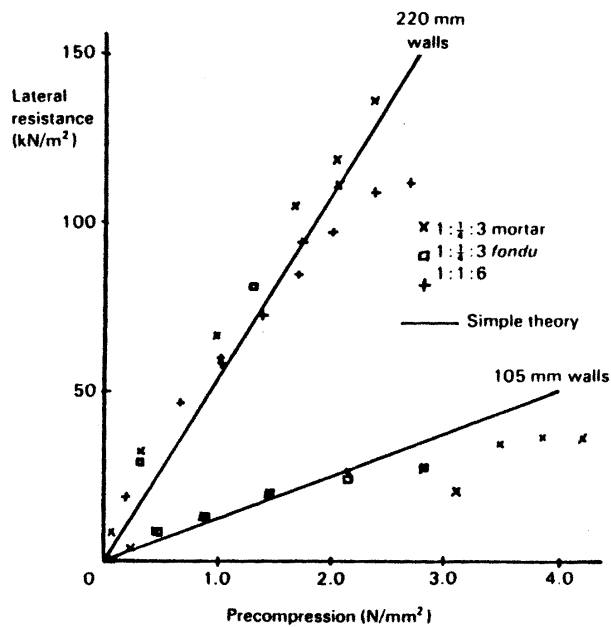
Figure 9.23 Upper bound method compared with theory taken from [38]

9.3.6 Load carrying capacity of transversely loaded one-way walls

The load carrying capacity of transversely loaded masonry one-way walls without tensile strength and without external normal forces is equal to zero when calculated by

the previous analysis. However using an upper bound solution where the mass of the masonry wall is considered a load carrying capacity different from zero may be found.
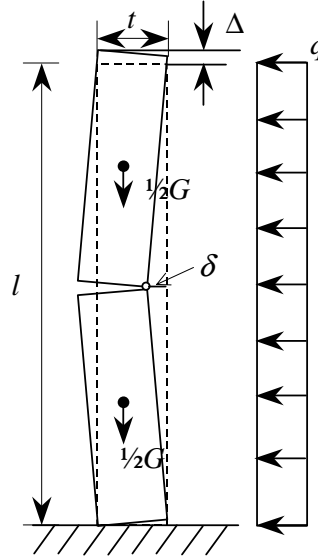
Figure 9.24 Lateral load carrying capacity of masonry without precompression

The geometrical relation between δ and Δ is given as

$$\Delta = 4 \cdot \delta \cdot \frac{t}{l} \tag{9.53}$$

The internal work is zero because of the assumption of zero tensile strength of the masonry. The external work then determines the load carrying capacity:

$$W_E = \frac{1}{2} \cdot q \cdot l \cdot b \cdot \delta - \left(\frac{1}{2} \cdot G \cdot \frac{1}{4} \cdot \Delta + \frac{1}{2} \cdot G \cdot \frac{3}{4} \cdot \Delta \right) \Leftrightarrow$$

$$W_E = \frac{1}{2} \cdot q \cdot b \cdot l \cdot \delta - 2 \cdot G \cdot \frac{t}{l} \cdot \delta \tag{9.54}$$

where b is the total thickness of the wall and $G = \gamma \cdot b \cdot t \cdot l$. γ being the specific weight.

Setting $W_E = 0$ a relation between the weight, G, and the transverse load, q, can be obtained.

$$q = 4 \cdot G \cdot \frac{t}{bl^2} = 4 \cdot \gamma \cdot \frac{t^2}{l} \tag{9.55}$$

The load carrying capacity of a one-way wall may, according to DS414, be calculated assuming a linear elastic stress variation along the cross-section. The maximum stress at

the edge in tension is equal to the tensile flexural strength. In pure bending the absolute value of the maximum compressive stress is also equal to the tensile flexural strength. The tensile flexural strength is determined from $f_{mor,tlk}$, which according to DS414 is the strength of the interface when the masonry is bent above the bed joint. Based on $f_{mor,tlk}$ the flexural strength may be taken from two tables (G.4e and G.4d in DS414). Thereby the moment capacity may be determined as:

$$M = \frac{1}{6} f_{tlk} b t^2 \qquad (9.56)$$

t	b	l	γ
[mm]	[mm]	[mm]	[kN/m^3]
108	1000	2500	18.2

Table 9.3 Geometry of the two walls

To compare the load carrying capacity calculated using (9.55) with the method in DS414, two walls with the same geometry (see Table 9.3) are considered. The walls are built with two different types of brick and mortar. The combinations of brick and mortar results in the strengths listed in Table 9.4 based on DS414. The mortar is of minor importance in determining f_{tlk}, from DS414. Using (9.56) the moment capacity listed in Table 9.4 may be obtained.

	$f_{mor,tlk} = 0.25$ MPa	$f_{mor,tlk} = 0.50$ MPa
	$f_{cb} = 30$ MPa	$f_{cb} = 30$ MPa
	$f_{tlk} = 0.24$ MPa	$f_{tlk} = 0.40$ Mpa
M: kNm	0.47	0.78

Table 9.4 Moment capacity according to DS414

From (9.55), the load carrying capacity may be calculated and thereby the moment having the simple relation

$$M = \frac{1}{8} q l^2 \qquad (9.57)$$

Using the values in Table 9.3 the moment calculated from (9.57) becomes 0.26 kNm. It is seen that the moment calculated using (9.55) and (9.57) is a significantly smaller than the value calculated according to DS414. However, the moment calculated

represents characteristic values of the moment capacity. A comparison of the two methods must be made with regards to the design values.

The design value of the moment capacity using (9.55) and (9.57) is obtained multiplying the moment obtained by 0.8, since according to the Danish code for the safety of structures, the mass must be multiplied with 0.8 when used to stabilize the structure. This gives a moment capacity of 0,21 kNm.

The design moment capacity using DS414 is calculated using a material safety factor, γ_m, for a structural element in normal safety class and control class. In this case, γ_m becomes 2.00 and the moment capacities become 0.23 kNm and 0.39 kNm, respectively.

It appears that in the case of $f_{mor,tlk} = 0.25$ MPa the two methods provide almost the same results. It may be noticed that $f_{mor,tlk} = 0.25$ MPa is the highest value, which can be achieved using DS414 alone. To obtain a higher moment capacity, $f_{mor,tlk}$ has to be known for the masonry used.

10 Reinforced masonry

10.1 Introduction

In this section, reinforced masonry will be analysed by different constitutive relations in compression, namely a parabolic stress-strain curve and a linear elastic one. Reinforcement is linear elastic perfectly plastic with the same yield stress f_y in tension and compression. A rigid plastic model will not be considered since it is only relevant when the beam-column is short and failure is due to material failure.

10.2 Instability of reinforced masonry columns

The analysis of reinforced columns is similar to the analysis of unreinforced masonry columns the only difference being that the contribution from the reinforcement must be added to the load carrying capacity determined by the Ritter or the Engesser equation (see equation (10.1)).

The critical load when using the Ritter or Engesser equations may be determined by

$$N_{cr} = \min \begin{cases} \sigma_{cr} A_c \cdot (1 + n \cdot \varphi) \\ \sigma_{cr} A_c + A_s \cdot f_y \end{cases} \qquad (10.1)$$

where $n = \dfrac{E_s}{E_0^*}$ and $\varphi = \dfrac{A_s}{A_{cm}}$. It appears that the reinforced contribution is simply added as in sectional analysis, i.e. the contribution from the reinforcement to the bending stiffness is neglected.

The theoretical method is based on the equilibrium method explained in section 10.3.1. The critical load for concentrically loaded columns is obtained by letting the deflection u go towards zero.

In Figure 10.1, the results of the different methods are shown in a specific example. It is seen that Ritter's equation provides a conservative result, making it suitable for practical purposes. The theoretical calculation leads to a flat plateau, which is due to yielding in the compression reinforcement. The strain distribution switches between the cases 37, 38 and 39, see the following Figure 10.2.

The reinforcement only renders a limited additional load carrying capacity. Thus, a simple and almost correct theory is Engesser's first theory where the contribution from the reinforcement is added as done in equation (10.1).
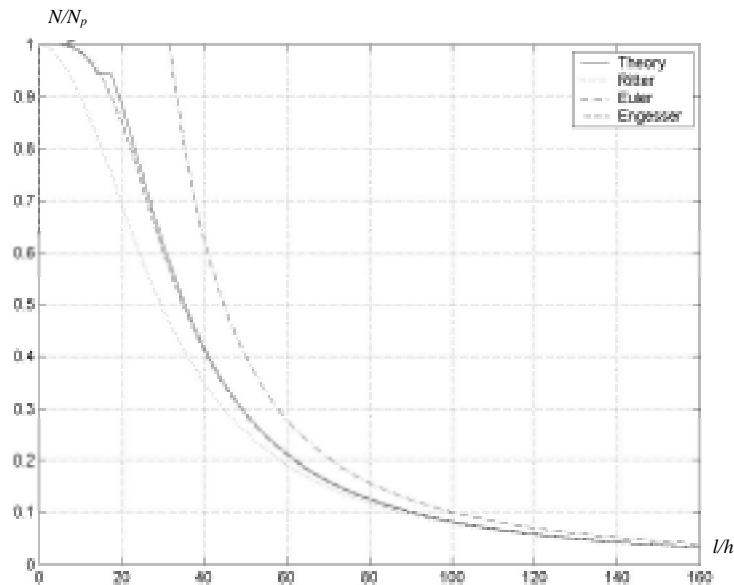
Figure 10.1 Concentrically loaded column. Theory compared with the Ritter, the Euler and the Engesser equation. In the calculations $f_{cm} = 25$MPa, $f_y = 300$MPa, $\Phi_0 = 0.05$, $h_c = 0.10h$ and $\alpha = 10$.

10.3 Instability of reinforced masonry beam-columns

In this section, the behaviour of reinforced masonry beam-columns will be investigated using a linear elastic and a parabolic material behaviour. Reinforcement is elastic-perfectly plastic with the same yield stress f_y in tension and compression.

To obtain the moment-curvature relationship, nine different situations have to be examined (see Figure 10.2).

10.3.1 Non-linear material behaviour

The nine different cross-section analyses are characterised by a number so that the conditions at failure[5] may be tracked. The nine cases are shown in Figure 10.2.

---

[5] A point of failure is characterized either as failure due to instability or to material failure.
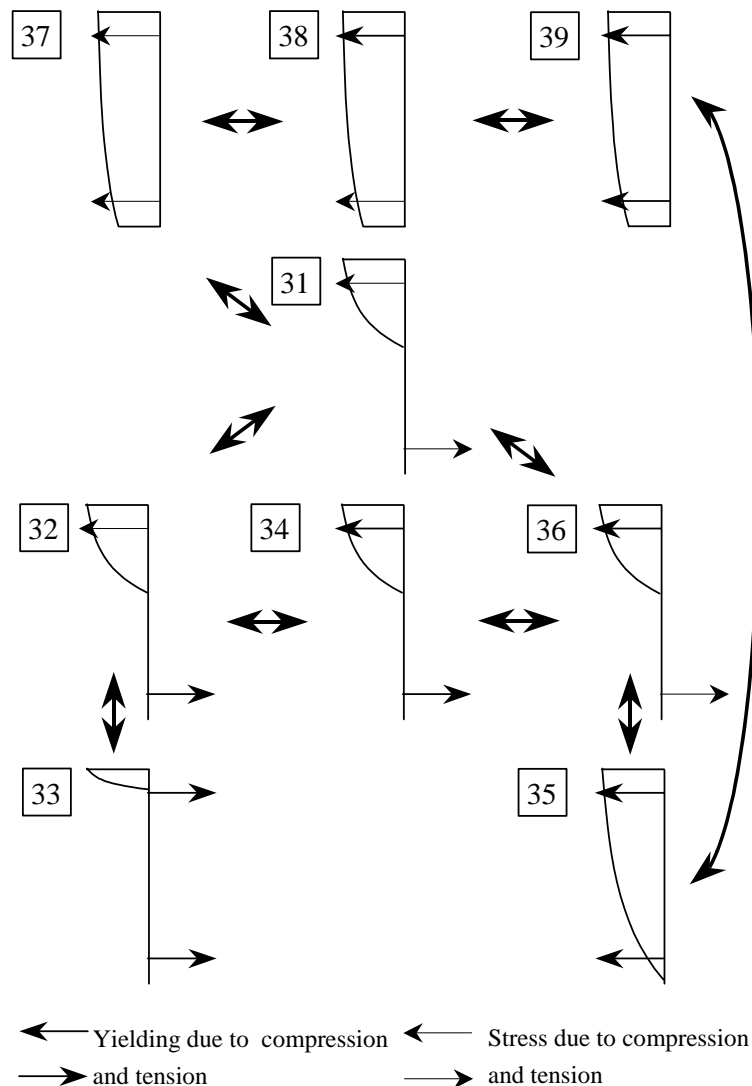
Figure 10.2 Calculation of the moment-curvature relationship is based on nine cross-section analyses.

For a prescribed normal force and masonry strain, the neutral axis is determined from the projection equation, whereby the curvature may be determined. From the moment equation, the bending moment is determined.

As before the normal force and the bending moment are referred to the midpoint of the section, see Figure 10.3. The cross section is shown in Figure 10.4.
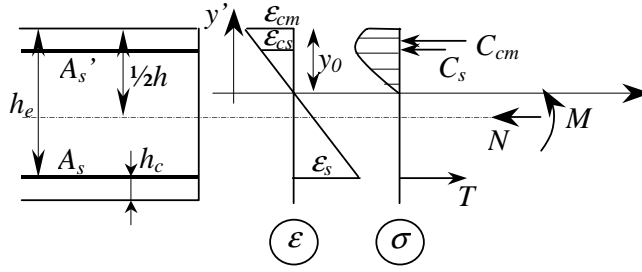
Figure 10.3 Stress and the strain distribution in a cross-section

The projection equation, when $y_0 \le h$ and the reinforcement is in the linear elastic range:

$$N = C_{cm} + C_s - T \qquad (10.2)$$

where

$$C_{cm} = b \int_0^{y_0} \sigma_{cm} dy'$$

$$C_{cm} = b \int_0^{y_0} f_{cm} \frac{\varepsilon_{cm} \frac{y'}{y_0}}{\varepsilon_{cmy}} \left(2 - \frac{\varepsilon_{cm} \frac{y'}{y_0}}{\varepsilon_{cmy}} \right) dy' = \frac{f_{cm} b}{\varepsilon_{cmy}} \varepsilon_{cm} \left(1 - \frac{\varepsilon_{cm}}{3\varepsilon_{cmy}} \right) y_0$$

$$C_s = \sigma_{cs} A_s' = \varepsilon_{sc} E_s A_s = \frac{y_0 - h_c}{y_0} \varepsilon_{cm} E_s A_s'$$

$$T = \sigma_s A_s = \varepsilon_s E_s A_s = \frac{h_e - y_0}{y_0} \varepsilon_{cm} E_s A_s'$$

The moment equation, when $y_0 \le h$ and the reinforcement is in the linear elastic range:

$$M = M_{cm} + C_s \left(y_0 - h_c \right) + T \left(h_e - y_0 \right) + N \left(\frac{h}{2} - y_0 \right) \qquad (10.3)$$

where

$$M_{cm} = b \int_0^{y_0} \sigma_{cm} y' dy'$$

$$M_{cm} = b \int_0^{y_0} f_{cm} \frac{\varepsilon_{cm} \frac{y'}{y_0}}{\varepsilon_{cmy}} \left(2 - \frac{\varepsilon_{cm} \frac{y'}{y_0}}{\varepsilon_{cmy}} \right) y' dy' = \frac{f_{cm} b}{\varepsilon_{cmy}} \varepsilon_{cm} \left(\frac{2}{3} - \frac{\varepsilon_{cm}}{4\varepsilon_{cmy}} \right) y_0^2$$

When the reinforcement yields, $E_s \varepsilon_s$ is replaced by f_y.

When these equations are solved in the nine cases the M-κ relationship and the M_0-κ relationship may be obtained for a specific beam-column.

The M-κ relationship depends on the reinforcement ratio, the compressive strength and the yield strength of the reinforcement. Results are shown in Figure 10.5.

The value of the axial load is set at 2/9 N_p, where $N_p = hbf_{cm} + 2A_sf_y$ assuming the reinforcement to yield when the masonry stress reaches its maximum value.
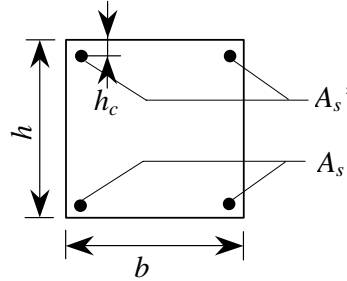
Figure 10.4 Cross-section used in the calculations

The calculations are carried out for the values listed in Table 10.11.

b	h	h_c	l	f_{cm}	ε_{cmy}	f_y	Φ_0
[mm]	[mm]	[mm]	[mm]	[MPa]	[‰]	[MPa]	[]
250	250	20	3000	15	2	300	0.05

Table 10.1. Data used in the calculation of the figures when values are not listed.

These data are used in the following unless otherwise stated. The maximum strain is set equal to 3,5‰ as done in Eurocode 6, [44].
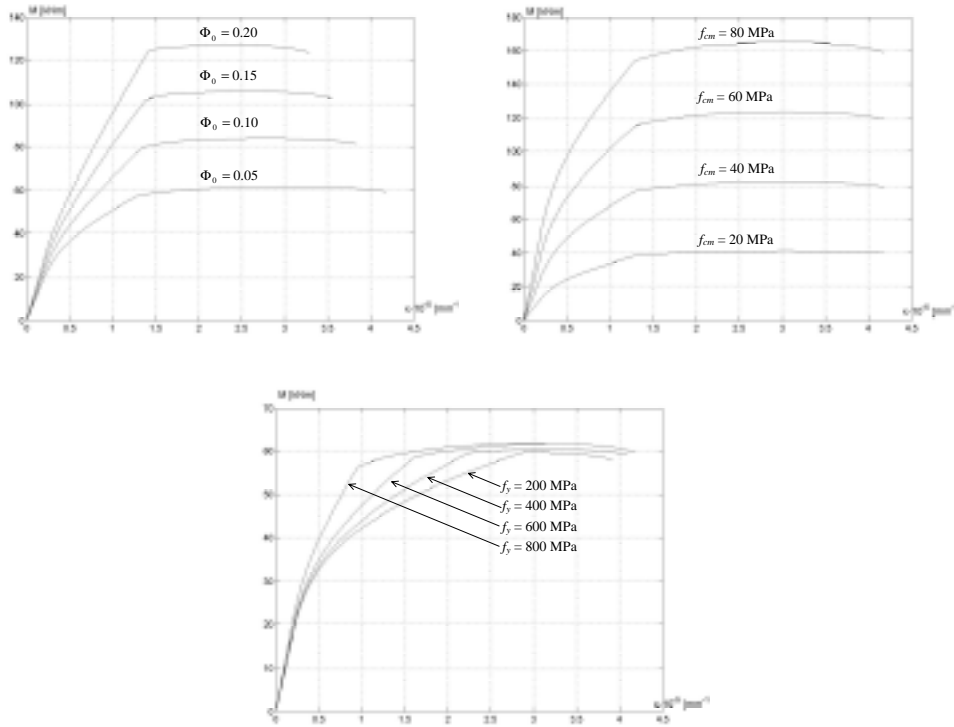
Figure 10.5 Moment-curvature relationship as a function of the degree of reinforcement, the compressive strength and the yield strength

Figure 10.6 and Figure 10.7 shows the moment-curvature relationship and applied moment-curvature relationship for different axial loads, respectively.
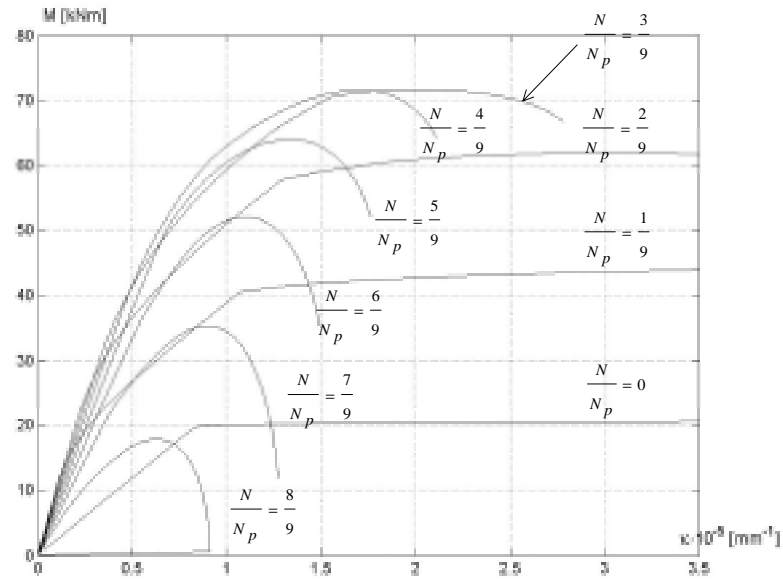
Figure 10.6 Moment-curvature relationship for different axial loads
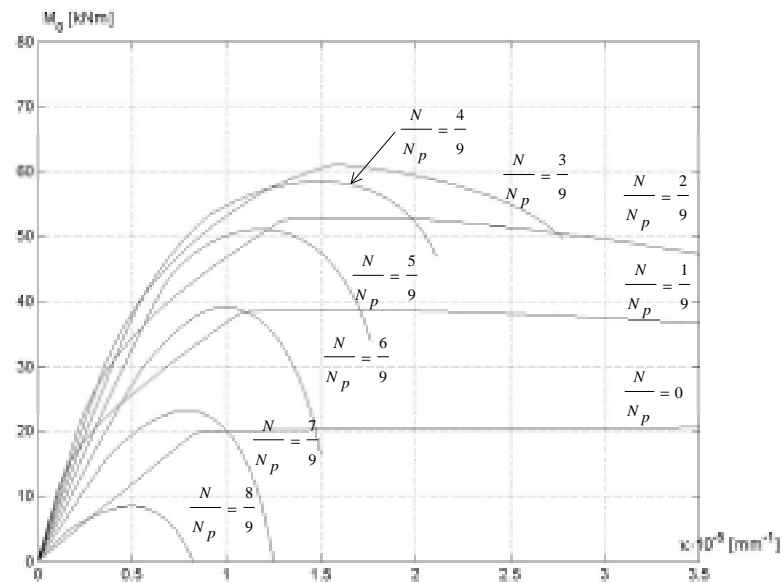
Figure 10.7 Simple moment-curvature relationship for the same axial loads as in Figure 10.6

Table 10.2 illustrates the different stress distributions met in the calculations of the moment-curvature relationships.

$\dfrac{N}{N_p}$	M interval in kNm	Case
0	$0 \leq M \leq 20$	31
	$M \geq 20$	32
$\dfrac{1}{9}$	$0 \leq M \leq 10$	37
	$10 \leq M \leq 40$	31
	$M \geq 40$	32 and 34
$\dfrac{2}{9}$	$0 \leq M \leq 20$	37
	$20 \leq M \leq 58$	31
	$58 \leq M \leq 60$	32
	$M \geq 60$	32 and 34
$\dfrac{3}{9}$	$0 \leq M \leq 29$	37
	$29 \leq M \leq 65$	31
	$M \geq 65$	34 and 36
$\dfrac{4}{9}$	$0 \leq M \leq 38$	37
	$38 \leq M \leq 60$	31
	$M \geq 60$	36
$\dfrac{5}{9}$	$0 \leq M \leq 45$	37
	$45 \leq M \leq 51$	31
	$M \geq 51$	36
$\dfrac{6}{9}$	$0 \leq M \leq 35$	37
	$M \geq 35$	36 and 38
$\dfrac{7}{9}$	$0 \leq M \leq 12$	37
	$M \geq 12$	37 and 38
$\dfrac{8}{9}$	$0 \leq M \leq 7$	37 and 38
	$M \geq 7$	38

Table 10.2 Cases for which the moment-curvature relationship is calculated

It appears that a great variety of N levels may be described by the same cases. All the curves in Figure 10.6 starts in situation 37 except the curve for pure bending, where the stress distribution starts in case 31. Then the case changes to one of the cases where the

compression depth is smaller than the depth of the cross section. For $\dfrac{N}{N_p} \leq \dfrac{5}{9}$ the case

reached after case 37 is case 31 (in general dependent on the degree of reinforcement). For N larger than this level the case will be 36, because when the axial load is large the top face reinforcement yields (in general dependent on the reinforcement ratio). The moment-curvature relationship changes in shape for an N level above $3/9N_p$. The reason is that the axial load is at a level where the compressive reinforcement begins to yield before the tension reinforcement yields, indicating that the depth of cracked cross section is decreasing. Thus, the moment-curvature relationship after this level will have no slope discontinuity for changes from uncracked to cracked cross section.

The point where the simple moment reaches its maximum value is the load carrying capacity of the column. This point may be influenced by the degree of reinforcement as shown in Figure 10.8 and the slenderness ratio as shown in Figure 10.9.

In Figure 10.8, the length l (500 mm) is small so the slenderness ratio has no effect.
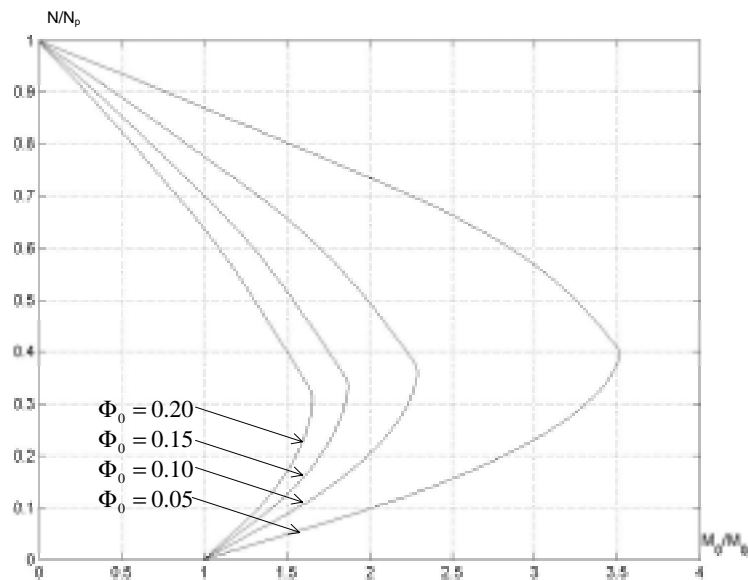
Figure 10.8 Influence of the degree of reinforcement

Figure 10.8 shows, that the effect of the axial load on the load carrying capacity is pronounced for low degrees of reinforcement.

The influence of the slenderness ratio is illustrated for one degree of reinforcement (Φ_0 = 0.05) in Figure 10.9.
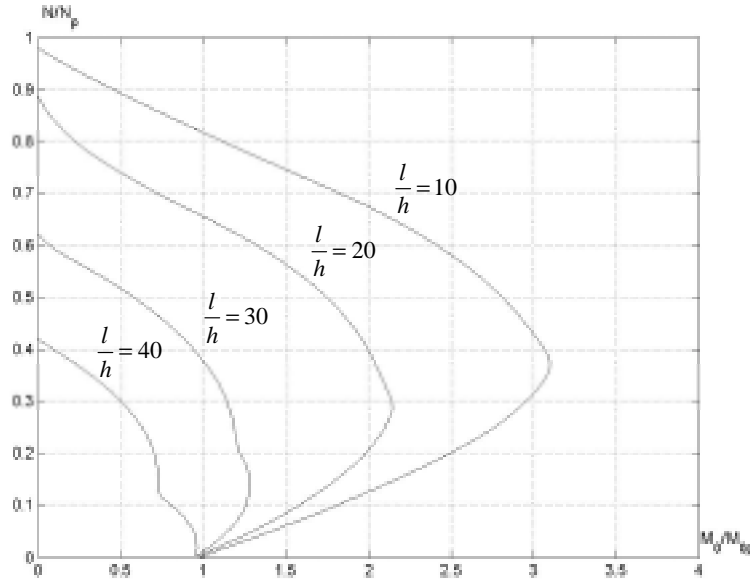
Figure 10.9 Influence of the slenderness ratio

Figure 10.9 shows, that the additional load carrying capacity due to the reinforcement is influenced a great deal by the slenderness ratio. A radical change in shape occurs, when the beam-column becomes slender (in the example for l/h = 30). The curves have a discontinuity in slope and they become non-convex. This phenomenon is due to a large change in the curvature for a small change in axial load. These large changes are illustrated in Figure 10.10 showing the maximum curvature as a function of the axial load for the same values of l/h as in Figure 10.9.

f_y=500 MPa, $\Phi_0 = 0.1$
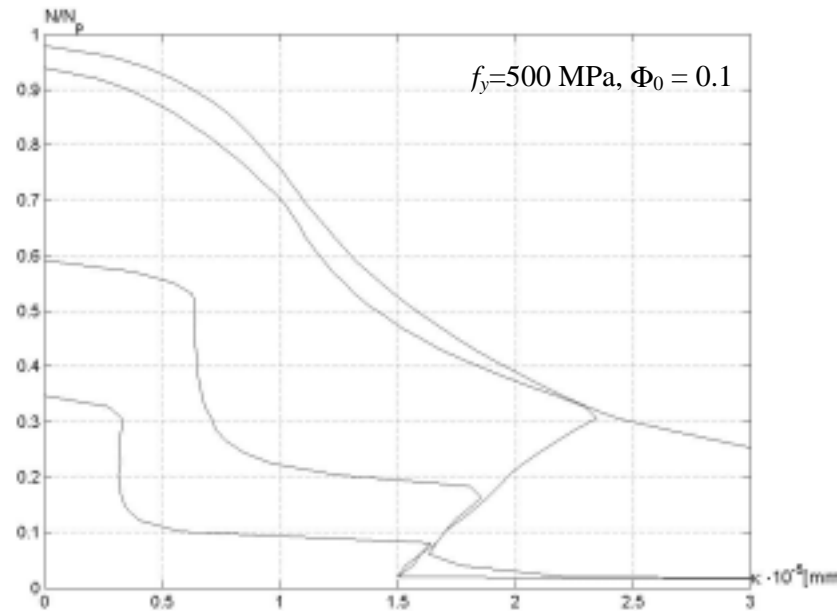
Figure 10.10 Maximum curvature versus axial load.

Large changes of curvature for small changes in the axial load may be understood by studying the moment-curvature relationship. Obviously, the phenomenon gets more pronounced for slender beam-columns. For slender beam-columns, the axial load is small, since the critical load is small. For small values of N the moment-curvature relationship has two points where the shape changes abruptly, see Figure 10.11. This takes place when we go from case 37 to case 31 and from case 31 to a case where the reinforcement yields.
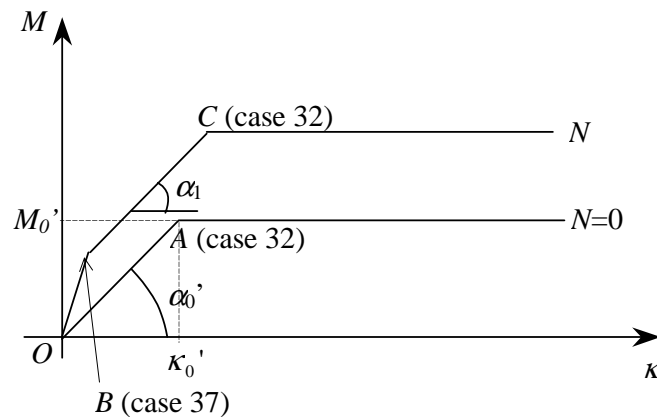
Figure 10.11 Schematical illustration of the moment-curvature relationship

For small values of N, the slope of the straight line OA valid for $N = 0$ is almost the same as the slope of the straight line BC. The real curve only deviates a little from a straight line, which means that the straight line $M=M_0 + Nu$ may be tangent to almost identical moment-curvature relationships at two very different points (κ, M). This is why a jump in the maximum moment and the corresponding curvature may be expected for small values of N.

Since OA and BC as stated above has almost the same slope, the level of axial load where the interaction curve changes shape may be found by equation (10.4).

$$\frac{N \cdot l^2}{\alpha} = \frac{M_0{}'}{\kappa_0{}'}$$
(10.4)

where the meaning of $M_0{}'$ and $\kappa_0{}'$ is explained in Figure 10.11.

The corresponding moment may be obtained from the cross-section analysis corresponding to C in Figure 10.11. This analysis is only valid for slender columns since for short columns the straight line approximation (OA) is no longer valid.

The criterion for a beam-column to be short is that the N level found from equation (10.4) is larger than the N level found for case 36 where the top and bottom reinforcement are yielding (the case may depend on the amount of reinforcement). On the other hand, if a beam-column is slender the N-level found from equation (10.4) has to be smaller than the N level found for case 36.

10.3.2 Linear elastic material behaviour

In this section calculations by a simple linear elastic method and the method used in the Danish code of Practice DS414 is presented. The two methods also comprise nine different cases.
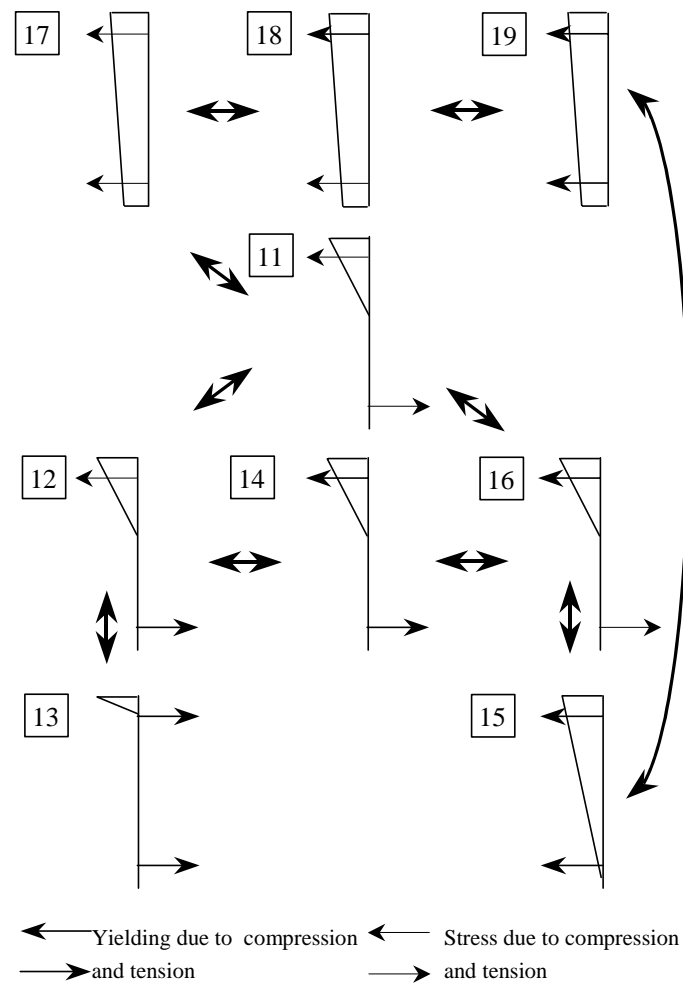
Figure 10.12 Cross-section analysis used in the linear elastic method

10.3.2.1 Linear elastic material

The masonry is assumed to reach its compressive strength f_{cm} at a strain $\varepsilon_{cmy} = f_{cm}/E_0{}^*$. In the interval where the stress goes from zero to f_{cm} the variation is linear as shown in Figure 10.13.
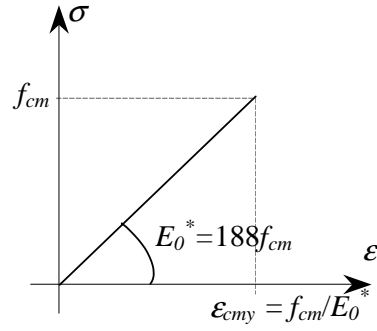
Figure 10.13. Linear elastic material behaviour

The moment-curvature relation for the linear elastic method is obtained in a similar way as in the previous section and results are shown in Figure 10.14.
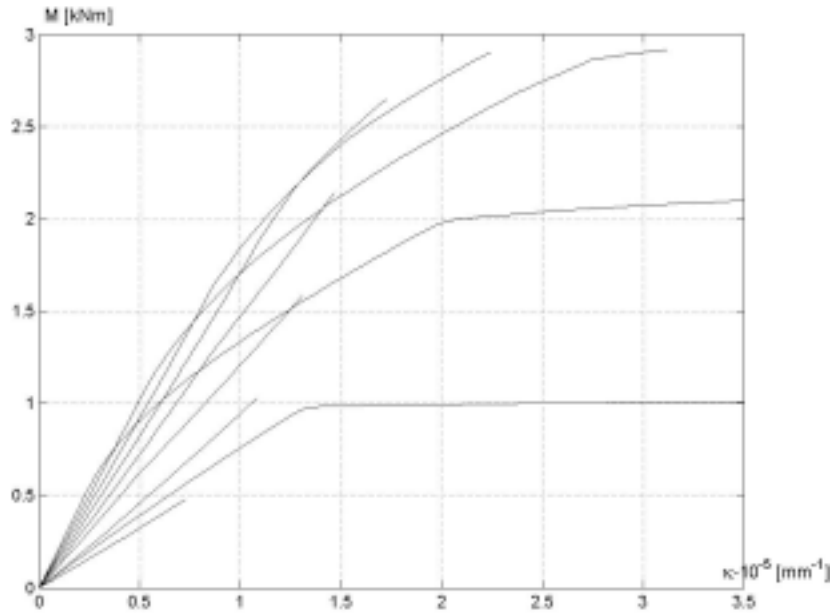
Figure 10.14 Moment-curvature relation using the linear elastic model

10.3.2.2DS414 method B

The masonry is assumed to reach its compressive strength f_{cm}^* at a strain $\varepsilon_{cmy} = f_{cm}^*/E_0^*$. In the interval where the stress goes from zero to f_{cm}^* the variation is linear as shown in Figure 10.15.
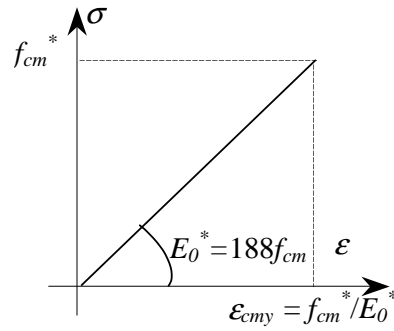
Figure 10.15. Linear elastic material behaviour used in DS414 method B

The moment-curvature relation for method B is obtained as before. However, the calculation of the deflection must be changed so the non-linear material behaviour is taken into consideration.

The Danish code, DS414, prescribes a stiffness that declines with the stress level as seen in equation (10.5).

$$E_{\sigma} = E_{0cr}\left(1 - 0,4\frac{\sigma_{cm,\max}}{f_{cm}} - 0,6\frac{\sigma_{cm,\min}}{f_{cm}}\right) \tag{10.5}$$

where $\sigma_{cm,\max}$ and $\sigma_{cm,,\min}$ are the maximum and minimum stresses in the masonry, respectively, and $E_{0cr} = 375f_{cm}$ in case of Danish masonry. If the cross-section is cracked $\sigma_{cm,,\min} = 0$.

The maximum stress in the masonry is determined by

$$f_{cm}^{*} = \begin{cases} 1,25f_{cm} \\ 1,25f_{cm}\left(1 - 0,2\dfrac{\sigma_{cm,\min}}{f_{cm}}\right) \end{cases} \tag{10.6}$$

The moment-curvature diagrams obtained from these calculations are shown in Figure 10.16.
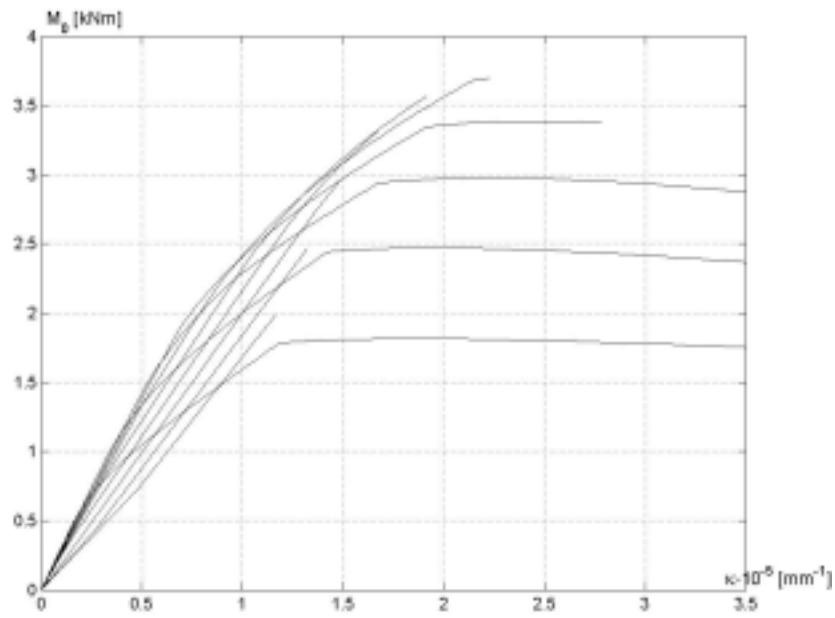
Figure 10.16 Moment-curvature relation using DS414 method B

10.3.3 Comparison of calculation methods

In this section the three methods are compared in an interaction diagram, see Figure 10.17
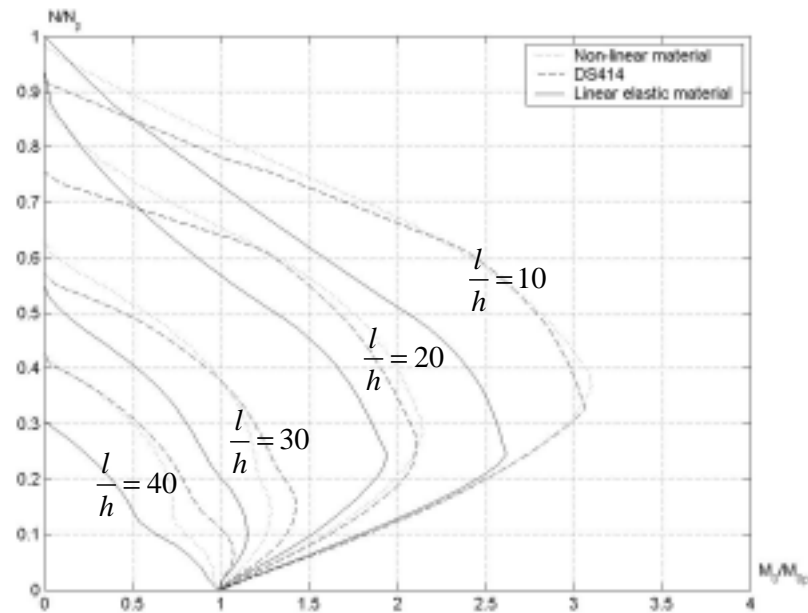
Figure 10.17 The influence of the slenderness ratio

As seen from Figure 10.17 the method of DS414 gives similar results as the method using a parabolic material behaviour. Further, the figure shows that the linear elastic model is conservative compared with the other methods.

10.3.4 DS414 Method A

In the Danish code of practice, DS414, another calculation method is described. The method is based on a cross-section analysis as outlined in Figure 10.18.
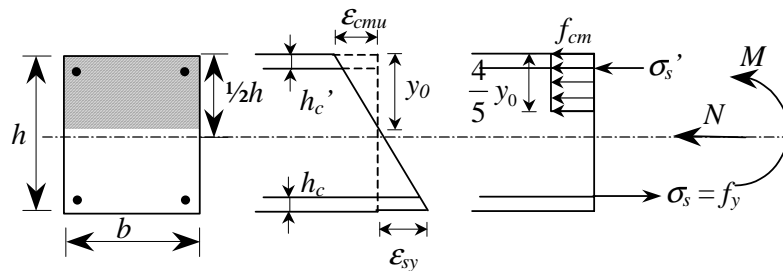
Figure 10.18 Cross section analysis, DS414, method A

The curvature is calculated from the strain diagram, i.e.:

$$\kappa = \frac{\varepsilon_{cmu} + \varepsilon_{sy}}{h} \tag{10.7}$$

where the maximum strain, ε_{cmu}, is equal to 3.5 $^0/_{00}$ according to DS414.

Thereby the deflection may be calculated in the normal way by $u = \frac{1}{\alpha}\kappa l^2$. However, the value of the maximum strain is questionable, since it is not related to the stress-strain relation of Danish masonry.
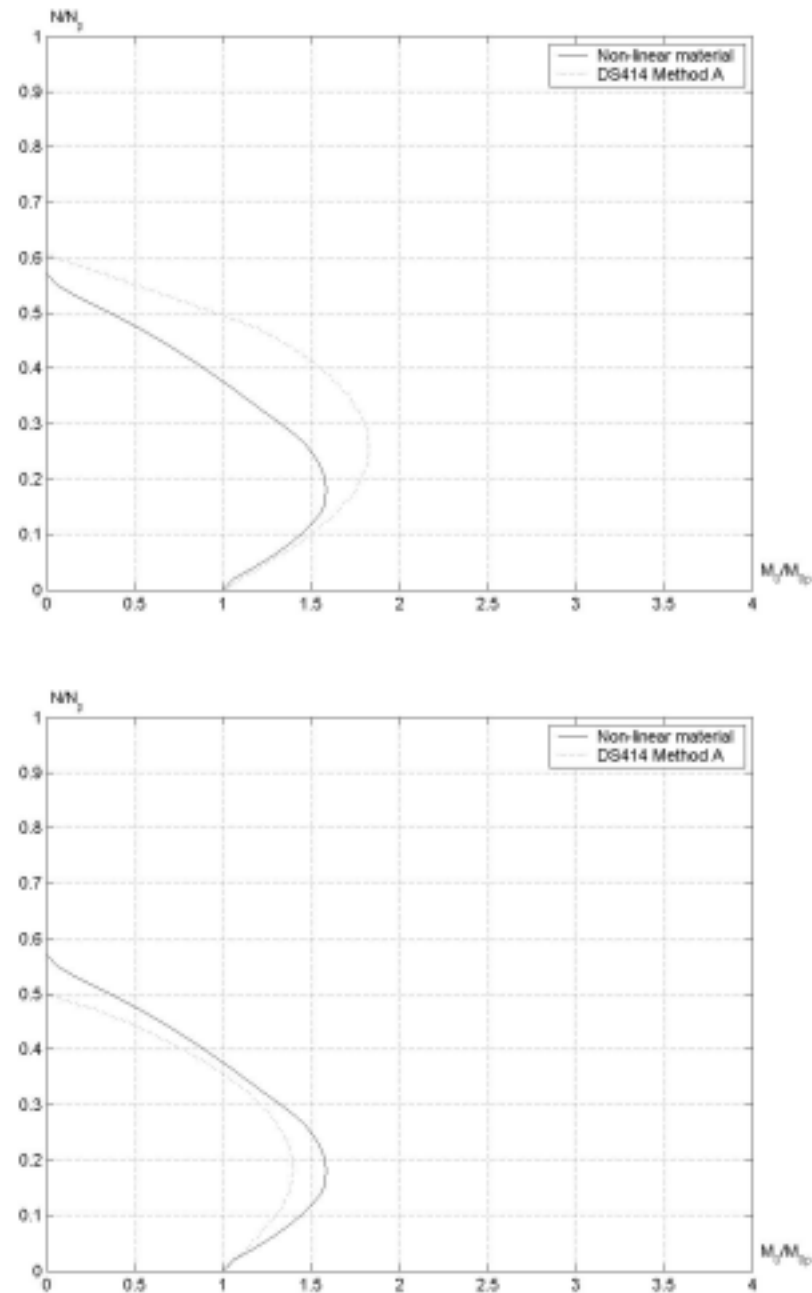
Figure 10.19 Interaction diagram comparing DS414 method A with calculations made by assuming non-linear material behaviour

In Figure 10.19, interaction diagrams for reinforced masonry beam-columns are shown. The deflection is calculated according to DS414 in the diagram at the top and at the

bottom diagram the deflection is calculated for a maximum strain equal to $\varepsilon_{cmy} = 5.33$ $^0\!/_{00}$.

Figure 10.19 shows that DS414 method A provides results, which, compared with calculations based on a parabolic stress-strain relation, overestimates the load carrying capacity. If the maximum strain is adjusted to the stress-strain relation of Danish masonry, it is seen that the methods provide almost similar results.

10.4 Practical calculation procedure

10.4.1 Simplified interaction diagram

A simple method for calculating the load carrying capacity of reinforced masonry beam-columns may be developed from the investigations made in the previous sections. This section describes a simple way of constructing an interaction diagram between the axial load and the additional moment on the beam-column. The simplified interaction diagram may be constructed from 3-4 cross-section analyses shown in Figure 10.20. In this figure, five cross-section analyses are outlined because B and E may substitute each other.

The cross-section analyses are as follows:

A: Pure bending, where the strain in the masonry is either equal to 3.5 $^0\!/_{00}$ or 6.8 $^0\!/_{00}$ in case of Danish masonry and where the stress in the masonry equals f_{cm}. The stress is constant over the stress block.

B: Bending with axial load, otherwise the same as A.

C: Compression in the entire cross-section, where the stress in the bottom face is zero and the maximum stress at the top face is 1.25 f_{cm}.

D: Bending with axial load, where the masonry is calculated as linear elastic and cracked and where the bottom reinforcement yields.

E: Bending with axial load. The masonry is assumed linear elastic with a maximum stress equal to 1.25 f_{cm} in the masonry and yielding in the bottom reinforcement.

In B and E, the top reinforcement might also yield for certain reinforcement ratios and yield strengths. B and E are cases characterising the top point of the interaction diagram in the case of short beam-columns.

I all the cross-section analyses assuming linear elastic material behaviour the modulus of elasticity is equal to the secant modulus, i.e. $500 f_{cm}$ or $188 \, f_{cm}$ in the case of Danish masonry.

The five situations are illustrated in Figure 10.20.
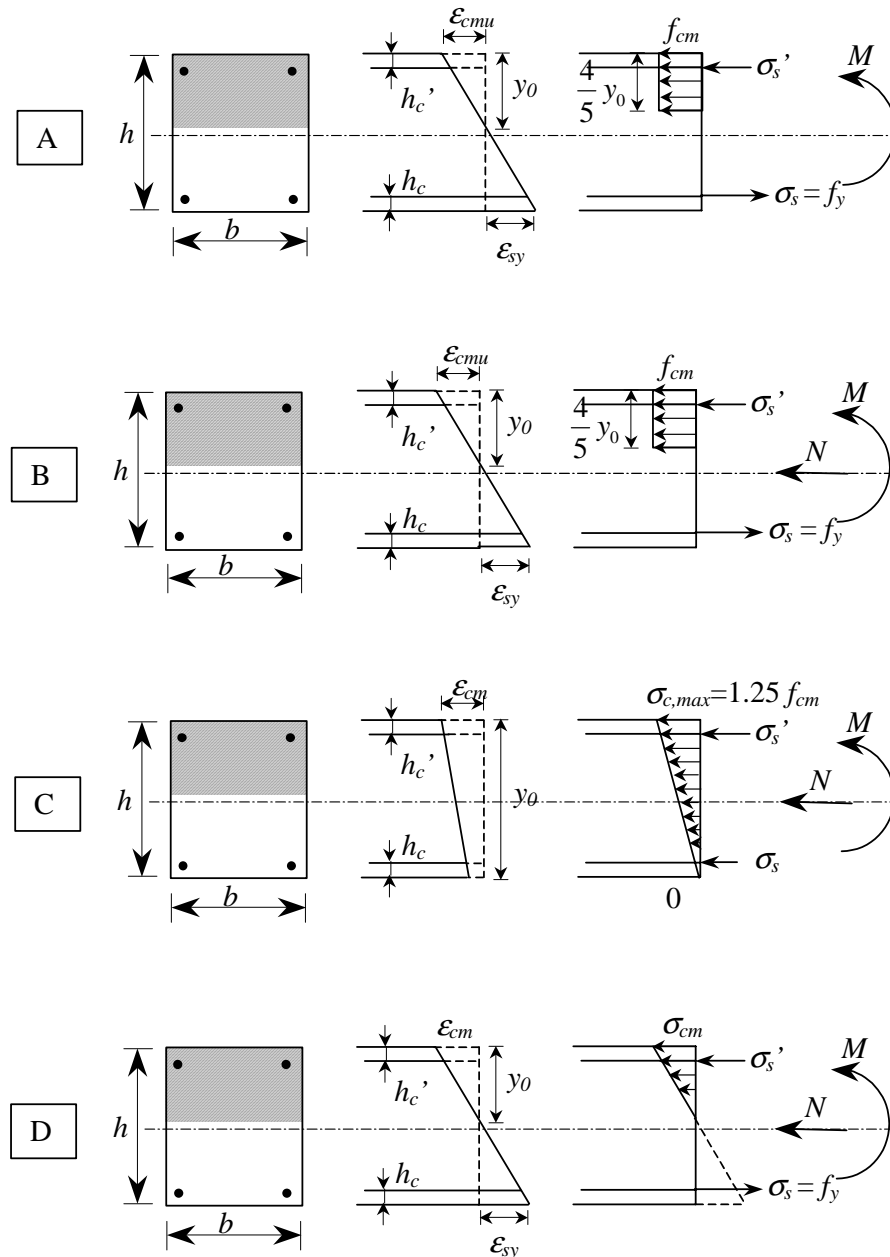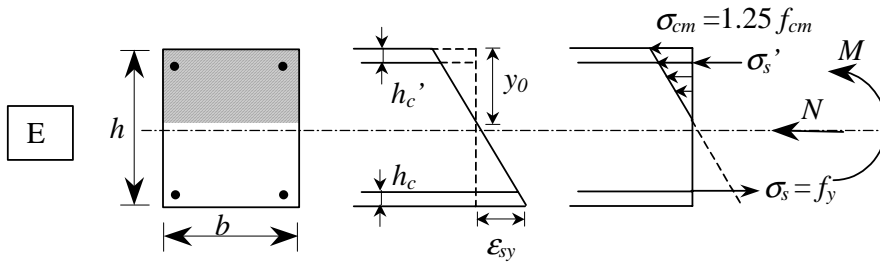
Figure 10.20 Cross-section analysis used to estimate the interaction curve between the simple moment and the axial load.

10.4.1.1 The calculation procedure

a. Determine the critical load by use of Ritter's equation for the critical stress.

b. Calculate the moment, simple moment and curvature from cross-section analysis D without N and determine N_i (see equation below).

c. Calculate the maximum M, N combination from cross-section analysis B or E and determine if the column is slender or short.

d. If the column is short, calculate the point obtained from C; plot this together with A, B or E and the critical load in an interaction diagram.

e. If the column is slender, calculate the point obtained from cross-section analysis D and plot this together with the point obtained from A and the critical load in an interaction diagram.

Re 1.

The critical stress determined by the Ritter equation is

$$\sigma_{cr} = \frac{f_c}{1 + \dfrac{f_c}{\pi^2 E_{0cr}}\left(\dfrac{l}{i}\right)^2}$$

where in the case of Danish masonry

$$E_{0cr} = 375 f_{cm}$$

The maximum axial load is determined by:

$$N_{cr} = \min \begin{cases} \sigma_{cr} A_c \cdot (1 + n \cdot \varphi) \\ \sigma_{cr} A_c + A_s \cdot f_y \end{cases}$$

Re 2.

Calculate $M_{D,N=0}$ and $\kappa_{D,N=0}$ from cross section analysis D when $N = 0$.

Calculate the N level N_i from the equation:

$$N_i = \frac{M_{D,N=0}}{\kappa_{D,N=0}} \frac{\alpha}{l^2}$$

Re 3.

Calculate the N, M_0 -combination from cross-section analysis B or E

If $N_i > N$ from B or E then the column is short

If $N_i < N$ from B or E then the column is slender

Point 4 and 5 do not require any more comments.

10.4.1.2 Interaction diagrams compared with theory

In this section, the simple procedure outlined in the previous section is compared with calculations using the parabolic stress-strain relation. First, the results for short columns will be shown and then the results for slender columns.

In the calculations, the parameters shown in Table 10.3 are used together with a maximum strain equal to 3.5 $^0/_{00}$. For the short columns the slenderness ratio is varied between:

$$5 \le \frac{l}{h} \le 30$$

For slender columns the slenderness ratio is varied within:

$$30 \le \frac{l}{h} \le 60$$

b	h	h_c	l	f_{cm}	ε_{cmy}	f_y	Φ_0
[mm]	[mm]	[mm]	[mm]	[MPa]	[‰]	[MPa]	[]
250	250	20	3000	30	2	300	0.1

Table 10.3. Data used when otherwise not stated
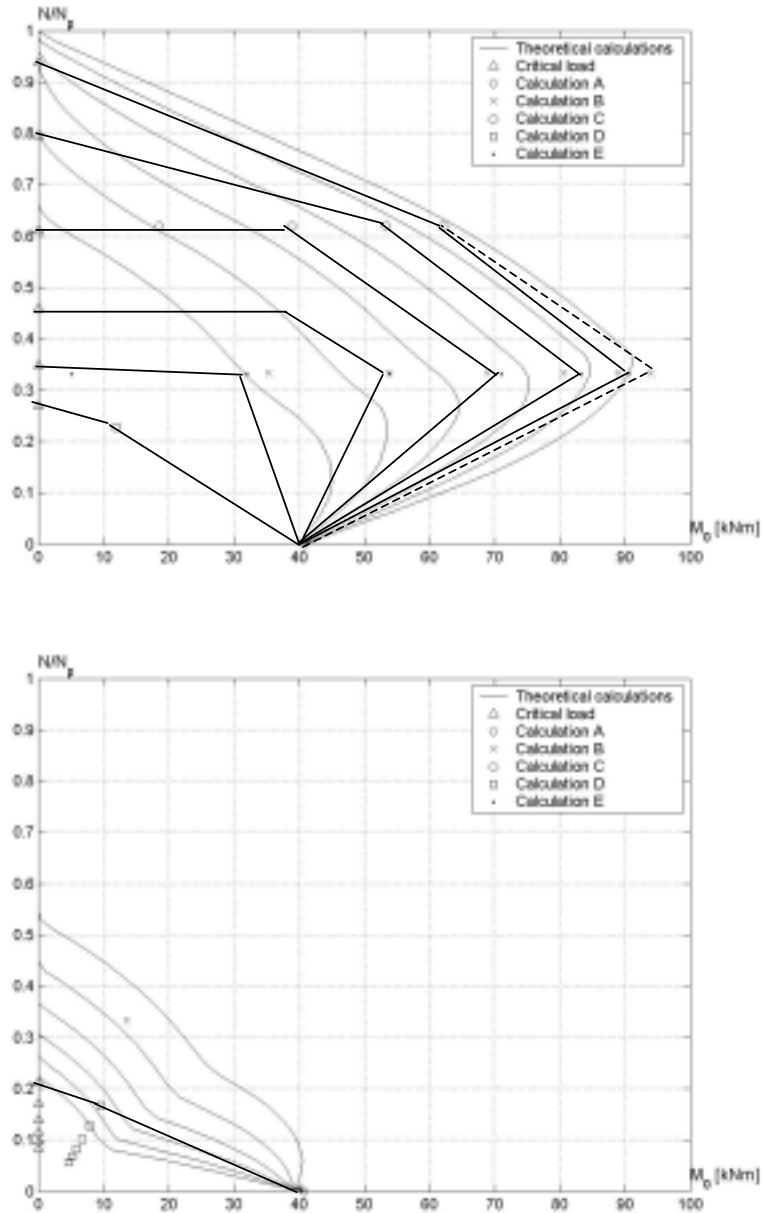
Figure 10.21 Interaction diagrams for short columns

In Figure 10.21, the solid straight line represents the simplified interaction diagram using the case E points and the broken straight line represents the simplified interaction diagram using the case B point as the top point. The curves illustrates that the simplifications made underestimate the load carrying capacity in the case of slender beam-columns. The reason is the applied value of the stiffness of the masonry. Since the stresses in the masonry are small for slender beam-columns, the stiffness is closer to the initial stiffness than to the secant stiffness.

11 Comparison with experiments

11.1 Introduction

In this section, experiments with unreinforced and reinforced masonry will be compared with the theories outlined in the previous sections.

11.2 Unreinforced masonry

This section compares the calculation methods for unreinforced masonry with experiments collected from the literature. In the case of investigations made in other countries than Denmark, a model similar to the one suggested in DS/ENV, 1996-1-1, [44], is used, see Figure 11.1. This model is similar to the one used for concrete and similar to the stress-strain relations suggested in [38].
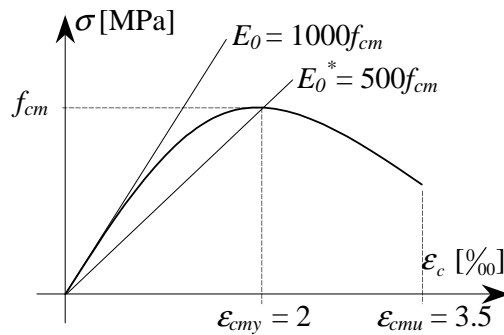
Figure 11.1 Parabolic model used for non-Danish masonry

The stiffness $E_0{}^*$ will be used in the linear elastic model and the modified linear elastic model.

In the case of Danish masonry the constitutive equations are formulated in the way explained in section 7.2 and section 9.3.1.1.

11.2.1 Investigations used in the comparisons

Rambøll, B. J., Clarbo, O. & Manniche, K. 1953 [19]

The experimental investigation made by Rambøll et. al. consists of 76 masonry wall columns, 44 of which were made using the same stone through the entire wall. This was "Flamme" stone (F), "Moler" stone (M), "Gasbeton" stone (G) and "Klinkerbeton" stone (K). The rest was made with "Flamme" stone on one side and another type of brick on the other side. The walls were all 1½ brick thick, 0.85 m wide, 2.6 m high and simply supported at both ends. The bricks were laid in English bond. Furthermore, 84 quadratic piers (1½ brick in side length and with a height of 1.2 m) were tested. The walls and piers were tested under three eccentricities. Three types of mortars were used, a lime mortar (7.5 % $Ca(OH)_2$ from Kjøbenhavns Mørtelværker A/S), a lime cement mortar (C:L = 1:2 by weight) and a pure cement mortar (C:S = 1:3 by weight). Measurements of the compressive strength of bricks, mortar and masonry were carried out. Measurements of the flexural strength of the mortar were also recorded. The relevant data for this investigation can be seen in section 14.1.1.

Report 9 1965 Structural Clay Product Research Foundation [21]

The experimental investigation in Report 9 from Structural Clay Product Research Foundation consists of 40 wall columns and 15 transversely loaded walls without precompression. The transverse load was applied by an air bag. The wall thickness was equal to the width of a brick. The bricks used had three holes with a diameter of 35 mm. The size of the bricks was 57 mm, 92 mm and 206 mm (height, width and length). The compressive strength of the bricks covered a span of 27 different types of bricks, which means that a high (111 MPa), mean (73.9 MPa) and low (43.5 MPa) strength brick was used. These are labelled H, M and L respectively. The mortar was a 1:½:4½ mortar (C:L:S) measured by volume. Water was added to the mix to produce workability

suitable for the mason. The tensile strength was also measured together with the flexural strength. The relevant data for this investigation can be seen in section 14.1.2.

Report 10 1966 Structural Clay Product Research Foundation [22]

The experimental investigation reported in Report 10 from Structural Clay Product Research Foundation consists of 35 wall columns and 10 transversely loaded walls without precompression. The transverse load was applied by an air bag. The wall thickness was equal to the length of a brick. The bricks used had three holes with a diameter of 35 mm. The size of the bricks was 57 mm, 92 mm and 206 mm (height, width and length). The compressive strength of the brick was kept constant equal to 73.9 MPa like the medium brick in Report 9. The walls were built as two walls with the thickness equal to the width of the brick and then they were held together with either metal ties for each 7 course or in one case with brick headers, which means that for each 7 course the bricks were turned 90 degrees. The mortar was a 1:½:4½ mortar (C:L:S) measured by volume. Water was added to the mix to produce workability suitable for the mason. The relevant data for this investigation can be seen in section 14.1.3.

Grenley, D. G, Cattaneo, L. E. & Pfrang, E. O. 1969 [26]

The scope of this investigation is to investigate the interaction between the axial load and the transverse load. 39 one-way walls were prepared. The walls were built in running bond. Three different types of bricks were used: A, B and S. The initial rate of absorption was 6.2 g, 2.6 g and 19.8 g per minute of suction for the A, B and S brick, respectively. Two different types of mortar were used, a conventional mortar and a high-bond mortar. The mix was 94 lb cement, 50 lb of lime and 360 lb of washed sand in the case of conventional mortar. In the case of the high bond mortar the contents of cement, lime and sand was the same but four gallons of liquid additive was added. The relevant data for this investigation can be seen in section 14.2.1.

Yokel, F. Y. , Mathey, R. G. and Dikkers, R. D. 1971 [28]

The experimental investigation made by Yokel et. al. consists of 36 transversely and axially loaded tests. Three different bricks were used A, B and S. The two first ones were perforated bricks and that last one was a solid brick. The compressive strength was

measured to 100 MPa, 142 MPa and 121 MPa, respectively. The IRA was measured to 0.32, 0.13 and 1 kg/m^2/min, respectively. The mortars used were 1:1:4 and the high bond mortar was also a 1:1:4 mortar. In the latter additives were added (poly vinylidene chloride named sarabond). The compressive strength of the mortar was 33.9 MPa. The strength of the normal 1:1:4 mortar was not reported. The relevant data for this investigation can be seen in section 14.2.2

Hasan, S. S. & Hendry, A. W. 1976 [31]

The investigation made by Hasan, S. S. and Hendry, A. W. consists of 72 wall columns, 48 concentrically loaded and 24 eccentrically loaded. The bricks used were third scale bricks. The mortar used was a 1:3 cement mortar (C:S). The wall thickness was equal to the width of the brick. The walls had different slenderness ratios varying between 6 and 25. Three different end conditions were used: hinged, flat and fixed ends. This led to a relative reduction in theoretical column length ratio, which was 1, 0.9 and 0.75, respectively. The relevant data for this investigation can be seen in section 14.1.4.

Fattal, S. G. and Gattano, L. E. 1976 [32]

The experimental investigation made by Fattal et. al. consist of 12 eccentrically loaded masonry walls. The bricks used had three holes and a compressive strength of 90.2 MPa. The IRA was measured to 1.09 kg/m^2/min. The mortar used was a 1:½:4½ (C:L:S) mortar, with a compressive strength of 10.4 MPa. The walls were simply supported at both ends. The relevant data for this investigation can be seen in section 14.1.5.

Murværkscenteret 1979 [33]

The experimental investigation made at Murværkscenteret consists of 21 story high wall columns tested together with 21 piers. The walls were built of six different types of bricks. Nine of the walls were built with a Danish "bredsten" (52mm x 168mm x 228 mm) and the rest with a normal size Danish brick (52mm x 108mm x 228 mm). The bricks selected were a weak brick, a strong brick and one in between. All of the bricks had several holes as illustrated in Figure 11.2. The wall columns were all simply

supported at both ends and those made of normal size brick were built in English bond so the wall thickness was 1/1 stone (228 mm).
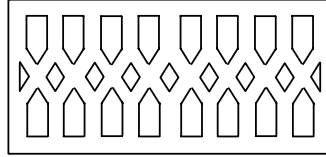
Figure 11.2 Example of a Danish brick with several holes.

The initial rate of absorption was in the interval from 3.6 –5.0, kg/m^2/min, measured according to the Danish code. Two different mortars were used. Both were cement lime mortars; the mix was C/L/S 50/50/750 and 20/80/550, respectively. The content of cement, lime and sand is by weight. The relevant data for this investigation can be seen in section 14.1.5.

Kalk og teglværkslaboratoriet 1984 [36]

The experimental investigation made at Kalk og teglværkslaboratoriet consists of 17 wall columns. The walls varied in height from 1600 mm to 4600 mm. The walls were built of one type of brick. The brick used were a massive normal size Danish brick (52mm x 108mm x 228 mm) with an initial rate of absorption of 1.5 kg/m^2/min and a compressive strength of 28.7 MPa.

Thirteen of the walls were built with 71 brick headers per m^2, two with 21 brick headers per m^2 and two with 16 metal ties per m^2. The wall columns were all simply supported in both ends. Two different mortars were used. Both were cement lime mortars with the mix C/L/S 50/50/750 and 20/80/550, respectively. The content of cement, lime and sand is by weight. The important data for this investigation can be seen in section 14.1.7.

The mean value (μ) and standard deviation (s) are calculated for each series. The results are shown in Table 11.1, where 1 indicates calculations according to a parabolic stress-strain relation, 2 indicates calculations according to a linear elastic stress-strain relation, 3 indicates calculations according to the modified linear elastic model and 4 indicates calculations according to DS414.

Investigation	Number of tests		1	2	3	4
Rambøll, B. J., Clarbo, O. & Manniche, K. 1953 [19]	40	μ	1.24	1.48	1.29	1.57
		s	0.27	0.31	0.28	0.35
Report 9 1965 [21]	39	μ	0.97		1.14	1.27
		s	0.18		0.22	0.24
Report 10 1966 [22]	39	μ	0.90		0.97	1.08
		s	0.26		0.29	0.32
Grenley, D. G, Cattaneo, L. E. & Pfrang, E. O. 1969 [26]	39	μ	0.97	1.33	1.11	
		s	0.29	0.44	0.38	
Yokel, F. Y. , Mathey, R. G. and Dikkers, R. D. 1971 [28]	35	μ	1.31	1.87	1.42	
		s	0.82	1.61	0.88	
Hasan, S. S. & Hendry, A. W. 1976 [31]	72	μ	1.01	1.19	1.13	1.72
		s	0.1	0.33	0.35	0.5
Fattal, S. G. and Gattano, L. E. 1976 [32]	10	μ	1.06	1.54	1.14	1.70
		s	0.20	0.52	0.24	0.34
Murværkscenteret 1979 [33]	18	μ	0.74		0.99	1.10
		s	0.11		0.13	0.15
Kalk og teglværks-laboratoriet 1984 [36]	15	μ	0.97	1.28	1.02	1.26
		s	0.14	0.34	0.16	0.18
Total	307					
Centrically/Eccentrically loaded	233					
Laterally loaded	74					

Table 11.1 Mean value and standard deviation for different constitutive equations

In the case of Danish masonry, the correlation is best for method 3 (the modified linear elastic calculation method). The mean value and standard deviation in the other comparisons have to be taken with some caution since a correct constitutive equation is not available. Problems of this kind seem to be particularly present in the investigations, which are hatched in Table 11.1.

11.2.2 Interaction diagrams

11.2.2.1 Concentrically loaded columns and one-way walls

a

b

c
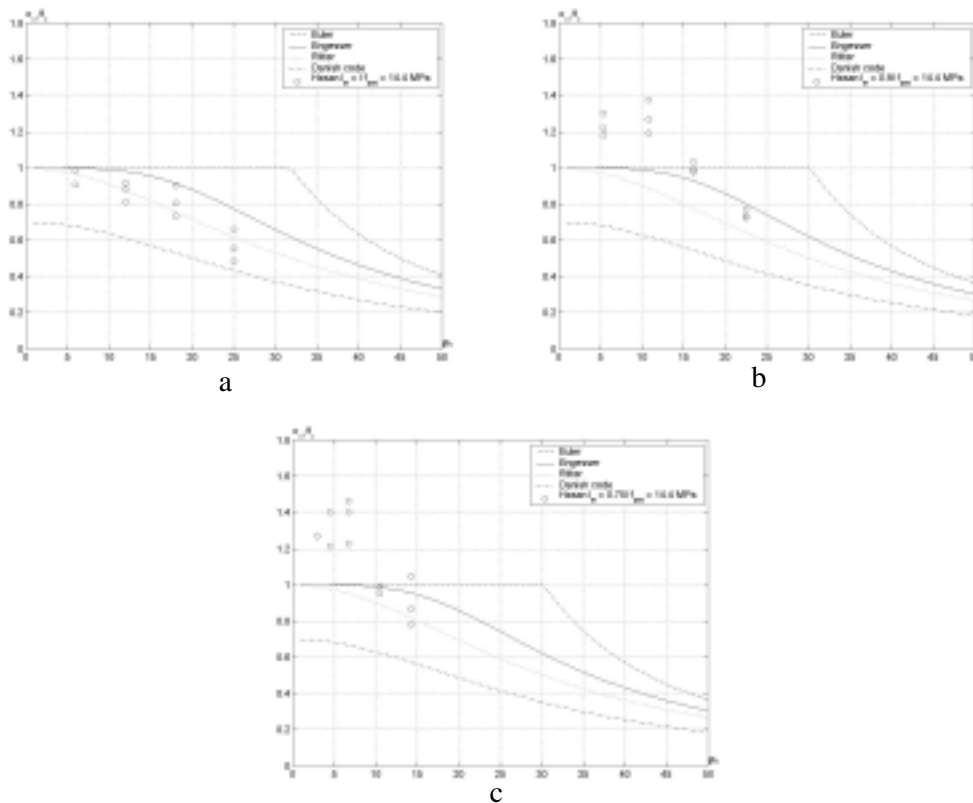
Figure 11.3 Results on columns with different end conditions

In Figure 11.3, load carrying capacity diagrams for three different end conditions are illustrated. The investigation is due to Hasan, S. S. and Hendry, A. W. [31]. Figure 11.3a deals with simply supported columns, Figure 11.3b with columns tested on flat ends and Figure 11.3c with rigidly supported columns. The diagrams indicate that the experiments with simply supported columns fit the Ritter equation. In the case of flat

end supports and rigid supports the test results do not fit as well for small slenderness ratios. This may be due to the support conditions where membrane action may be introduced.

In Figure 11.4 a comparison between Ritter's equation and all column experiments are shown. The agreement is seen to be good.
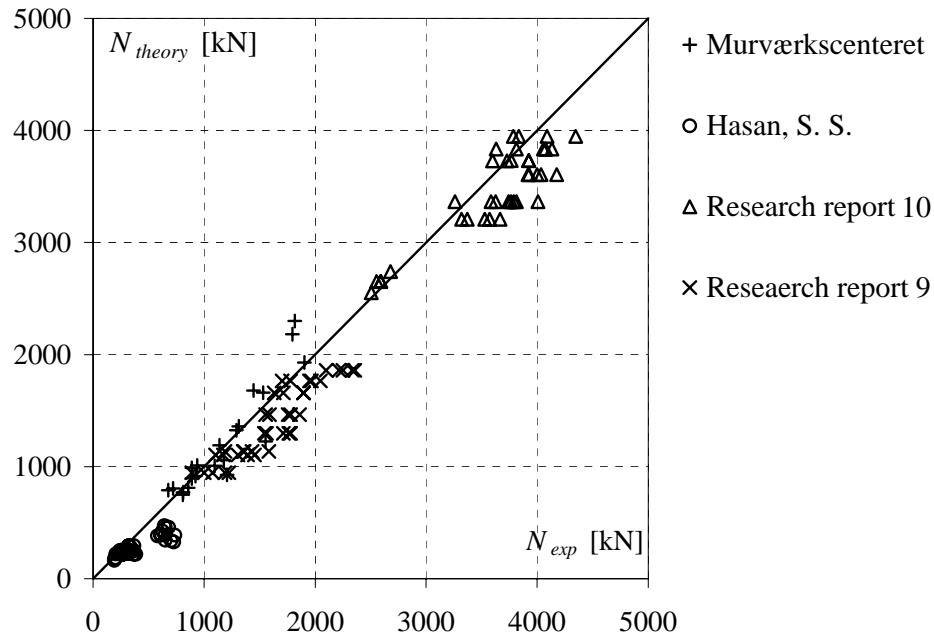
Figure 11.4 Ritter's equation compared with experiments

11.2.2.2 Eccentrically loaded columns and one-way walls

In Figure 11.5-Figure 11.6 the results from the investigation reported in [31] is shown.
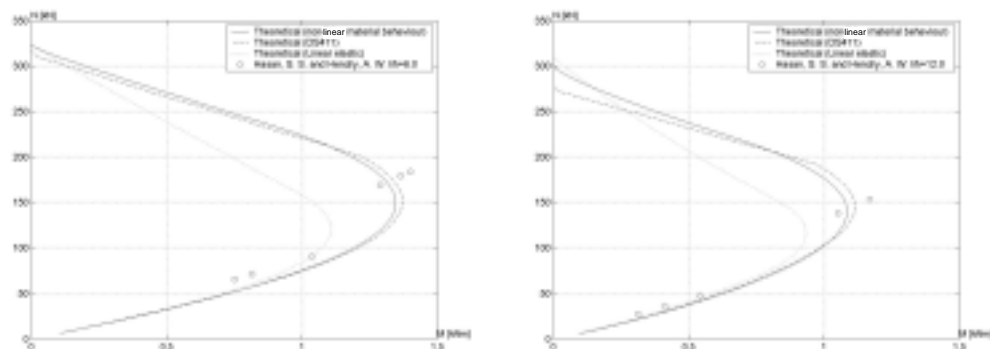
Figure 11.5 Results of tests shown in an interaction diagrams valid for *l/h* = 6.0 and *l/h* = 12.0
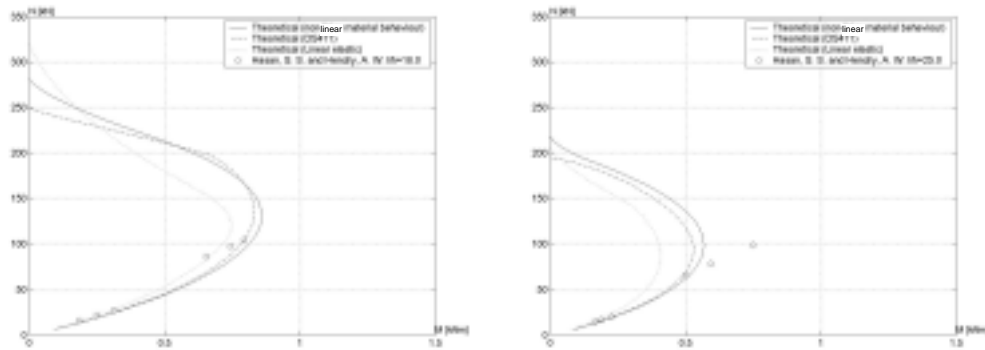
Figure 11.6 Results of tests shown in a interaction diagrams valid for *l/h* = 18.0 and *l/h* = 25.0

Interaction diagrams like the ones shown above may be found in Chapter 10.

The interaction diagrams show that the modified linear elastic model provides good agreement with experiments.

In Figure 11.7, all experiments collected from the literature are compared with calculations made by the modified linear elastic model.
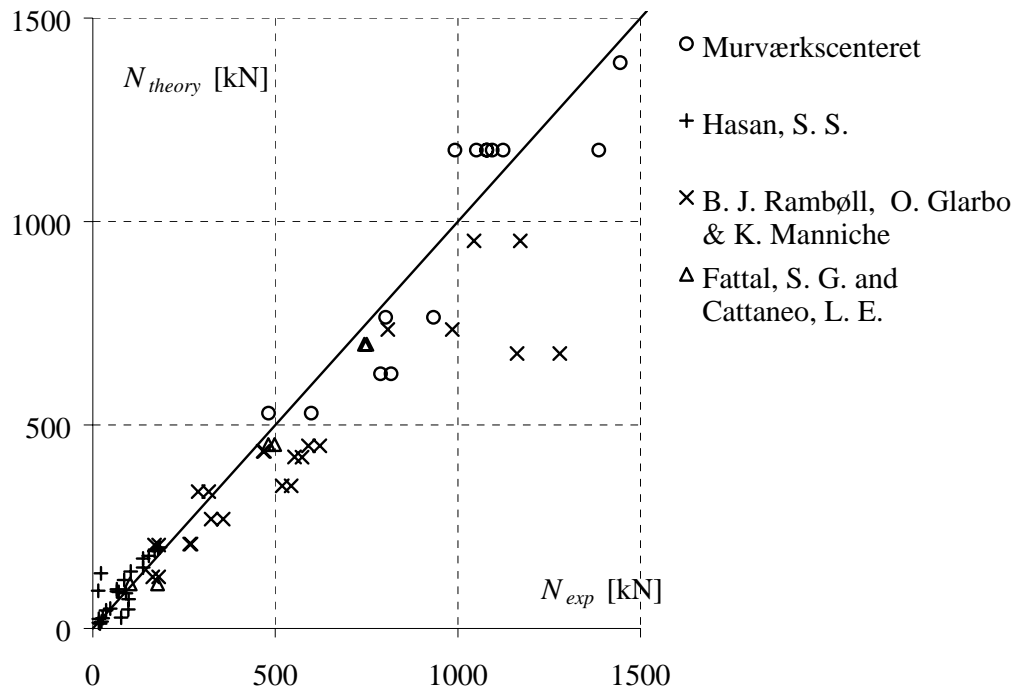
Figure 11.7 Modified linear elastic theory compared with experiments

The correlation is seen to be good.

11.2.2.3 Laterally and concentrically loaded one-way walls

In Figure 11.8 results taken from Grenley, G, A et. al. and Yokel, F. Y. et. al. are shown. It is seen that a linear elastic prediction is conservative.
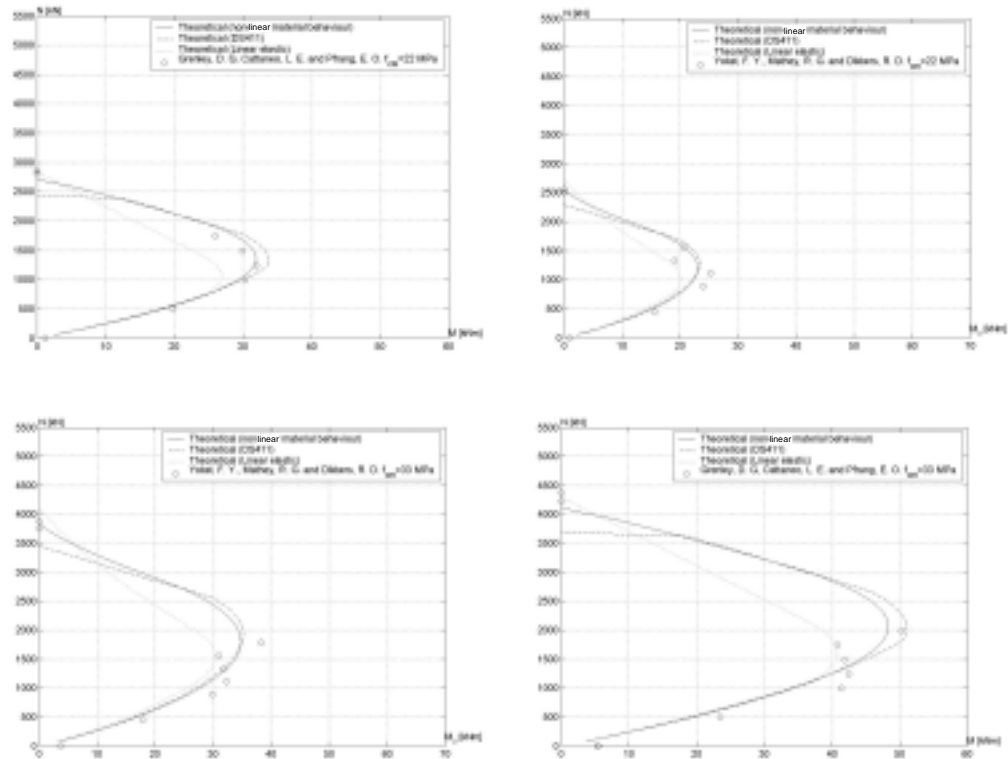
Figure 11.8 Results of tests reported in [26] and [28] shown in interaction diagrams

Further, it is seen that the results have a large scatter. The modified linear elastic calculation method seems to fit best to the results. In Figure 11.9, this method is compared with all the tests available from the literature.
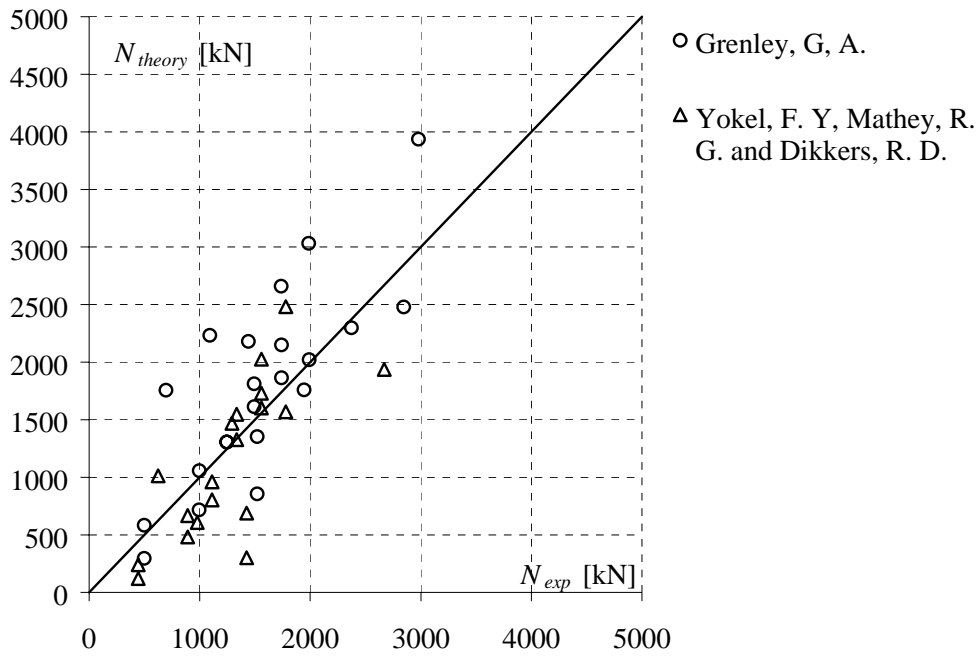
Figure 11.9 Linear elastic theory compared with experiments

11.2.2.4 Laterally loaded one-way walls

The comparisons for laterally loaded masonry are based on experiments reported in [21] and [22].
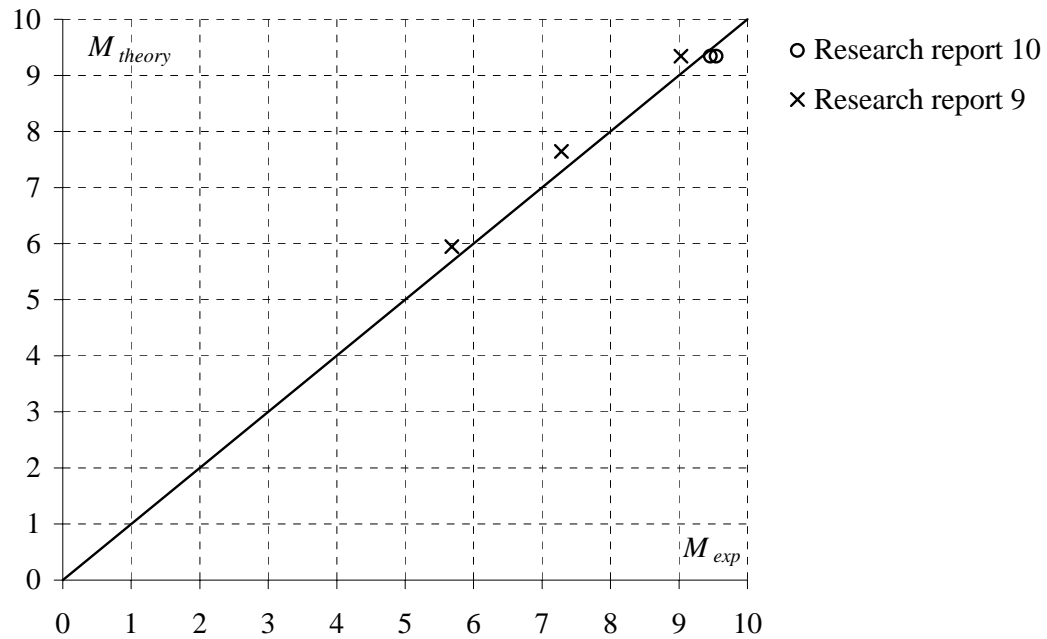
Figure 11.10 Results of the theory in section 9.3.6 compared with experiments

However, it must be noted that the gravity of the bricks and the mortar have not been reported. Nevertheless, if the gravity for the specimens reported in [22] is set to 22 kN/m^2 and for the specimens reported in [21] to 22, 18, 14 kN/m^2, respectively, the results shown in Figure 11.10 are obtained. The reason why the gravity is varied for the specimens reported in [21] is that the IRA indicates that the bricks have had different densities.

11.3 Reinforced masonry

In this section experiments on reinforced masonry are compared with the theories outlined in Chapter 10. As for unreinforced masonry, the initial stiffness is calculated in different ways. For the tests in [15] the compressive strength of masonry has not been reported and cannot be calculated. Thus, this test series has been disregarded.

11.3.1 Investigations used in the comparisons

Davey, N. & Thomas, F. G. 1949-50 [17]

The experimental investigation made by Davey et. al. dealt with reinforced masonry, where the entire cross-section was of masonry (see Figure 11.11). The piers were prepared on a concrete base and a concrete cap was cast on the top after 7 days. The eccentrical axial load was applied on the concrete cap through a knife-edge. The reinforcement was symmetrically placed as shown in Figure 11.11 and had a diameter of 6.35 mm (~ ¼ inch). The piers were built of Felton bricks with a compressive strength of 21.4 MPa and a 1:¼:3 mortar with a cube strength of 27.6 MPa after 28 days. The relevant data for this investigation can be seen in section 15.1.1.

127 mm
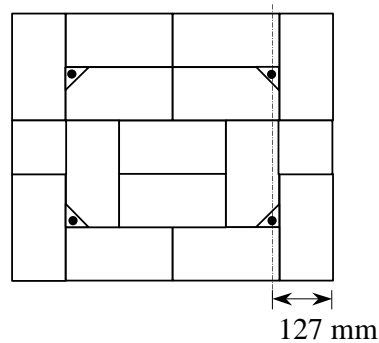
Figure 11.11 Cross-section for the reinforced piers

Anderson, D. E. & Hoffman, E. S. 1969 [27]

The experimental investigation made by Anderson et. al. consists of reinforced masonry piers, where the core was crout (see Figure 11.12). The piers are simply supported in the top and rigidly supported at the bottom. The column length was reported to be 0.75 of the entire length. The bricks used had a compressive strength of 93.1 MPa. The mortar used was an ASTM Type S. The crout had an average compressive strength of 25 MPa. This gave a masonry compressive strength of 36.2 MPa. The reinforcement used were four steel bars with a diameter of 16 mm (~5/8 in ~ #5) and a yield strength of 275.8 MPa. The important data for this investigation can be seen in section 15.1.2.
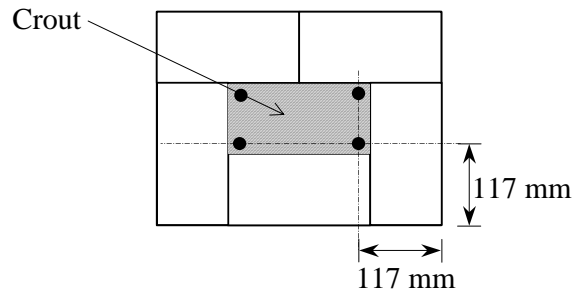
Figure 11.12 Cross-section for the reinforced piers

The mean value (μ) and the standard deviation (s) for calculations using the parabolic stress-strain relation (1), the model used in DS414, method B (2) and the linear elastic model (3) are presented in Table 11.2 for all experiments.

Investigator	Number of tests		1	2	3
Davey, N. & Thomas, F. G. 1949-50 [17]	13	μ	0,82	0,98	0,87
		s	0,08	0,09	0,09
Anderson, D. E. & Hoffman, E. S. 1969 [27]	11	μ	1,16	1,35	1,14
		s	0,15	0,19	0,12
Total	24				

Table 11.2 Mean value and standard deviation for reinforced masonry columns

It is seen that the best correlation is achieved with calculations made according to DS414 method B.

11.3.2 Interaction diagrams

11.3.2.1 Eccentrically loaded columns and one-way slabs

In this section, eccentrically loaded masonry beam-columns are compared with the theories by means of interaction diagrams: The results are shown in Figure 11.13
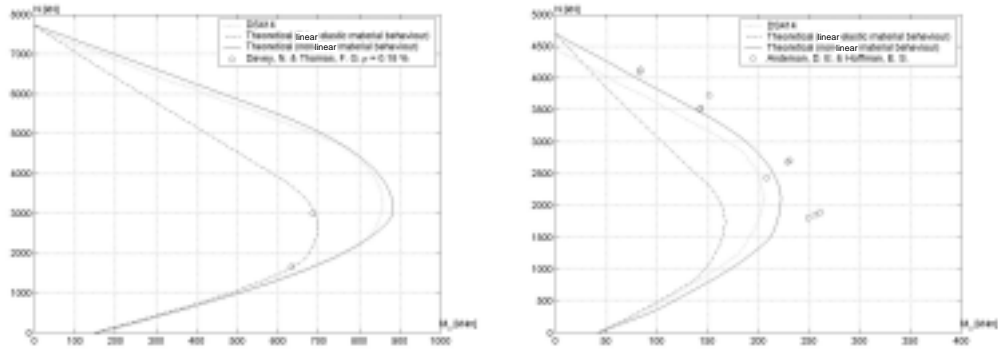
Figure 11.13 Interaction diagrams for reinforced masonry compared with tests from [17] and [27]

The remaining of the interaction diagrams may be found in Chapter 10.

All experiments are plotted in Figure 11.14 together with calculated values using DS414, method B. The agreement is seen to be good.
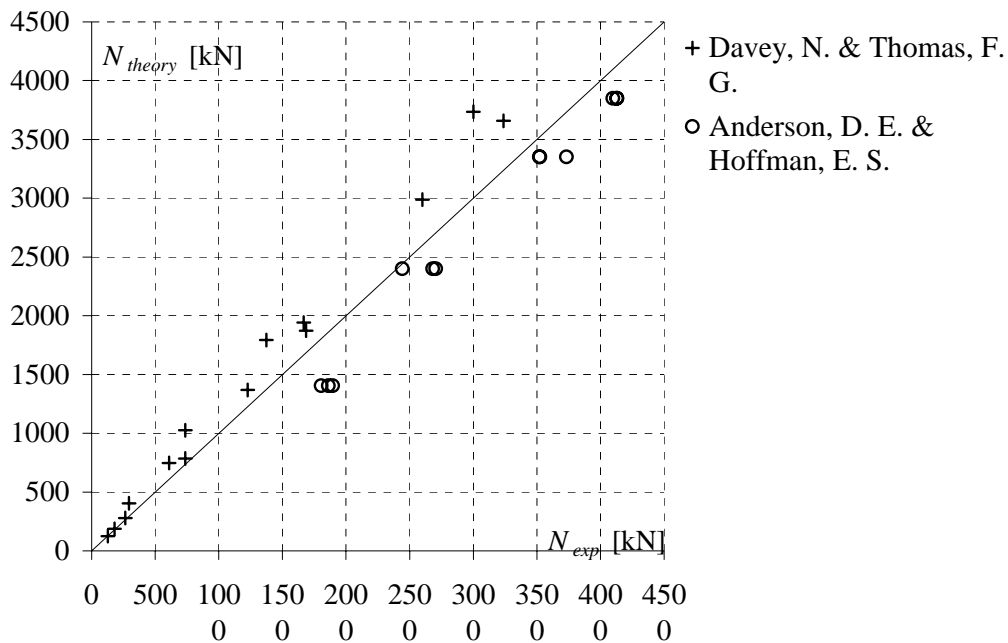
Figure 11.14 Comparison between DS414, method B and experiments

12 Conclusion

In this report, unreinforced and reinforced masonry columns and beam columns have been treated by different constitutive models. The models have been compared individually and with experiments. The tensile strength has been set at zero. To provide tensile strength to masonry reinforcement must be used.

Unreinforced masonry

In the report, expressions have been derived for the load carrying capacity of columns and beam-columns with and without membrane action and for laterally loaded masonry without axial load. Comparison with experiments shows that concentrically loaded columns may be calculated by Ritter's equation without the kind of correction factor suggested in the Danish Code of Practice, DS414. Results for unreinforced masonry beam-columns have been compared with experiments. The comparison shows that calculations made by using a modified linear elastic model overall provide the best results. The method developed is iterative. Simple conservative calculations may be made by using a simplified linear elastic model, and then closed form solutions may be given. All-together 307 experiments have been collected and used for the comparison.

Furthermore, it has been shown that masonry made by Danish bricks have an initial stiffness which may be taken as $375f_{cm}$, where f_{cm} is the compressive strength of the masonry in MPa. This value is much smaller than the initial stiffness used in other countries in Europe. Thus, an investigation of the behaviour of Danish masonry in compression has been undertaken.

Regarding masonry members with membrane action, it has been shown that a small pressure perpendicular to the bed joints increases the lateral strength notably.

Furthermore, it has been shown how the lateral strength of masonry walls without other external axial compression may be calculated by taken the weight of the masonry into account.

Reinforced masonry

In the report, reinforced masonry has been treated by the same methods as used for unreinforced masonry. Experiments collected from the literature are very limited in number so a thorough comparison has not been possible. Only 24 experiments have been found. However, it seems fair to conclude that reinforced masonry beam-columns may be calculated by using the method given in DS414.

In the report, practical calculation methods have been derived by using interaction diagrams between axial load and bending moment.

13 Literature

[1]   SHANLEY, F. R.: Inelastic Column Theory, *Journal of the Aeronautical Sciences, Vol. 4, No. 5, May 1947.*

[2]   VAN DEN BROEK, J. A.: Euler's Paper on the Strength of Columns, *American journal of physics, 1947 July-August, p 315.*

[3]   TIMOSHENKO, S. P. and GERE, J. M.: Theory of Elastic Stability, *International student edition, McGraw-Hill. 1961.*

[4]   NIELSEN, J.: Ekscentrisk beslastede jernbetonsøjler, *Bygningsstatiske meddelelser, Årgang XXIV, Nr. 2, 1953, p 53.*

[5]   POULSEN, E.: Betonsøjlers bæreevne, *Festskrift til Professor Anker Engelund, Laboratoriet for bygningsteknik, DTH, meddelelse nr. 10. 1959.*

[6]   HUTCHINSON, J. W.: On the Postbuckling Behaviour of Imperfection-Sensitive Structures in the Plastic Range, *Journal of Applied Mechanics, March 1972.*

[7]   NIELSEN, M. P. and HANSEN, L. P.: Mekanik 3.2. Søjler og Bjælkesøjler, *Danmarks Ingeniørakadami Bygningsafdelingen Aalborg, Den Private Ingeniørfond, 1973.*

[8]   NIELSEN, M. P. and RATHKJEN, A.: Mekanik 2.1. Plane spændings og deformationstilstande, *Danmarks Ingeniørakadami, Bygningsafdelingen Aalborg, Den Private Ingeniørfond, 1979.*

[9]   NIELSEN, M. P. and RATHKJEN, A.: Mekanik 5.1 del 1 og 2. Skiver og plader, *Danmarks Ingeniørakadami, Bygningsafdelingen Aalborg, Den Private Ingeniørfond, 1981.*

[10]   JÖNSSON, J.: Continuum Mechanics of Beam and Plate Flexure, *Aalborg University, July 1995.*

[11]   NIELSEN, M. P.: Limit Analysis and Concrete Plasticity, *Second Edition, CRC Press, 1998*

[12]   NIELSEN, M. P.: Beton 2 del 1, Bjælke- og rammekonstruktioner, Skæv bøjning, *Danmarks Tekniske Universitet Institut for Bærende Konstruktioner og Materialer, 1. udgave*, *Lyngby, 2001.*

[13]   NIELSEN, M. P., HANSEN, L. P. and RATHKJEN, A.: Mekanik 2.2 del 1. Rumlige spændings og deformationstilstande, *Danmarks Tekniske Universitet Institut for Bærende Konstruktioner og Materialer, København/Aalborg, 2001.*

[14]   NIELSEN, M. P., HANSEN, L. P. and RATHKJEN, A.: Mekanik 2.2 del 2. Rumlige spændings og deformationstilstande, *Danmarks Tekniske Universitet Institut for Bærende Konstruktioner og Materialer, København/Aalborg, 2001.*

Literature on masonry:

[15]   LYSE, I.: Tests on reinforced brick columns, *Journal American Ceramic Society, No. 16, pp 584-597, 1933.*

[16]   SUENSON, E. & DÜHRKOP, H.: Forsøg med murværk af molersten og almindelige teglsten, *Ingeniørvidenskabelige skrifter, 1944 Nr. 1.*

[17]   DAVEY, N. and THOMAS, F. G.: The Structural Use of Brickwork, Structural Paper No. 24, Institution of Civil Engineers, London, 1950.

[18]   SUENSON, E.: Teglstens-pillers trykstyrke og sammentrykkelighed naar hveranden sten er stærk og hver anden svag, *Ingeniørvidenskabelige skrifter, 1951 Nr. 1.*

[19]   RAMBØLL, B. J., CLARBO, O & MANNICHE, K.: Beretning fra udvalget til forsøg med murværks styrke og elasticitetsforhold, *Akademiet for de Tekniske Videnskaber, Beretning nr. 14, 1953.*

[20]   THOMAS, F. G.: The Strength of Brickwork, Struct. Engr., 31, 1953, pp 35-46.

[21]   Compressive, Transverse and Ranking Strength Tests of Four-inch Brick Walls, Research Paper No. 9, Structural Clay Products Research Foundation, Geneva, Ill., 1965.

[22]   Compressive, Transverse and Ranking Strength Tests of Eight-inch Brick Walls, *Research Paper No. 10, Structural Clay Products Research Foundation, Geneva, Ill., 1966.*

[23]   HELLERS, B.: Eccentrically Compressed Columns without Tensile Strength Subjected to Uniformly Distributed Lateral Load, *Rapport 35, Byggforskning, Stockholm 1967.*

[24]   SAHLIN, S. and HELLERS, B.: Transversalbelastning på mellan bjælklag inspända vägger utan draghållfasthet, *Rapport 9, Byggforskning, Stockholm 1968.*

[25]   HALLER, P.: Load Capacity in Brick Masonry, *ed. F.B. Johnson, Gulf, Houston, Texas, 1969, pp 129-49.*

[26]   GRENLEY, D. G. and GATTANEO, L. E.: Effect of edge load on flexural strength of clay masonry systems utilizing improved mortars, *ed. F.B. Johnson, Gulf, Houston, Texas, 1969, pp 119-28.*

[27]   ANDERSON, D. E. & HOFFMAN, E. S.: Design of brick masonry columns *ed. F.B. Johnson, Gulf, Houston, Texas, 1969, pp 94-100.*

[28]   YOKEL, F. Y., MATHEY, R. G. and DIKKERS, R. D.: Strength of Masonry Walls Under Compression and Transverse Loads, *NBS Building science series 34, 1971.*

[29]   MONDORF, P. E.: Murværkskonstruktioner, *Polyteknisk Forlag, 1972.*

[30]   HASAN, S. S.: Investigation of the effect of slenderness ratio on the compressive strength of masonry wall panels, *Ph.d thesis, University of Edinburgh, 1975.*

[31]   HASAN, S. S. and HENDRY, A. W.: Effects of Slenderness and Eccentricity on the Compressive Strength of Walls, Proceedings of the Fourth International Brick Masonry Conference (Brugge) 1976, Paper 4.d.3.

[32]   FATTAL, S. G. & GATTANEO, L. E.: Structural Performance of Masonry Walls Under Compression and Flexure, *NBS Building science series 73, 1976*

[33]   Murværkscenteret: Murværks bæreevne, *Murværkscenteret DTI-Byggeri Hasselager 1979.*

[34]   CAJDERT, A.: Laterally Loaded Masonry Walls, *Chalmers University of Technology, Publication 80:5, Göteborg 1980.*

[35]   EXNER, H.: Plasticitetsteori for Coulomb-materialer, *Afdelingen for Bærende Konstruktioner, DTH, 1983.*

[36]   Kalk- og Teglværkslaboratoriet: Bæreevne for murværk af mangehulsten og massive sten, *Hasselager 1984*

[37]   VILLUMSEN, K. & PEDERSEN, F. B.: *Murværk, beregningsmetoder, Murerfagets Oplysningsråd, Januar 1987.*

[38]   HENDRY, A. W.: Structural Masonry, *MacMillan, 1990.*

[39]   HENDRY, A. W.: Reinforced & Prestressed Masonry, *Longmann Scientific & Technical, 1991.*

[40]   KNUTSON, H. H.: Vertical Load Bearing Masonry – The Danish Approach, *Masonry International, Vol. 5, No. ,1 pp 23-26, 1991.*

[41]   KHALAF, F. M., HENDRY, A. W. and FAIRBAIRN, D. R.: Reinforced Blockwork Masonry Cloumns, *ACI Structural Journal, Vol. 90, No. 5, September-October 1993.*

[42]   DS414 Code of Practice for the structural use of masonry, *5. udgave / 1. oplag, 1998.*

[43]   DS411 Code of Practice for the structural use of concrete, *4. udgave / 1. oplag, 1999.*

[44]   DS/ENV 1996-1-1, Eurocode 6: Murværkskonstruktioner Del 1-1_ Generelle regler for bygningskonstruktioner. Regler for armeret og uarmeret murværk, 1999.

[45]   HAGSTEN, L.G.: Plasticitetsteori for murværk Del 1: Trykstyrke, *Department of Structural Engineering and Materials, DTU, Series R, No. 72, 2000.*

[46]   HAGSTEN, L.G.: Plasticitetsteori for murværk Del 2: Trækstyrke parallelt med liggefugerne, *Department of Structural Engineering and Materials, DTU, Series R, No. 73, 2000.*

[47]   HAGSTEN, L.G.: Plasticitetsteori for murværk Del 3: Koncentreret last, *Department of Structural Engineering and Materials, DTU, Series R, No. 74, 2000.*

[48]   HAGSTEN, L.G.: Plasticitetsteori for murværk Del 4: Teglbjælkers forskydningskapacitet, *Department of Structural Engineering and Materials, DTU, Series R, No. 75, 2000.*

[49]   HAGSTEN, L.G.: Plasticitetsteori for murværk Del 5: Tværbelastet murværk, *Department of Structural Engineering and Materials, DTU, Series R, No. 76, 2000.*

[50]   HAGSTEN, L.G. and NIELSEN, M. P.: Murværk, Lærebog for ingeniører, Første foreløbige udgave, *Department of Structural Engineering and Materials, DTU, December 2000.*

[51]   HANSEN, L. Z. & GUDMAND-HØYER, T.: Strength effects from the initial rate of absorption on masonry, *Bygningsstatiske meddelser, Vol. LXVIII, Nos 2-3, p. 35.*

14 Appendix 1. Experiments, unreinforced masonry

Eccentrically and concentrically loaded columns and one-way slabs.

B. J. Rambøll, O. Glarbo & K. Manniche

Research report number 9, Structural Clay Product Research Foundation

Research report number 10, Structural Clay Product Research Foundation

Hasan, S. S. & Hendry, A. W.

Fattal, S. G. and Cattaneo, L. E.

Murværkscenteret

Kalk- og teglværkslaboratoriet Hasselager

Laterally loaded beam columns

Grenley, G, A.

Yokel, F. Y., Mathey, R. G. and Dikkers, R. D.

In almost all of the interaction curves, the compressive strength is calculated using the test results for pure compression, i.e. without any applied external moment. In the case of the investigation made at Murværkscenteret (The Danish centre of masonry) this was not possible. Instead, the compressive strength was calculated by the formula suggested by Hagsten [45]. Thus the compressive strengths reported in the tables are either measured values or values calculated by means of Hagsten's formula.

14.1 Concentrically and eccentrically loaded columns

14.1.1 B. J. Rambøll, O. Glarbo & K. Manniche

Ref no.	b	h	$f_{c,m}$	e_i/h	l/h	N_{exp}	$M_{0,exp}$	$\dfrac{N_{exp}}{N_{theo,par}}$	$\dfrac{N_{exp}}{N_{theo,el}}$	$\dfrac{N_{exp}}{N_{theo,DS411}}$	$\dfrac{N_{exp}}{N_{theo,DS414}}$
	[mm]	[mm]	[MPa]			[kN]	[kNm]				
1	850,00	163,30	4,57	0,00	15,92	678,85	0,00	1,11	1,43	1,29	1,43
2	850,00	163,30	4,57	0,00	15,92	590,56	0,00	0,97	1,25	1,12	1,25
5	850,00	163,30	4,57	0,08	15,92	466,96	6,35	1,06	1,21	1,07	1,27
6	850,00	163,30	4,57	0,08	15,92	469,90	6,39	1,06	1,22	1,08	1,28
7	850,00	163,30	4,57	0,17	15,92	317,84	8,65	0,96	1,14	0,95	1,22
8	850,00	163,30	4,57	0,17	15,92	288,41	7,85	0,87	1,03	0,86	1,11
11	850,00	163,30	4,57	0,25	15,92	180,50	7,37	0,88	1,00	0,88	1,15
12	850,00	163,30	4,57	0,25	15,92	168,73	6,89	0,82	0,94	0,82	1,08
14	850,00	163,30	10,00	0,00	15,92	1458,75	0,00	1,09	1,41	1,27	1,41
15	850,00	163,30	10,00	0,00	15,92	1318,46	0,00	0,99	1,27	1,14	1,27
16	850,00	163,30	10,00	0,08	15,92	1043,78	14,20	1,08	1,24	1,10	1,30
17	850,00	163,30	10,00	0,08	15,92	1171,31	15,94	1,21	1,39	1,23	1,46
18	850,00	163,30	10,00	0,17	15,92	984,92	26,81	1,37	1,61	1,34	1,73
19	850,00	163,30	10,00	0,17	15,92	808,34	22,00	1,12	1,32	1,10	1,42
20	850,00	163,30	10,00	0,25	15,92	621,95	25,39	1,38	1,58	1,38	1,81
29	850,00	163,30	10,00	0,25	15,92	590,56	24,11	1,31	1,50	1,31	1,72
21	850,00	163,30	15,05	0,00	15,92	2220,98	0,00	1,11	1,42	1,28	1,42
22	850,00	163,30	15,05	0,00	15,92	1956,11	0,00	0,97	1,25	1,13	1,25
23	850,00	163,30	15,05	0,08	15,92	2181,74	29,69	1,50	1,72	1,52	1,81
24	850,00	163,30	15,05	0,08	15,92	1975,73	26,89	1,36	1,56	1,38	1,63
25	850,00	163,30	15,05	0,17	15,92	1661,81	45,23	1,53	1,80	1,50	1,94
28	850,00	163,30	15,05	0,17	15,92	1534,28	41,76	1,41	1,67	1,39	1,79
26	850,00	163,30	15,05	0,25	15,92	1279,22	52,22	1,89	2,15	1,89	2,48
27	850,00	163,30	15,05	0,25	15,92	1161,50	47,42	1,72	1,96	1,72	2,25
30	850,00	163,30	2,82	0,00	15,92	420,85	0,00	1,12	1,44	1,30	1,44
31	850,00	163,30	2,82	0,00	15,92	361,99	0,00	0,96	1,24	1,11	1,24
32	850,00	163,30	2,82	0,08	15,92	323,73	4,41	1,19	1,36	1,21	1,43
33	850,00	163,30	2,82	0,08	15,92	357,08	4,86	1,31	1,50	1,33	1,58
36	850,00	163,30	2,82	0,17	15,92	268,79	7,32	1,32	1,56	1,30	1,67

37	850,00	163,30	2,82	0,17	15,92	265,85	7,24	1,31	1,54	1,28	1,66
38	850,00	163,30	2,82	0,25	15,92	163,83	6,69	1,29	1,47	1,29	1,69
39	850,00	163,30	2,82	0,25	15,92	180,50	7,37	1,43	1,62	1,43	1,87
49	850,00	163,30	1,57	0,00	15,92	413,00	0,00	1,97	2,54	2,29	2,54
75	850,00	163,30	5,73	0,00	15,92	756,35	0,00	0,99	1,27	1,15	1,27
76	850,00	163,30	5,73	0,00	15,92	834,83	0,00	1,09	1,41	1,26	1,41
77	850,00	163,30	5,73	0,17	15,92	572,90	15,59	1,39	1,63	1,36	1,76
78	850,00	163,30	5,73	0,17	15,92	552,30	15,03	1,34	1,57	1,31	1,69
71	850,00	163,30	4,77	0,00	15,92	735,75	0,00	1,16	1,49	1,34	1,49
72	850,00	163,30	4,77	0,00	15,92	587,62	0,00	0,92	1,19	1,07	1,19
73	850,00	163,30	4,77	0,17	15,92	518,95	14,12	1,51	1,78	1,48	1,91
74	850,00	163,30	4,77	0,17	15,92	543,47	14,79	1,58	1,86	1,55	2,00

Table 14.1 Data for the calculation of tests taken from [19]. Only results of walls built with the same brick and mortar through the entire wall are found useful. The compressive strength is calculated by using Hagstens formula

Figure 14.1 Results of tests shown in an interaction diagram, FIKM is "Flamme" stones with lime mortar

Figure 14.2 Results of tests shown in an interaction diagram, FIKCM is "Flamme" stones with lime cement mortar
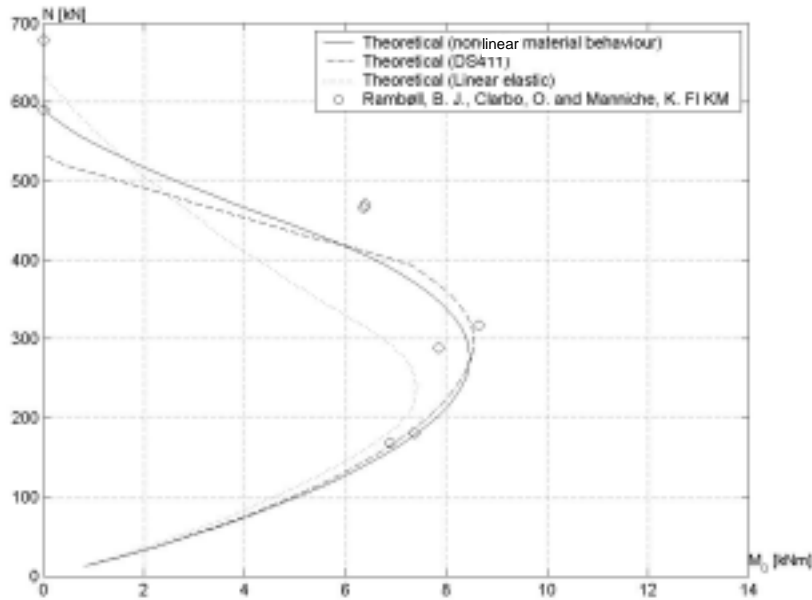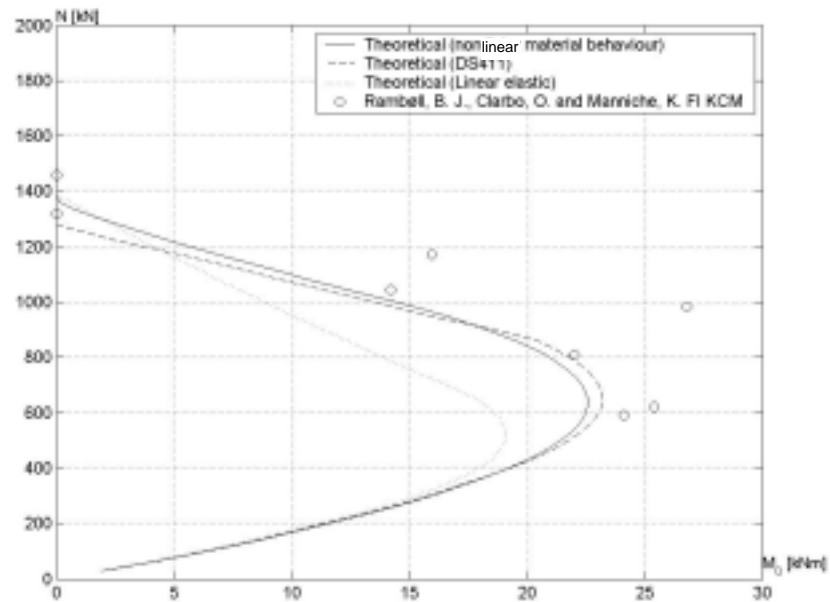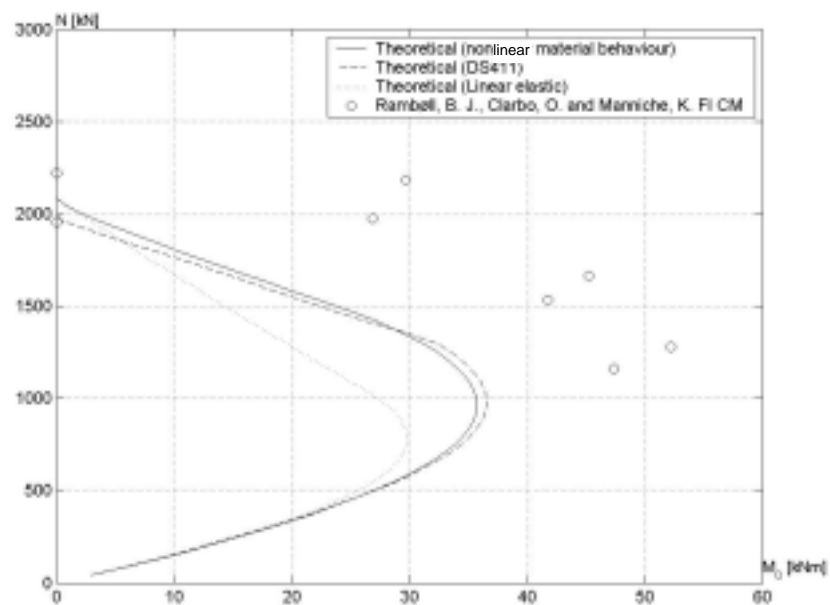

Figure 14.3 Results of tests shown in an interaction diagram, FICM is "Flamme" stones with cement mortar
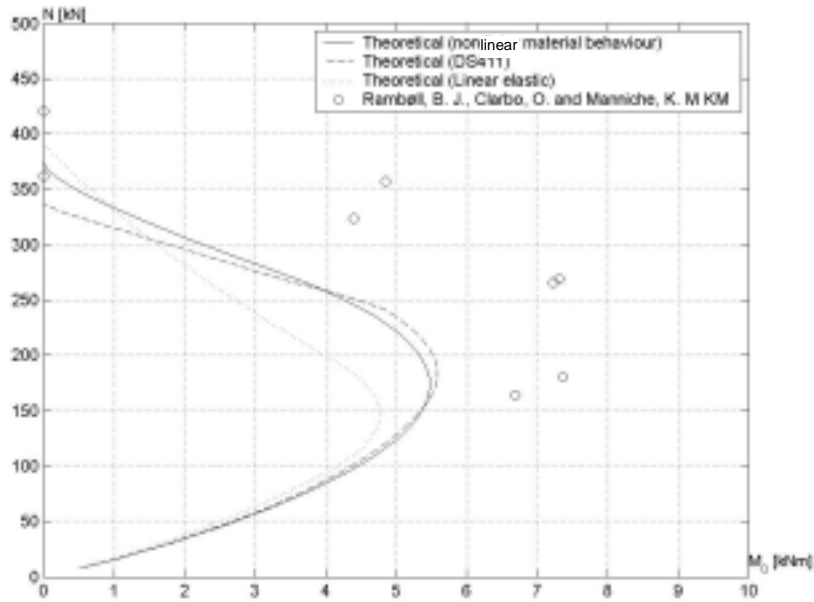
Figure 14.4 Results of tests shown in an interaction diagram, MKM is "Moler" stones with lime mortar,

14.1.2 Research report 9. Structural Clay Product Research Foundation.

Ref no.	b	h	$f_{c,m}$	e_i/h	l/h	N_{exp}	$M_{0,exp}$	$\dfrac{N_{exp}}{N_{theo,par}}$	$\dfrac{N_{exp}}{N_{Ritter}}$	$\dfrac{N_{exp}}{N_{theo,DS414}}$
	[mm]	[mm]	[MPa]			[kN]	[kNm]			
c8-1	609,60	101,60	38,10	0,00	23,75	2099,46	0,00	0,95	1,13	1,26
c8-2	609,60	101,60	38,10	0,00	23,75	2215,10	0,00	1,00	1,19	1,32
c8-3	609,60	101,60	38,10	0,00	23,75	2250,69	0,00	1,02	1,21	1,35
c8-4	609,60	101,60	38,10	0,00	23,75	2335,20	0,00	1,06	1,26	1,40
c8-5	609,60	101,60	38,10	0,00	23,75	2357,44	0,00	1,07	1,27	1,41
c3-1	609,60	101,60	29,73	0,00	9,75	2046,08	0,00	1,11	1,16	1,29
c3-2	609,60	101,60	29,73	0,00	9,75	1779,20	0,00	0,97	1,01	1,12
c3-3	609,60	101,60	29,73	0,00	9,75	1948,22	0,00	1,06	1,10	1,23
c3-4	609,60	101,60	29,73	0,00	9,75	1703,58	0,00	0,93	0,97	1,07
c3-5	609,60	101,60	29,73	0,00	9,75	1966,02	0,00	1,07	1,11	1,24
c5-1	609,60	101,60	29,73	0,00	15,50	0,00	0,00	0,00	0,00	0,00
c5-2	609,60	101,60	29,73	0,00	15,50	1894,85	0,00	1,04	1,14	1,27
c5-3	609,60	101,60	29,73	0,00	15,50	1632,42	0,00	0,90	0,98	1,09
c5-4	609,60	101,60	29,73	0,00	15,50	1894,85	0,00	1,04	1,14	1,27
c5-5	609,60	101,60	29,73	0,00	15,50	1712,48	0,00	0,94	1,03	1,15
c8-6	609,60	101,60	29,73	0,00	23,75	1859,26	0,00	1,07	1,27	1,41
c8-7	609,60	101,60	29,73	0,00	23,75	1779,20	0,00	1,03	1,22	1,35
c8-8	609,60	101,60	29,73	0,00	23,75	1756,96	0,00	1,01	1,20	1,33
c8-9	609,60	101,60	29,73	0,00	23,75	1587,94	0,00	0,92	1,09	1,21
c8-10	609,60	101,60	29,73	0,00	23,75	1552,35	0,00	0,90	1,06	1,18
c10-1	609,60	101,60	29,73	0,00	30,25	1779,20	0,00	1,11	1,37	1,52
c10-2	609,60	101,60	29,73	0,00	30,25	1761,41	0,00	1,10	1,36	1,51
c10-3	609,60	101,60	29,73	0,00	30,25	1561,25	0,00	0,98	1,20	1,34
c10-4	609,60	101,60	29,73	0,00	30,25	1543,46	0,00	0,97	1,19	1,32
c10-5	609,60	101,60	29,73	0,00	30,25	1712,48	0,00	1,07	1,32	1,47
c12-6	609,60	101,60	29,73	0,00	36,75	1583,49	0,00	1,11	1,39	1,55
c12-7	609,60	101,60	29,73	0,00	36,75	1361,09	0,00	0,96	1,20	1,33
c12-8	609,60	101,60	29,73	0,00	36,75	1187,62	0,00	0,84	1,04	1,16
c12-9	609,60	101,60	29,73	0,00	36,75	1352,19	0,00	0,95	1,19	1,32
c12-10	609,60	101,60	29,73	0,00	36,75	1432,26	0,00	1,01	1,26	1,40
c15-1	609,60	101,60	29,73	0,00	45,50	1076,42	0,00	0,92	1,14	1,27
c15-2	609,60	101,60	29,73	0,00	45,50	889,60	0,00	0,76	0,94	1,05
c15-3	609,60	101,60	29,73	0,00	45,50	1000,80	0,00	0,85	1,06	1,18

c15-4	609,60	101,60	29,73	0,00	45,50	1223,20	0,00	1,04	1,29	1,44
c15-5	609,60	101,60	29,73	0,00	45,50	1187,62	0,00	1,01	1,26	1,40
c8-11	609,60	101,60	22,21	0,00	23,75	1103,10	0,00	0,85	1,00	1,11
c8-12	609,60	101,60	22,21	0,00	23,75	1454,50	0,00	1,12	1,32	1,46
c8-13	609,60	101,60	22,21	0,00	23,75	1392,22	0,00	1,07	1,26	1,40
c8-14	609,60	101,60	22,21	0,00	23,75	1303,26	0,00	1,00	1,18	1,31
c8-15	609,60	101,60	22,21	0,00	23,75	1174,27	0,00	0,90	1,06	1,18

Table 14.2 Data for the calculation of tests taken from [21]
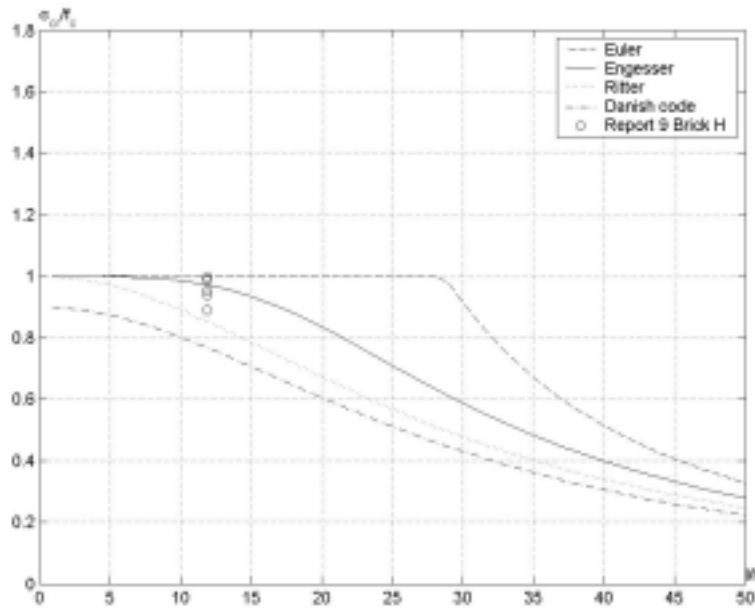

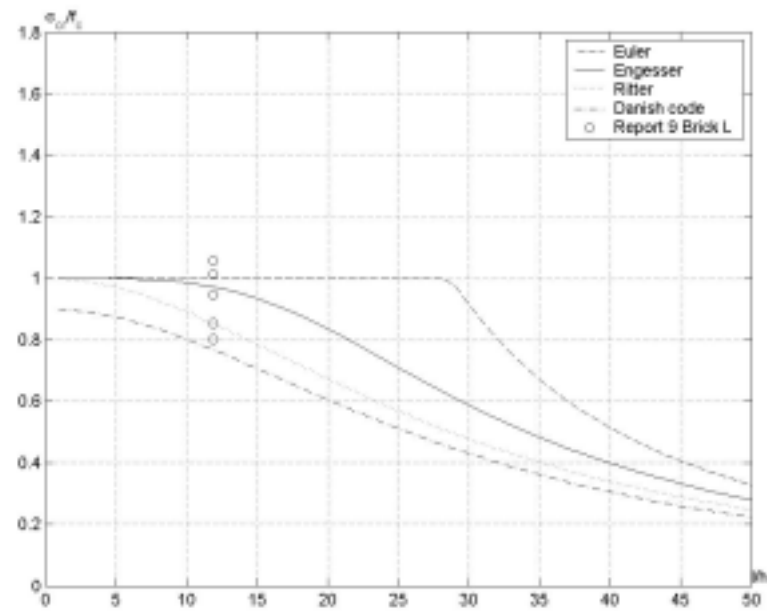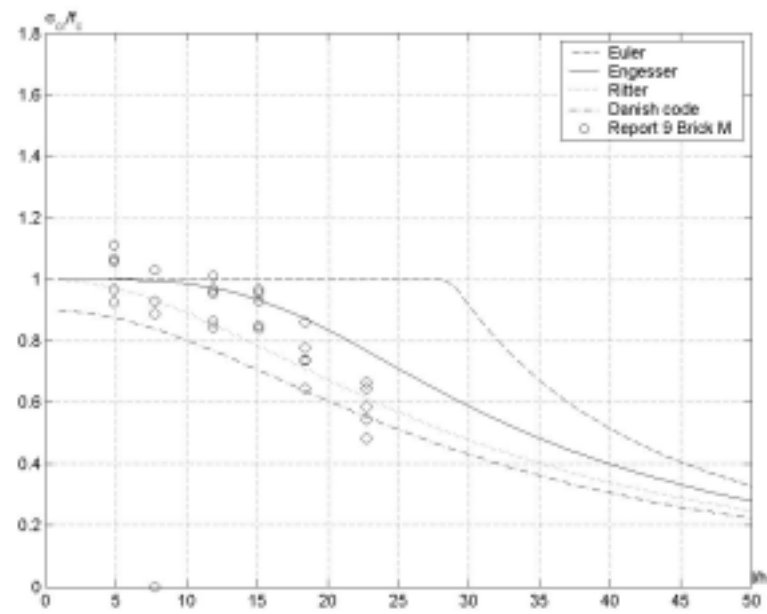**Figure 14.5 Results of tests**

Figure 14.6 Results of tests

Figure 14.7 Results of tests

14.1.3 Research report 10. Structural Clay Product Research Foundation.

Ref no.	b	h	$f_{c,m}$	e_i/h	l/h	N_{exp}	$M_{0,exp}$	$\dfrac{N_{exp}}{N_{theo,par}}$	$\dfrac{N_{exp}}{N_{theo,el}}$	$\dfrac{N_{exp}}{N_{theo,DS}}$
	[mm]	[mm]	[MPa]			[kN]	[kNm]			
CPR-S1	406,40	203,20	33,31	0,00	2,61	2677,70	0,00	0,97	0,98	1,09
CPR-S2	406,40	203,20	31,03	0,00	2,61	2504,22	0,00	0,98	0,98	1,09
CPR-S3	406,40	203,20	32,22	0,00	2,61	2588,74	0,00	0,97	0,98	1,09
CPR-S4	406,40	203,20	32,19	0,00	2,61	2553,15	0,00	0,96	0,96	1,07
CPR-S5	406,40	203,20	32,16	0,00	2,61	2593,18	0,00	0,98	0,98	1,09
C3-1	609,60	203,20	32,18	0,00	4,83	3785,25	0,00	0,95	0,96	1,07
C3-2	609,60	203,20	32,18	0,00	4,83	4345,70	0,00	1,09	1,10	1,22
C3-3	609,60	203,20	32,18	0,00	4,83	4087,71	0,00	1,03	1,04	1,15
C3-4	609,60	203,20	32,18	0,00	4,83	0,00	0,00	0,00	0,00	0,00
C3-5	609,60	203,20	32,18	0,00	4,83	3834,18	0,00	0,96	0,97	1,08
C6-1	609,60	203,20	32,18	0,00	9,33	4056,58	0,00	1,02	1,06	1,18
C6-2	609,60	203,20	32,18	0,00	9,33	3629,57	0,00	0,91	0,95	1,05
C6-3	609,60	203,20	32,18	0,00	9,33	4074,37	0,00	1,02	1,06	1,18
C6-4	609,60	203,20	32,18	0,00	9,33	4132,19	0,00	1,04	1,08	1,20
C6-5	609,60	203,20	32,18	0,00	9,33	3811,94	0,00	0,96	0,99	1,10
C8-1	609,60	203,20	32,18	0,00	12,23	3727,42	0,00	0,94	1,00	1,11
C8-2	609,60	203,20	32,18	0,00	12,23	3767,46	0,00	0,95	1,01	1,12
C8-3	609,60	203,20	32,18	0,00	12,23	3598,43	0,00	0,91	0,96	1,07
C8-4	609,60	203,20	32,18	0,00	12,23	3923,14	0,00	0,99	1,05	1,17
C8-5	609,60	203,20	32,18	0,00	12,23	3923,14	0,00	0,99	1,05	1,17
C10-1	609,60	203,20	32,18	0,00	15,13	3998,75	0,00	1,01	1,11	1,23
C10-2	609,60	203,20	32,18	0,00	15,13	3927,58	0,00	1,00	1,09	1,21
C10-3	609,60	203,20	32,18	0,00	15,13	3918,69	0,00	0,99	1,09	1,21
C10-4	609,60	203,20	32,18	0,00	15,13	4034,34	0,00	1,02	1,12	1,24
C10-5	609,60	203,20	32,18	0,00	15,13	4176,67	0,00	1,06	1,16	1,29
C13-1	609,60	203,20	32,18	0,00	19,95	3585,09	0,00	0,93	1,07	1,18
C13-2	609,60	203,20	32,18	0,00	19,95	3811,94	0,00	0,99	1,13	1,26
C13-3	609,60	203,20	32,18	0,00	19,95	3789,70	0,00	0,98	1,13	1,25
C13-4	609,60	203,20	32,18	0,00	19,95	4007,65	0,00	1,04	1,19	1,32
C13-5	609,60	203,20	32,18	0,00	19,95	3763,01	0,00	0,98	1,12	1,24
CB13-1	609,60	203,20	32,18	0,00	19,95	3625,12	0,00	0,94	1,08	1,20
CB13-2	609,60	203,20	32,18	0,00	19,95	3740,77	0,00	0,97	1,11	1,24
CB13-3	609,60	203,20	32,18	0,00	19,95	0,00	0,00	0,00	0,00	0,00

CB13-4	609,60	203,20	32,18	0,00	19,95	3260,38	0,00	0,84	0,97	1,08
CB13-5	609,60	203,20	32,18	0,00	19,95	0,00	0,00	0,00	0,00	0,00
C15-1	609,60	203,20	32,18	0,00	22,86	3571,74	0,00	0,95	1,11	1,24
C15-2	609,60	203,20	32,18	0,00	22,86	3665,15	0,00	0,97	1,14	1,27
C15-3	609,60	203,20	32,18	0,00	22,86	3371,58	0,00	0,89	1,05	1,17
C15-4	609,60	203,20	32,18	0,00	22,86	3527,26	0,00	0,93	1,10	1,22
C15-5	609,60	203,20	32,18	0,00	22,86	3318,21	0,00	0,88	1,03	1,15

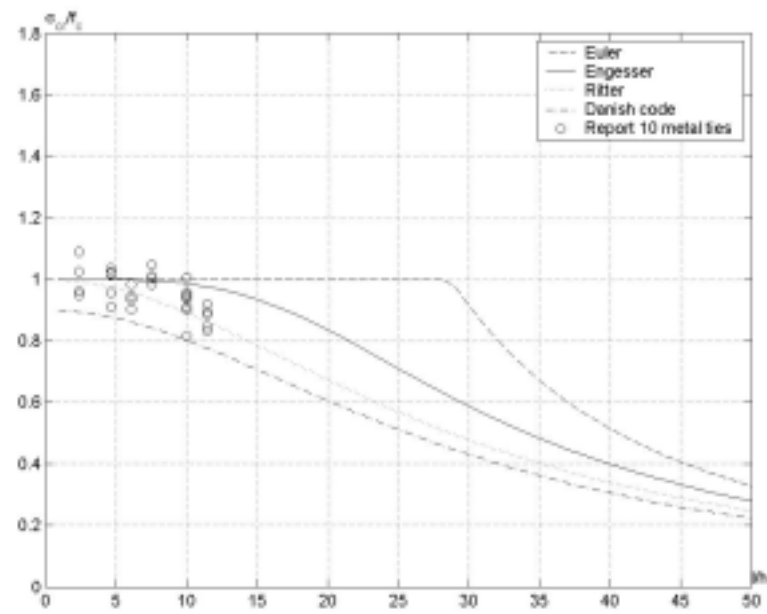**Table 14.3 Data for the calculation of tests taken from [22]**
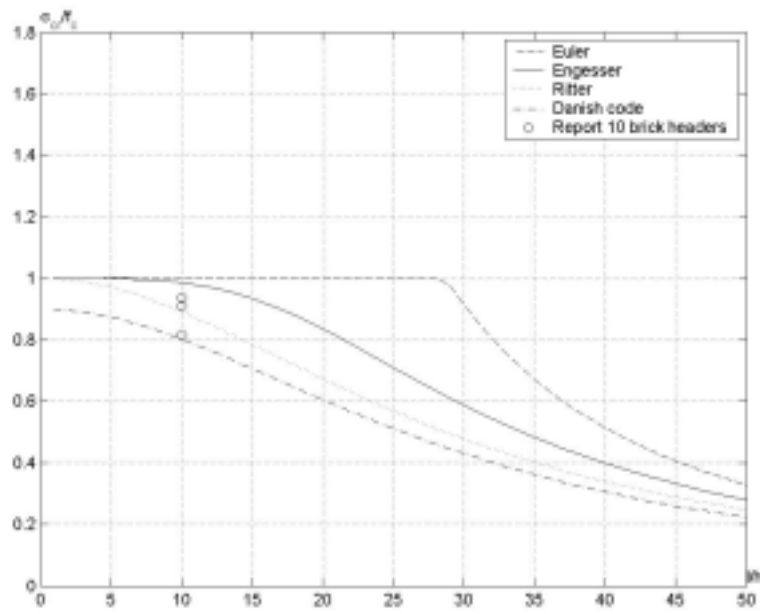

Figure 14.8 Results of tests, metal ties

Figure 14.9 Results of tests, brick headers

14.1.4 Hasan, S. S. & Hendry, A. W.

Ref no.	b	h	$f_{c,m}$	e_i/h	l/h	N_{exp}	$M_{0,exp}$	$\frac{N_{exp}}{N_{theo,par}}$	$\frac{N_{exp}}{N_{theo,el}}$	$\frac{N_{exp}}{N_{theo,DS}}$
	[mm]	[mm]	[MPa]			[kN]	[kNm]			
B1W6-1	380,00	76,20	14,19	0,00	6,00	611,80	0,00	1,49	1,56	2,23
B1W6-2	380,00	76,20	17,11	0,00	6,00	641,70	0,00	1,30	1,36	1,94
B1W6-3	380,00	76,20	16,65	0,00	6,00	679,30	0,00	1,42	1,48	2,12
B1W8-1	380,00	76,20	15,89	0,00	8,00	627,70	0,00	1,37	1,48	2,11
B1W8-2	380,00	76,20	14,59	0,00	8,00	647,70	0,00	1,54	1,66	2,37
B1W8-3	380,00	76,20	17,20	0,00	8,00	651,60	0,00	1,32	1,42	2,03
B1W12-1	380,00	76,20	15,70	0,00	12,00	579,90	0,00	1,32	1,52	2,17
B1W12-2	380,00	76,20	16,00	0,00	12,00	737,30	0,00	1,65	1,90	2,71
B1W12-3	380,00	76,20	15,99	0,00	12,00	607,80	0,00	1,36	1,56	2,24
B1W18-1	380,00	76,20	16,32	0,00	18,00	726,40	0,00	1,79	2,21	3,15
B1W18-2	380,00	76,20	17,13	0,00	18,00	649,65	0,00	1,53	1,89	2,70
B1W18-3	380,00	76,20	16,77	0,00	18,00	701,50	0,00	1,68	2,07	2,96
WM6-1	480,00	38,10	14,53	0,00	6,00	320,84	0,00	1,21	1,27	1,81
WM6-2	480,00	38,10	14,63	0,00	6,00	310,90	0,00	1,16	1,22	1,74
WM6-3	480,00	38,10	14,13	0,00	6,00	342,76	0,00	1,33	1,39	1,99
WM12-1	480,00	38,10	15,22	0,00	12,00	333,80	0,00	1,20	1,43	2,04
WM12-2	480,00	38,10	14,10	0,00	12,00	362,70	0,00	1,41	1,67	2,39
WM12-3	480,00	38,10	14,53	0,00	12,00	313,80	0,00	1,18	1,41	2,01
WM18-1	480,00	38,10	17,29	0,00	18,00	258,00	0,00	0,82	1,17	1,68
WM18-2	480,00	38,10	17,06	0,00	18,00	272,00	0,00	0,87	1,25	1,79
WM18-3	480,00	38,10	16,90	0,00	18,00	261,06	0,00	0,84	1,21	1,73
WM25-1	480,00	38,10	16,56	0,00	25,00	191,31	0,00	0,63	1,16	1,66
WM25-2	480,00	38,10	18,74	0,00	25,00	203,30	0,00	0,59	1,10	1,58
WM25-3	480,00	38,10	17,77	0,00	25,00	193,20	0,00	0,59	1,10	1,57
WS4-1	480,00	38,10	15,79	0,00	4,00	334,67	0,00	1,16	1,18	1,68
WS4-2	480,00	38,10	15,84	0,00	4,00	334,67	0,00	1,16	1,18	1,68
WS6-1	480,00	38,10	16,58	0,00	6,00	320,04	0,00	1,06	1,09	1,56
WS6-2	480,00	38,10	16,68	0,00	6,00	369,42	0,00	1,21	1,25	1,79
WS9-1	480,00	38,10	17,35	0,00	9,00	323,70	0,00	1,03	1,10	1,57
WS9-2	480,00	38,10	12,70	0,00	9,00	385,88	0,00	1,67	1,78	2,55
WS9-3	480,00	38,10	14,74	0,00	9,00	369,42	0,00	1,38	1,48	2,11
WS14-1	480,00	38,10	16,47	0,00	14,00	261,52	0,00	0,89	1,03	1,46

WS14-2	480,00	38,10	16,27	0,00	14,00	250,55	0,00	0,87	0,99	1,42
WS14-3	480,00	38,10	16,32	0,00	14,00	250,55	0,00	0,87	0,99	1,42
WS19-1	480,00	38,10	16,07	0,00	19,00	205,74	0,00	0,77	0,93	1,33
WS19-2	480,00	38,10	16,18	0,00	19,00	228,60	0,00	0,85	1,03	1,47
WS19-3	480,00	38,10	17,11	0,00	19,00	276,15	0,00	0,97	1,18	1,69
W06-1	480,00	38,10	16,56	0,00	6,00	238,84	0,00	0,79	1,17	0,82
W06-2	480,00	38,10	18,59	0,00	6,00	259,69	0,00	0,76	1,14	0,80
W06-3	480,00	38,10	17,80	0,00	6,00	259,69	0,00	0,80	1,19	0,83
W66-1	480,00	38,10	17,56	0,17	6,00	179,22	1,14	0,93	0,92	0,92
W66-2	480,00	38,10	17,05	0,17	6,00	169,35	1,08	0,91	0,89	0,89
W66-3	480,00	38,10	17,94	0,17	6,00	183,79	1,17	0,94	0,92	0,92
W36-1	480,00	38,10	17,17	0,33	6,00	90,71	1,15	1,09	1,05	1,05
W36-2	480,00	38,10	18,17	0,33	6,00	65,84	0,84	0,75	0,72	0,72
W36-3	480,00	38,10	17,94	0,33	6,00	71,32	0,91	0,82	0,79	0,79
W012-1	480,00	38,10	16,97	0,00	12,00	213,97	0,00	0,71	1,16	0,81
W012-2	480,00	38,10	17,82	0,00	12,00	232,26	0,00	0,73	1,20	0,84
W012-3	480,00	38,10	17,76	0,00	12,00	241,40	0,00	0,76	1,24	0,87
W612-1	480,00	38,10	14,88	0,17	12,00	138,07	0,88	0,96	0,92	0,92
W612-2	480,00	38,10	17,82	0,17	12,00	153,62	0,98	0,89	0,86	0,86
W612-3	480,00	38,10	17,05	0,17	12,00	138,07	0,88	0,83	0,80	0,80
W312-1	480,00	38,10	16,41	0,33	12,00	36,03	0,46	0,77	0,82	0,82
W312-2	480,00	38,10	18,14	0,33	12,00	47,55	0,60	0,92	0,98	0,98
W312-3	480,00	38,10	17,23	0,33	12,00	27,43	0,35	0,56	0,59	0,59
W018-1	480,00	38,10	17,05	0,00	18,00	193,85	0,00	0,70	1,23	0,86
W018-2	480,00	38,10	18,49	0,00	18,00	237,74	0,00	0,80	1,40	0,98
W018-3	480,00	38,10	18,77	0,00	18,00	212,14	0,00	0,70	1,23	0,86
W618-1	480,00	38,10	15,79	0,17	18,00	97,66	0,62	0,80	0,82	0,82
W618-2	480,00	38,10	18,56	0,17	18,00	85,95	0,55	0,60	0,61	0,61
W618-3	480,00	38,10	18,01	0,17	18,00	104,24	0,66	0,75	0,77	0,77
W318-1	480,00	38,10	16,45	0,33	18,00	21,95	0,28	0,93	0,93	0,93
W318-2	480,00	38,10	17,59	0,33	18,00	16,20	0,21	0,64	0,64	0,64
W318-3	480,00	38,10	18,61	0,33	18,00	27,43	0,35	1,03	1,03	1,03
W025-1	480,00	38,10	15,89	0,00	25,00	146,30	0,00	0,71	1,26	0,89
W025-2	480,00	38,10	18,54	0,00	25,00	173,74	0,00	0,72	1,29	0,90
W025-3	480,00	38,10	18,69	0,00	25,00	128,02	0,00	0,53	0,94	0,66
W625-1	480,00	38,10	14,28	0,17	25,00	77,91	0,49	1,01	1,09	1,09
W625-2	480,00	38,10	19,15	0,17	25,00	98,39	0,62	0,95	1,02	1,02

W625-3	480,00	38,10	18,37	0,17	25,00	65,84	0,42	0,67	0,71	0,71
W325-1	480,00	38,10	13,29	0,33	25,00	14,63	0,19	1,22	1,22	1,22
W325-2	480,00	38,10	15,79	0,33	25,00	19,75	0,25	1,40	1,40	1,40
W325-3	480,00	38,10	19,06	0,33	25,00	16,64	0,21	0,97	0,97	0,97

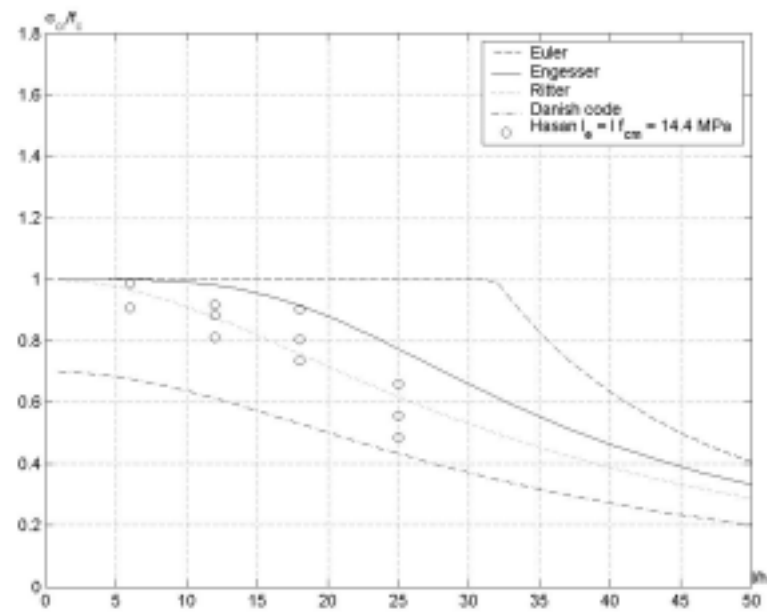**Table 14.4 Data for the calculation of tests taken from [31]**
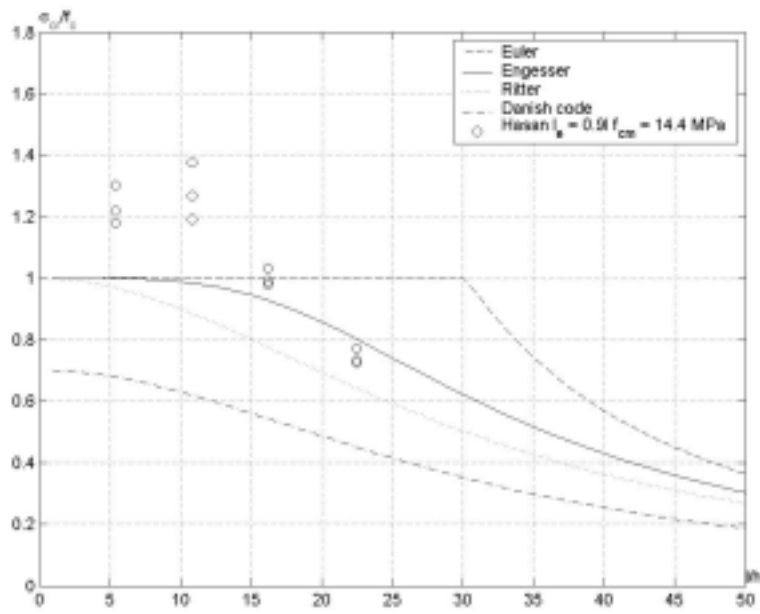

Figure 14.10 Results of tests
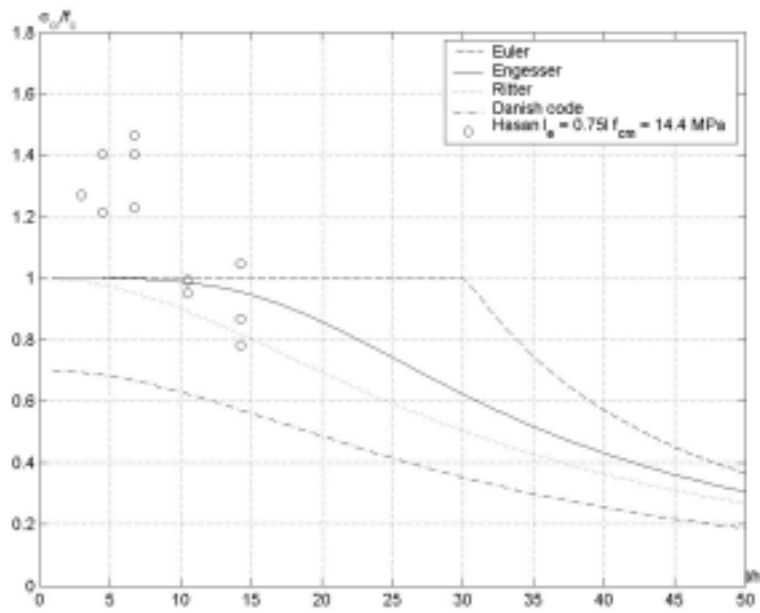
Figure 14.11 Results of tests
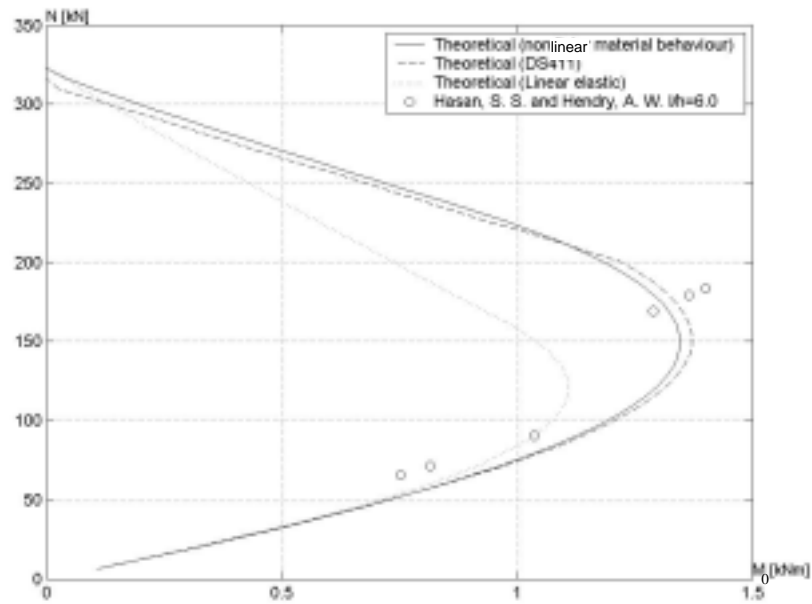

Figure 14.12 Results of tests

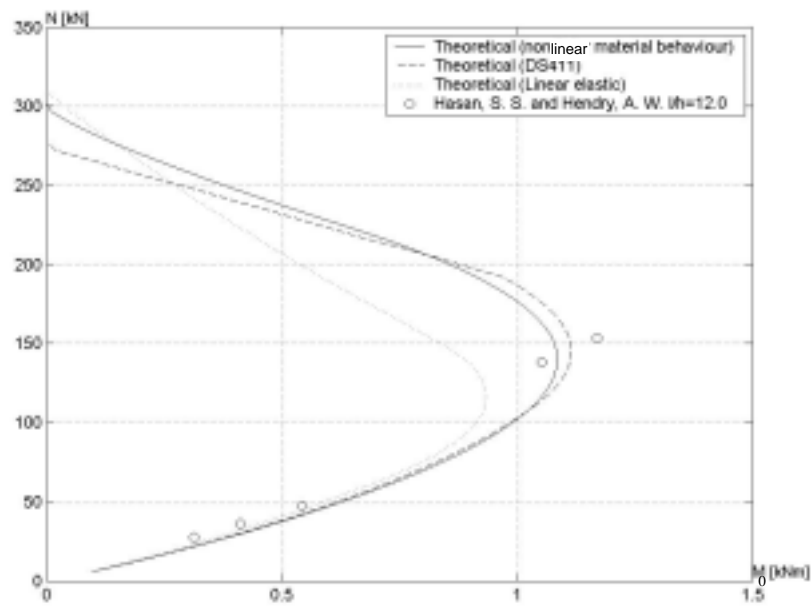**Figure 14.13 Results of tests shown in an interaction diagram *l/h* = 6.0**

Figure 14.14 Results of tests shown in an interaction diagram *l/h* = 12.0
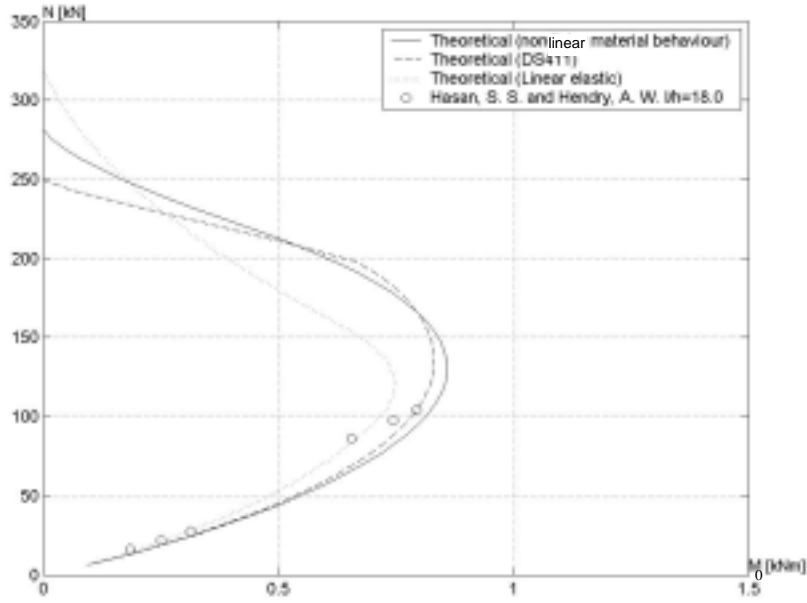
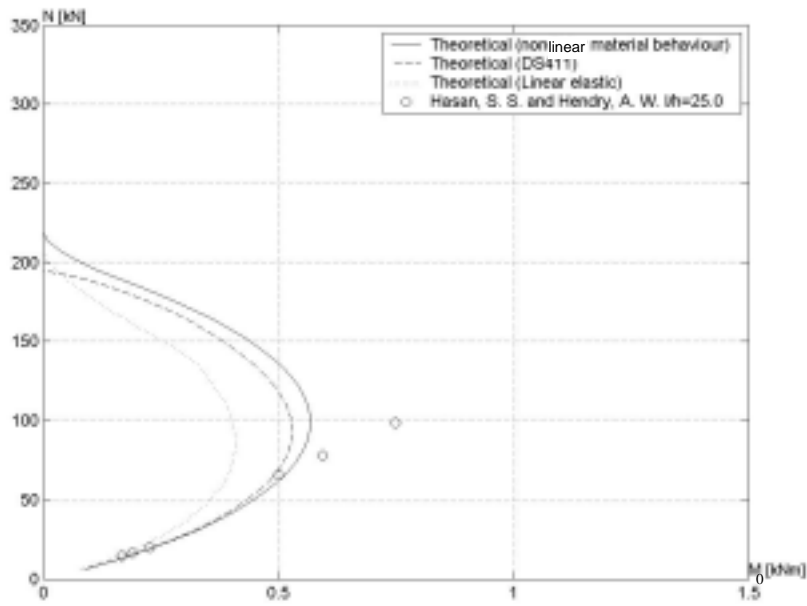**Figure 14.15 Results of tests shown in an interaction diagram *l/h* = 18.0**

Figure 14.16 Results of tests shown in an interaction diagram *l/h* = 25.0

14.1.5 Fattal, S. G. and Gattano, L. E.

Ref no.	b	h	$f_{c,m}$	e_i/h	l/h	N_{exp}	$M_{0,exp}$	$\dfrac{N_{exp}}{N_{theo,par}}$	$\dfrac{N_{exp}}{N_{theo,el}}$	$\dfrac{N_{exp}}{N_{theo,DS411}}$	$\dfrac{N_{exp}}{N_{theo,DS414}}$
	[mm]	[mm]	[MPa]			[kN]	[kNm]				
4A7	812,80	101,60	26,96	0,00	24,00	2228,45	0,00	1,65	1,89	1,70	2,27
4A8	812,80	101,60	26,96	0,00	24,00	2224,00	0,00	1,65	1,89	1,70	2,26
4A1	812,80	101,60	16,93	0,00	24,00	1365,54	0,00	1,55	1,85	1,66	2,13
4A2	812,80	101,60	16,93	0,00	24,00	1430,03	0,00	1,62	1,93	1,74	2,23
4A9	812,80	101,60	16,93	0,07	24,00	750,38	5,66	1,03	1,22	1,07	1,63
4A10	812,80	101,60	16,93	0,07	24,00	744,15	5,61	1,02	1,21	1,07	1,61
4A3	812,80	101,60	16,93	0,15	24,00	480,38	7,24	1,00	1,35	1,06	1,60
4A4	812,80	101,60	16,93	0,15	24,00	498,18	7,50	1,04	1,40	1,10	1,65
4A5	812,80	101,60	16,93	0,30	24,00	177,48	5,35	1,44	2,59	1,62	2,36
4A6	812,80	101,60	16,93	0,30	24,00	102,30	3,08	0,83	1,49	0,93	1,36

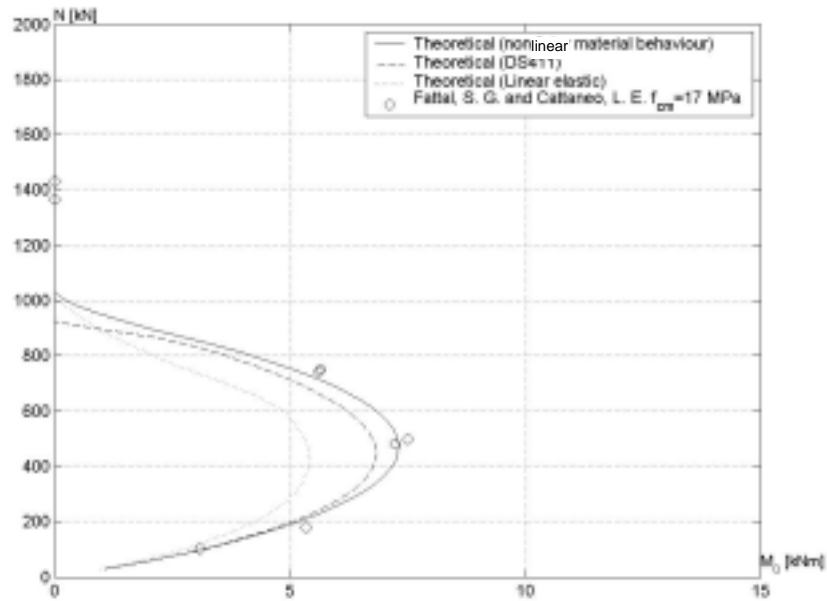**Table 14.5 Data for the calculation of tests taken from [32]**

Figure 14.17 Results of tests shown in an interaction diagram

14.1.6 Kalk og teglværkslaboratoriet

Ref no.	b	h	$f_{c,m}$	e_i/h	l/h	N_{exp}	$M_{0,exp}$	$\dfrac{N_{exp}}{N_{theo,par}}$	$\dfrac{N_{exp}}{N_{theo,el}}$	$\dfrac{N_{exp}}{N_{theo,DS411}}$	$\dfrac{N_{exp}}{N_{theo,DS414}}$
	[mm]	[mm]	[MPa]			[kN]	[kNm]				
1	960,00	228,00	13,70	0,17	7,02	1400,83	53,23	0,87	1,01	0,85	1,06
2	960,00	228,00	13,70	0,17	7,02	1269,50	48,24	0,79	0,92	0,77	0,96
3	960,00	228,00	13,70	0,17	11,40	1050,62	39,92	0,85	0,99	0,89	1,14
4	960,00	228,00	13,70	0,17	11,40	1079,81	41,03	0,87	1,02	0,92	1,17
5	960,00	228,00	13,70	0,17	11,40	1386,24	52,68	1,12	1,31	1,18	1,50
6	960,00	228,00	13,70	0,17	11,40	992,26	37,71	0,80	0,94	0,84	1,07
7	960,00	228,00	13,70	0,17	11,40	1123,58	42,70	0,91	1,06	0,96	1,22
10	960,00	228,00	13,70	0,17	15,79	802,56	30,50	0,98	1,44	1,05	1,26
11	960,00	228,00	13,70	0,17	15,79	933,89	35,49	1,13	1,67	1,22	1,46
12	960,00	228,00	13,70	0,17	20,18	598,27	22,73	1,07	1,70	1,13	1,32
13	960,00	228,00	13,70	0,17	20,18	481,54	18,30	0,86	1,37	0,91	1,06
16	960,00	228,00	13,70	0,17	11,40	1079,81	41,03	0,87	1,02	0,92	1,17
17	960,00	228,00	13,70	0,17	11,40	1094,40	41,59	0,89	1,03	0,93	1,19
8	960,00	228,00	16,20	0,17	11,40	1619,71	61,55	1,11	1,29	1,17	1,48
9	960,00	228,00	16,20	0,17	11,40	1444,61	54,90	0,99	1,15	1,04	1,32
14	960,00	228,00	16,20	0,17	20,18	787,97	29,94	1,19	1,89	1,26	1,47
15	960,00	228,00	16,20	0,17	20,18	817,15	31,05	1,24	1,96	1,31	1,53

Table 14.6 Data for the calculation of tests taken from [36]. The compressive strength has been calculated by using Hagstens formula
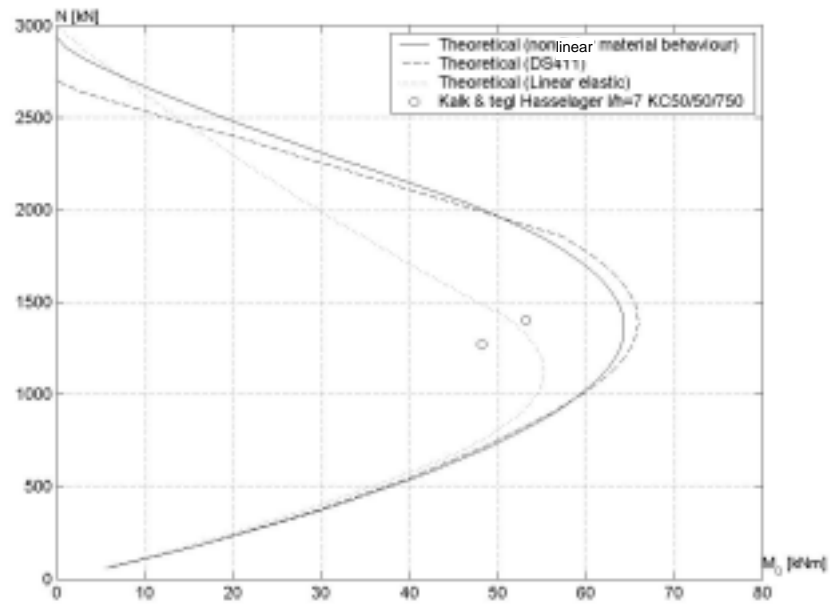
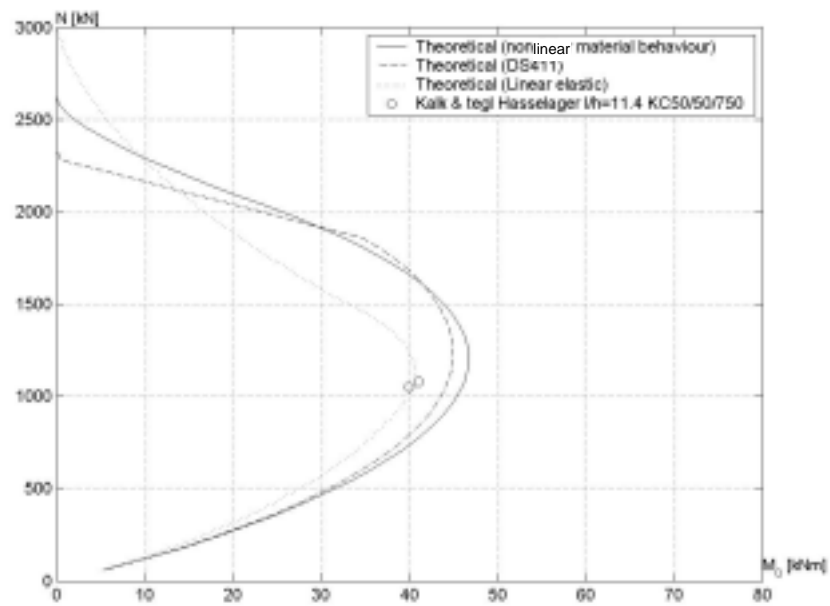**Figure 14.18 Results of tests shown in an interaction diagram, KC50/50/750**

Figure 14.19 Results of tests shown in an interaction diagram, KC50/50/750
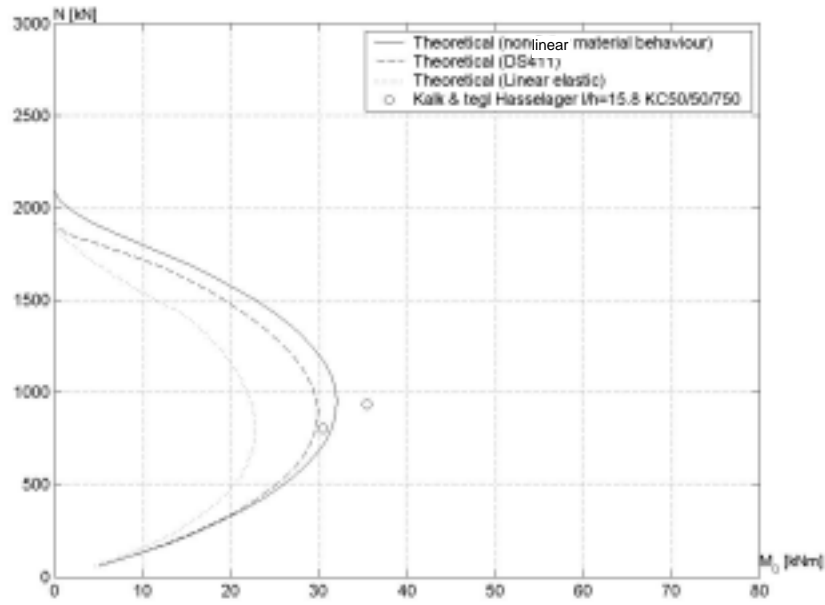
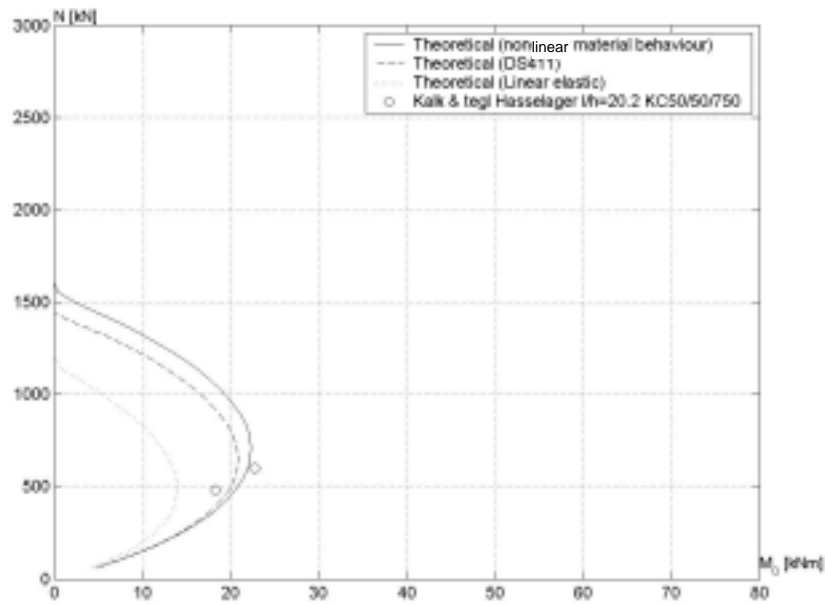**Figure 14.20 Results of tests shown in an interaction diagram, KC50/50/750**

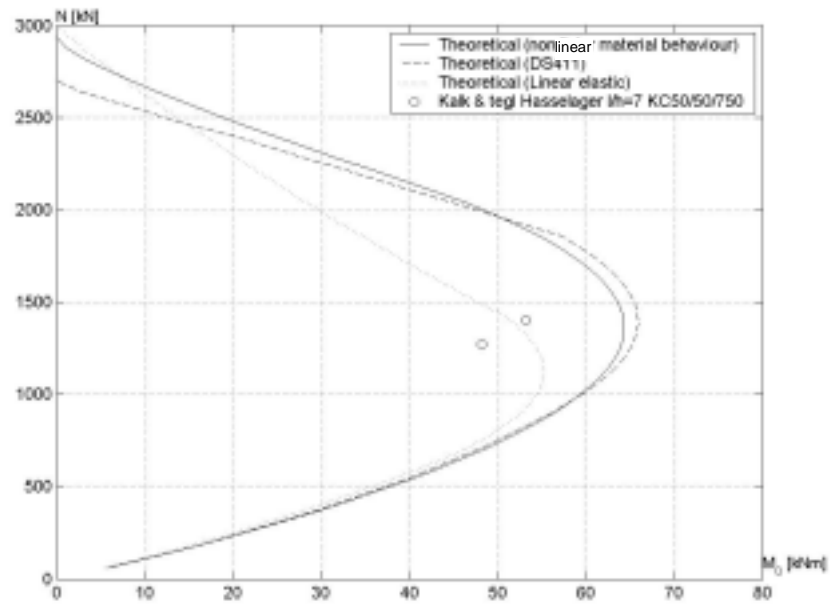**Figure 14.21 Results of tests shown in an interaction diagram, KC50/50/750**

Figure 14.22 Results of tests shown in an interaction diagram, KC20/80/550
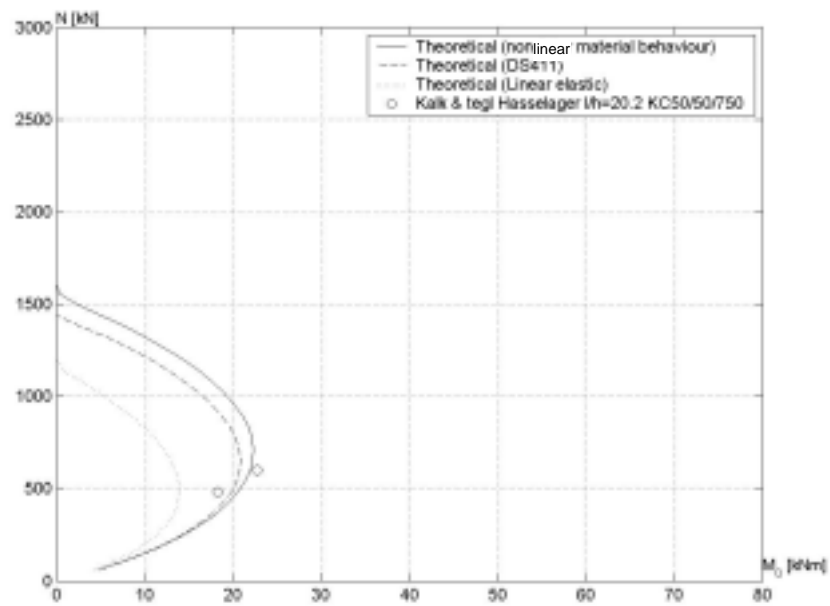

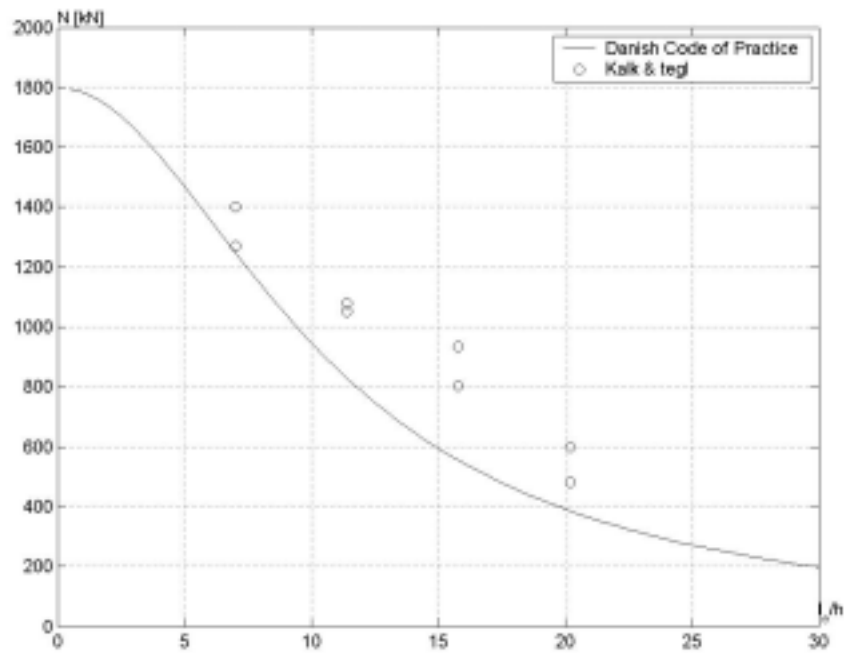**Figure 14.23 Results of tests shown in an interaction diagram, KC20/80/550**
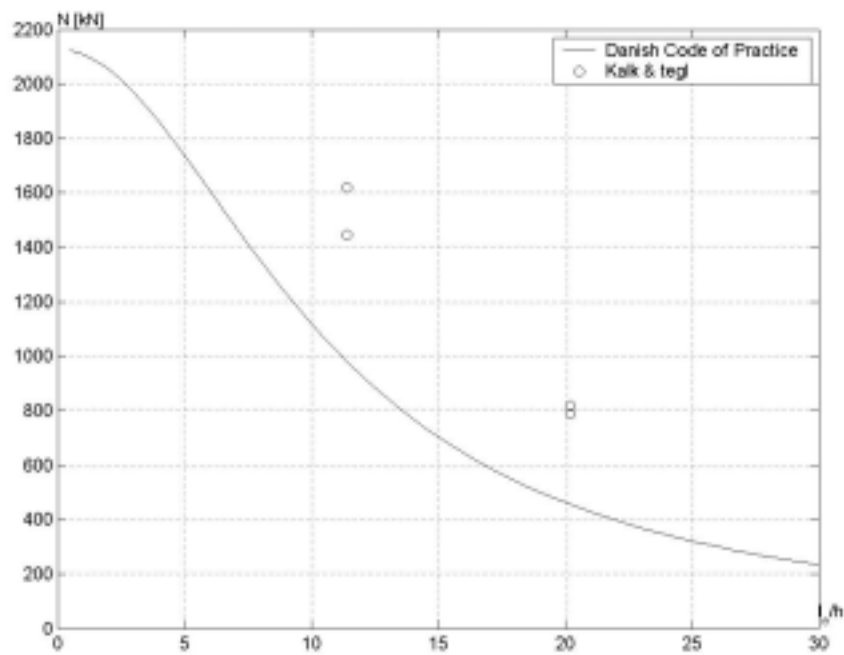
Figure 14.24 Results of tests, KC50/50/750

Figure 14.25 Results of tests, KC20/80/550

14.1.7 Murværkscenteret

Ref no.	b	h	$f_{c,m}$	e_i/h	l/h	N_{exp}	$M_{0,exp}$	$\dfrac{N_{exp}}{N_{theo,par}}$	$\dfrac{N_{exp}}{N_{Ritter}}$	$\dfrac{N_{exp}}{N_{theo,DS}}$
	[mm]	[mm]	[MPa]			[kN]	[kNm]			
1	960,00	228,00	4,70	0,00	11,40	678,53	0,00	0,72	0,86	0,96
2	960,00	228,00	4,60	0,00	11,40	809,86	0,00	0,87	1,05	1,17
3	960,00	228,00	4,80	0,00	11,40	722,30	0,00	0,75	0,90	1,00
4	960,00	228,00	7,10	0,00	11,40	1138,18	0,00	0,80	0,96	1,06
5	960,00	228,00	8,10	0,00	11,40	1313,28	0,00	0,80	0,97	1,07
6	960,00	228,00	7,90	0,00	11,40	1291,39	0,00	0,81	0,97	1,08
7	960,00	228,00	9,90	0,00	11,40	1532,16	0,00	0,77	0,92	1,02
8	960,00	228,00	10,00	0,00	11,40	1444,61	0,00	0,72	0,86	0,96
9	960,00	228,00	7,30	0,00	11,40	1554,05	0,00	1,06	1,27	1,41
19	960,00	228,00	11,50	0,00	11,40	1904,26	0,00	0,82	0,99	1,10
20	960,00	228,00	13,00	0,00	11,40	1794,82	0,00	0,68	0,82	0,91
21	960,00	228,00	13,70	0,00	11,40	1816,70	0,00	0,66	0,79	0,88
10	960,00	168,60	7,20	0,00	15,42	809,28	0,00	0,69	1,08	1,20
11	960,00	168,60	7,80	0,00	15,42	857,84	0,00	0,68	1,06	1,17
12	960,00	168,60	8,60	0,00	15,42	890,21	0,00	0,64	0,99	1,11
13	960,00	165,50	10,00	0,00	15,71	1096,27	0,00	0,69	1,09	1,21
14	960,00	165,50	10,50	0,00	15,71	1175,71	0,00	0,70	1,11	1,24
15	960,00	165,50	9,20	0,00	15,71	1207,49	0,00	0,83	1,30	1,45
16	960,00	168,60	8,80	0,00	15,42	922,58	0,00	0,65	1,01	1,12
17	960,00	168,60	9,50	0,00	15,42	890,21	0,00	0,58	0,90	1,00
18	960,00	168,60	9,70	0,00	15,42	938,76	0,00	0,60	0,93	1,03

Table 14.7 Data for the calculation of tests taken from [33]. The compressive strength was measured

Figure 14.26 Results of tests on elements simply supported in both ends, block course, KC5050750

Figure 14.27 Results of tests on elements simply supported in both ends, block course, KC5050750
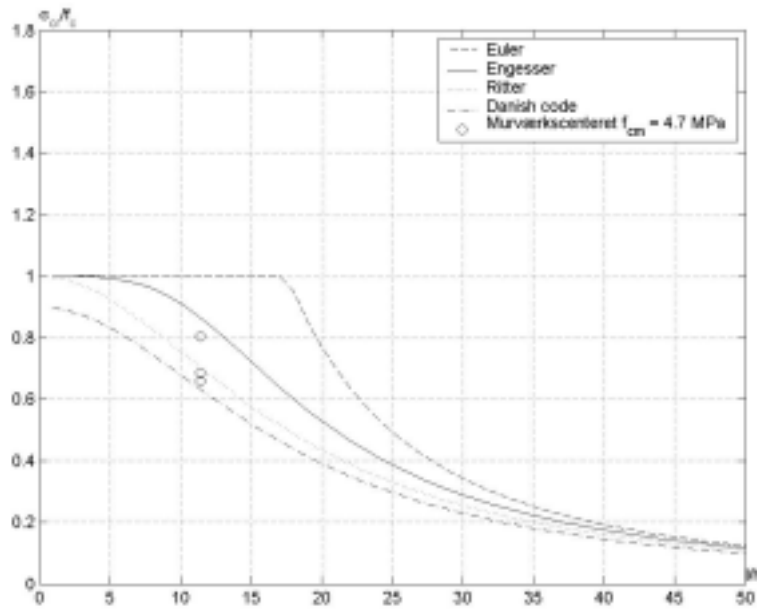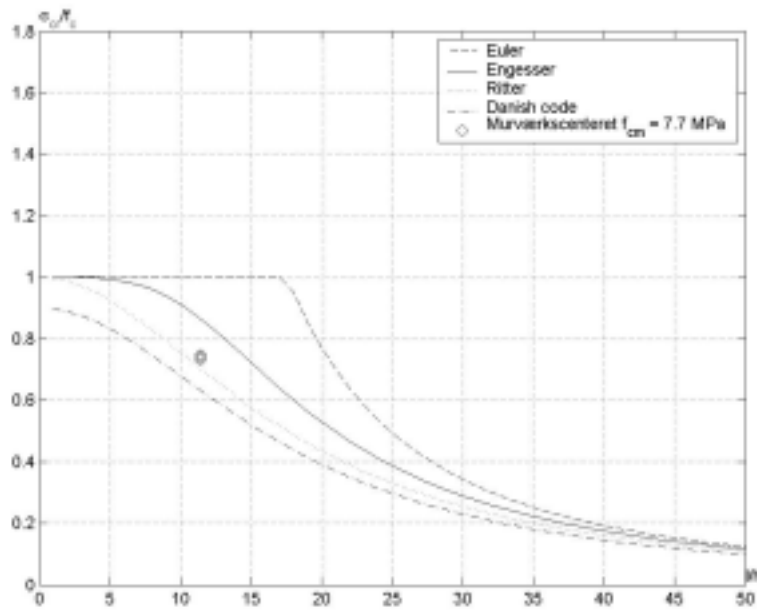
Figure 14.28 Results of tests on elements simply supported in both ends, block course, KC5050750

Figure 14.29 Results of tests on elements simply supported in both ends, block course, KC2080550
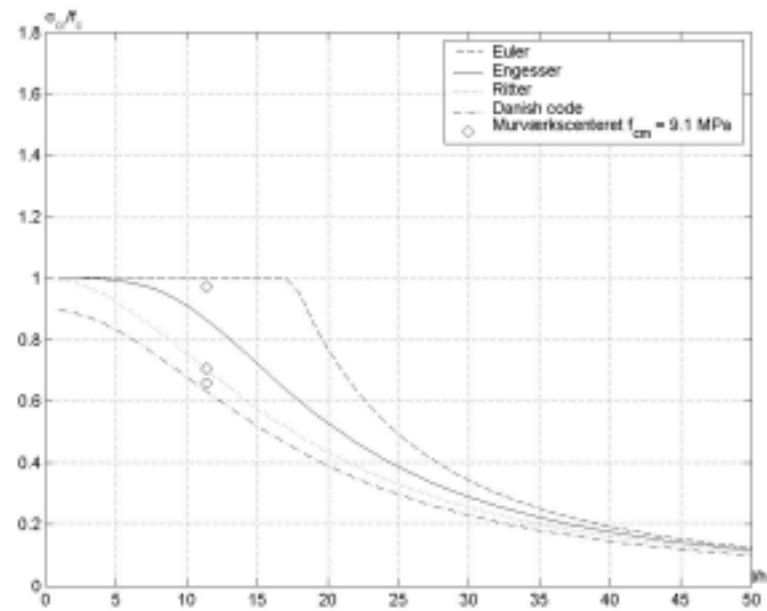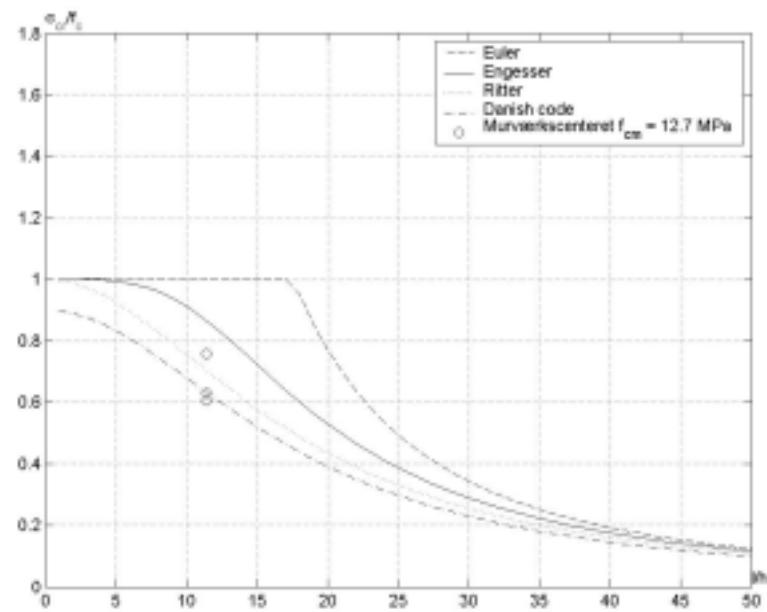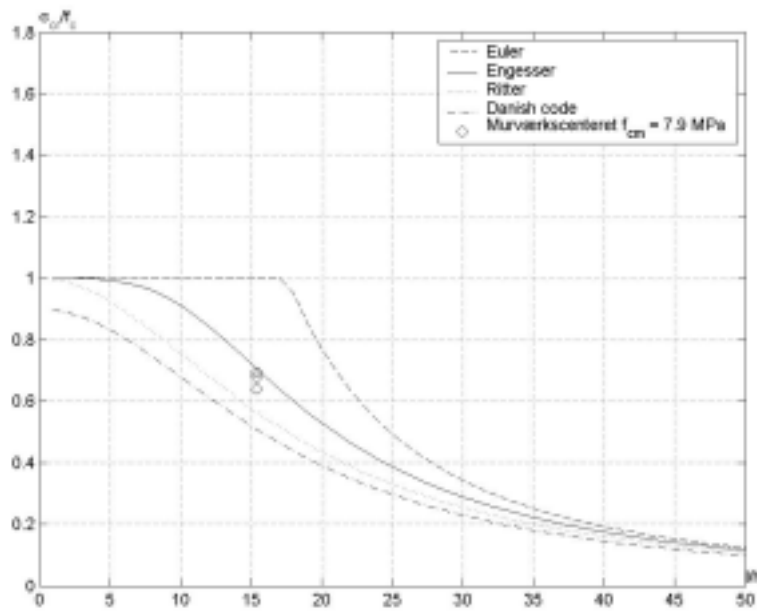
Figure 14.30 Results of tests on elements simply supported in both ends, running course, KC5050750
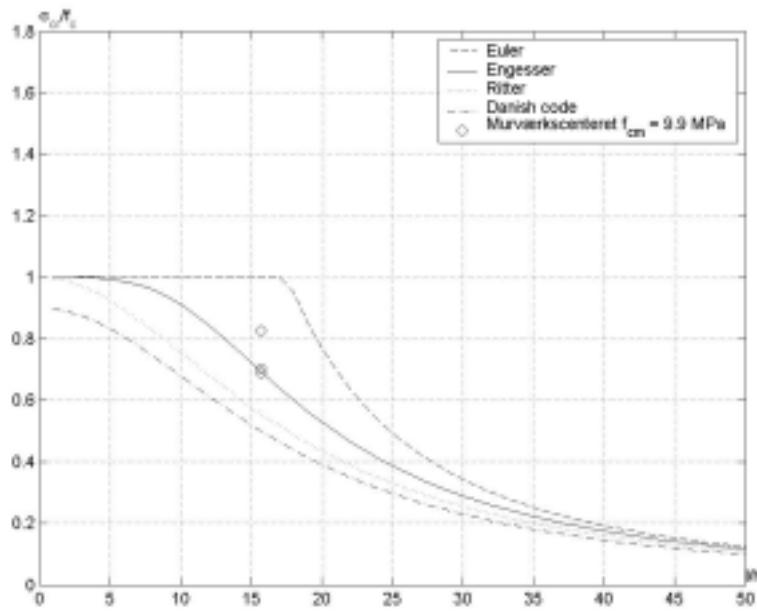

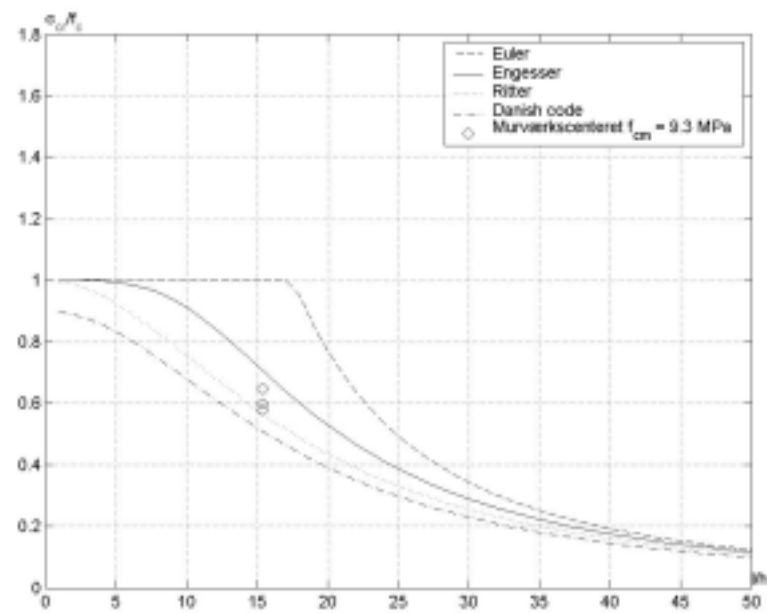**Figure 14.31 Results of tests on elements simply supported in both ends, running course, KC5050750**

Figure 14.32 Results of tests on elements simply supported in both ends, running course, KC5050750

14.2 Laterally loaded beam columns

14.2.1 Grenley, D. G, Cattaneo, L. E. & Pfrang, E. O

Ref no.	b	h	$f_{c,m}$	e_i/h	l/h	N_{exp}	$M_{0,exp}$	$\dfrac{N_{exp}}{N_{theo,par}}$	$\dfrac{N_{exp}}{N_{theo,el}}$	$\dfrac{N_{exp}}{N_{theo,DS411}}$
	[mm]	[mm]	[MPa]			[kN]	[kNm]			
1	1270,0	101,60	22,00	0,00	20,63	0,00	1,21	-	-	-
2	1270,0	101,60	22,00	0,00	20,63	0,00	1,17	-	-	-
3	1270,0	101,60	22,00	0,00	20,63	497,33	19,80	0,89	1,05	0,85
4	1270,0	101,60	22,00	0,00	20,63	995,55	30,33	0,94	1,15	0,94
5	1270,0	101,60	22,00	0,00	20,63	1243,77	31,97	0,95	1,18	0,95
6	1270,0	101,60	22,00	0,00	20,63	1492,88	29,96	0,94	1,17	0,93
7	1270,0	101,60	22,00	0,00	20,63	1741,10	25,97	0,93	1,16	0,93
8	1270,0	101,60	22,00	0,00	20,63	2812,26	0,00	0,99	1,67	1,50
9	1270,0	101,60	22,00	0,00	20,63	2862,09	0,00	1,01	1,70	1,53
10	1270,0	101,60	33,30	0,00	20,63	0,00	5,41	-	-	-
11	1270,0	101,60	33,30	0,00	20,63	0,00	5,42	-	-	-
12	1270,0	101,60	33,30	0,00	20,63	498,22	23,53	1,69	2,37	1,69
13	1270,0	101,60	33,30	0,00	20,63	994,66	41,38	1,39	1,69	1,39
14	1270,0	101,60	33,30	0,00	20,63	1243,77	42,50	0,95	1,18	0,95
15	1270,0	101,60	33,30	0,00	20,63	1492,88	41,90	0,84	1,04	0,82
16	1270,0	101,60	33,30	0,00	20,63	1741,10	40,84	0,81	1,01	0,81
17	1270,0	101,60	33,30	0,00	20,63	1990,20	50,32	0,98	1,24	0,98
18	1270,0	101,60	33,30	0,00	20,63	4230,41	0,00	0,98	1,66	1,49
19	1270,0	101,60	33,30	0,00	20,63	4369,20	0,00	1,02	1,71	1,54
20	1270,0	101,60	35,65	0,00	20,63	0,00	5,66	-	-	-
21	1270,0	101,60	35,65	0,00	20,63	0,00	7,14	-	-	-
22	1270,0	101,60	35,65	0,00	20,63	759,78	37,74	-	-	-
23	1270,0	101,60	35,65	0,00	20,63	1518,68	61,50	1,77	2,25	1,77
24	1270,0	101,60	35,65	0,00	20,63	1518,68	52,88	1,12	1,40	1,12
25	1270,0	101,60	35,65	0,00	20,63	1945,72	58,57	1,11	1,39	1,11
26	1270,0	101,60	35,65	0,00	20,63	2372,76	56,68	1,05	1,28	1,03
27	1270,0	101,60	35,65	0,00	20,63	2846,96	61,27	1,15	1,44	1,15
28	1270,0	101,60	35,65	0,00	20,63	4544,46	0,00	0,99	1,67	1,50
29	1270,0	101,60	35,65	0,00	20,63	4649,44	0,00	1,01	1,70	1,53

30	1270,0	101,60	42,06	0,00	20,63	0,00	3,39	-	-	-
31	1270,0	101,60	42,06	0,00	20,63	0,00	3,19	-	-	-
32	1270,0	101,60	42,06	0,00	20,63	694,84	22,94	0,40	0,48	0,40
33	1270,0	101,60	42,06	0,00	20,63	1092,52	31,17	0,49	0,60	0,49
34	1270,0	101,60	42,06	0,00	20,63	1439,50	41,63	0,66	0,82	0,66
35	1270,0	101,60	42,06	0,00	20,63	1737,54	42,02	0,65	0,82	0,65
36	1270,0	101,60	42,06	0,00	20,63	1985,76	40,71	0,67	0,81	0,65
37	1270,0	101,60	42,06	0,00	20,63	2978,63	31,55	0,75	0,89	0,76
38	1270,0	101,60	42,06	0,00	20,63	5446,59	0,00	1,00	1,69	1,52
39	1270,0	101,60	42,06	0,00	20,63	5301,58	0,00	0,98	1,65	1,48

Table 14.8 Data for the calculation of tests taken from [26]. Only some of the results are used. The compressive strength was measured
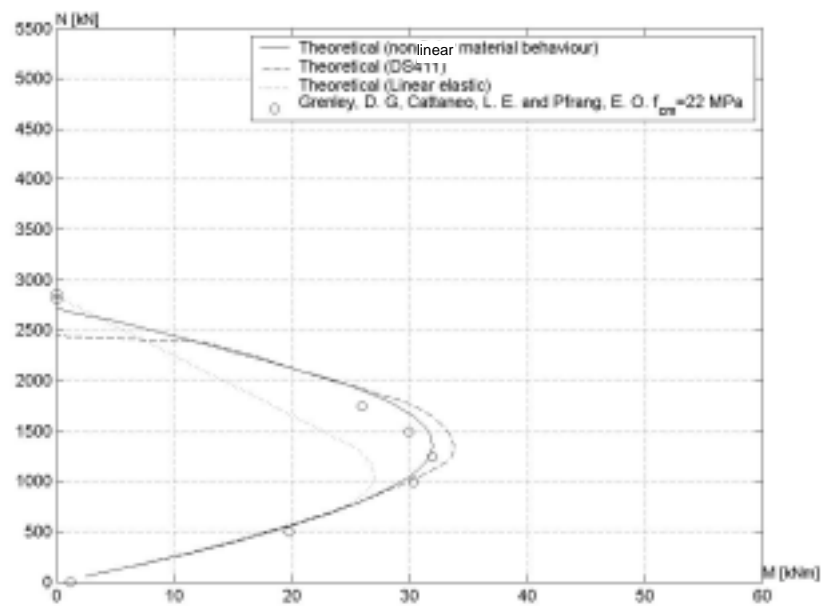

Figure 14.33 Results of tests shown in an interaction diagram, conventional mortar brick A
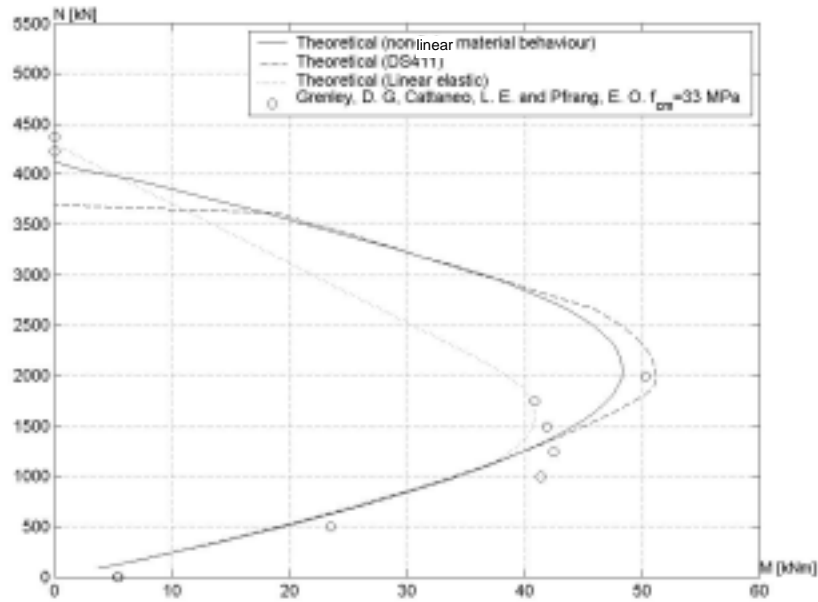
Figure 14. Results of tests shown in an interaction diagram, high bond mortar brick A
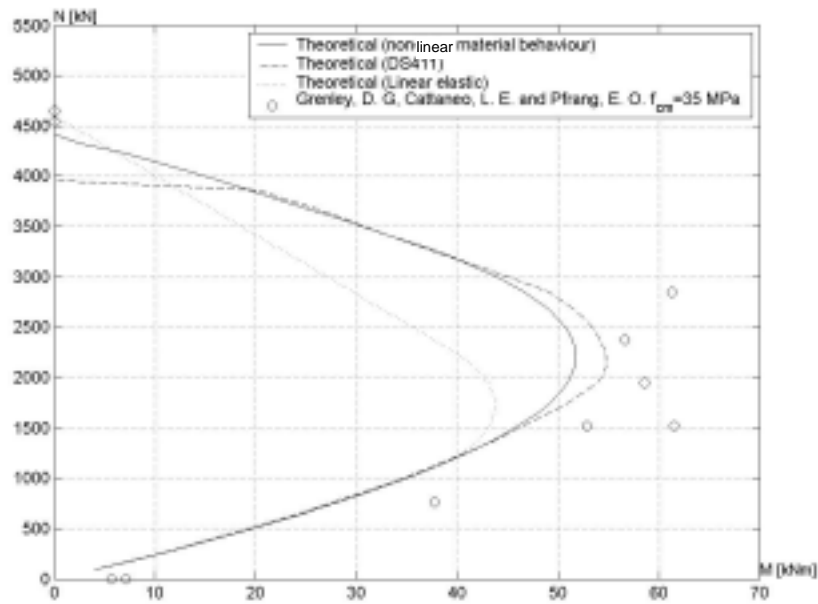

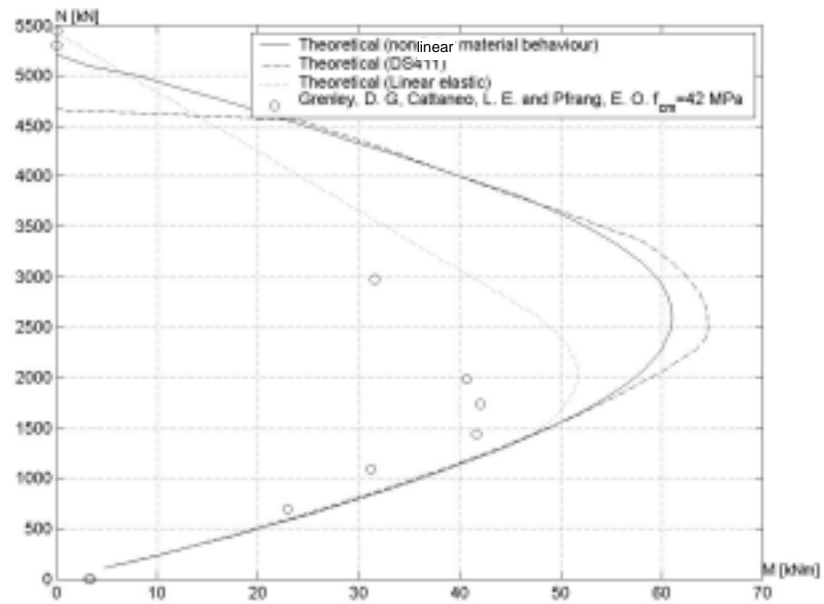**Figure 14.34 Results of tests shown in an interaction diagram, high bond mortar brick B**

Figure 14.35 Results of tests shown in an interaction diagram, high bond mortar brick S

14.2.2 Yokel, F. Y. , Mathey, R. G. and Dikkers, R. D.

Ref no.	b	h	$f_{c,m}$	e_i/h	l/h	N_{exp}	$M_{0,exp}$	$\dfrac{N_{exp}}{N_{theo,par}}$	$\dfrac{N_{exp}}{N_{theo,el}}$	$\dfrac{N_{exp}}{N_{theo,DS411}}$
	[mm]	[mm]	[MPa]			[kN]	[kNm]			
.4-1	1219,2	101,60	21,97	0,00	20,63	0,00	0,92	-	-	-
.4-2	1219,2	101,60	21,97	0,00	20,63	0,00	0,92	-	-	-
.4-3	1219,2	101,60	21,97	0,00	20,63	444,80	15,60	1,67	2,78	1,85
.4-4	1219,2	101,60	21,97	0,00	20,63	889,60	23,99	1,23	1,59	1,33
.4-5	1219,2	101,60	21,97	0,00	20,63	1112,00	25,29	1,13	1,30	1,16
.4-6	1219,2	101,60	21,97	0,00	20,63	1334,40	19,10	0,89	1,04	0,86
.4-7	1219,2	101,60	21,97	0,00	20,63	1556,80	20,63	1,01	1,17	0,97
.4-8	1219,2	101,60	21,97	0,00	20,63	2499,78	0,00	0,97	1,28	1,15
.4-9	1219,2	101,60	21,97	0,00	20,63	2562,05	0,00	1,00	1,31	1,18
.5-1	1219,2	101,60	33,14	0,00	20,63	0,00	3,69	-	-	-
.5-2	1219,2	101,60	33,14	0,00	20,63	0,00	3,69	-	-	-
.5-3	1219,2	101,60	33,14	0,00	20,63	444,80	17,90	3,69	5,53	3,69
.5-4	1219,2	101,60	33,14	0,00	20,63	889,60	29,90	1,84	2,76	1,84
.5-5	1219,2	101,60	33,14	0,00	20,63	1112,00	32,30	1,26	1,73	1,38
.5-6	1219,2	101,60	33,14	0,00	20,63	1334,40	31,84	0,98	1,11	1,01
.5-7	1219,2	101,60	33,14	0,00	20,63	1556,80	31,05	0,90	1,02	0,90
.5-8	1219,2	101,60	33,14	0,00	20,63	1779,20	38,25	1,11	1,26	1,13
.5-9	1219,2	101,60	33,14	0,00	20,63	3754,11	0,00	0,97	1,27	1,15
.5-10	1219,2	101,60	33,14	0,00	20,63	3878,66	0,00	1,00	1,32	1,18
.6-1	1219,2	101,60	41,71	0,00	20,63	0,00	1,85	-	-	-
.6-2	1219,2	101,60	41,71	0,00	20,63	0,00	2,49	-	-	-
.6-3	1219,2	101,60	41,71	0,00	20,63	622,72	18,18	0,56	0,77	0,61
.6-4	1219,2	101,60	41,71	0,00	20,63	978,56	32,76	1,49	2,42	1,61
.6-5	1219,2	101,60	41,71	0,00	20,63	1289,92	32,76	0,85	0,98	0,88
.6-6	1219,2	101,60	41,71	0,00	20,63	1556,80	32,90	0,77	0,85	0,77
.6-7	1219,2	101,60	41,71	0,00	20,63	1779,20	32,02	0,73	0,84	0,72
.6-8	1219,2	101,60	41,71	0,00	20,63	4839,42	0,00	0,99	1,30	1,17
.6-9	1219,2	101,60	41,71	0,00	20,63	4670,40	0,00	0,96	1,26	1,13
.7-1	1219,2	101,60	35,44	0,00	20,63	0,00	5,08	-	-	-
.7-2	1219,2	101,60	35,44	0,00	20,63	0,00	6,18	-	-	-
.7-3	1219,2	101,60	35,44	0,00	20,63	711,68	31,88	-	-	-
.7-4	1219,2	101,60	35,44	0,00	20,63	1423,36	52,09	4,13	8,27	4,73

.7-5	1219,2	101,60	35,44	0,00	20,63	1423,36	44,67	1,95	3,01	2,07
.7-6	1219,2	101,60	35,44	0,00	20,63	2668,80	51,72	1,38	1,59	1,38
.7-7	1219,2	101,60	35,44	0,00	20,63	4216,70	0,00	1,02	1,34	1,20
.7-8	1219,2	101,60	35,44	0,00	20,63	4314,56	0,00	1,04	1,37	1,23

Table 14.9 Data for the calculation of tests taken from [28]
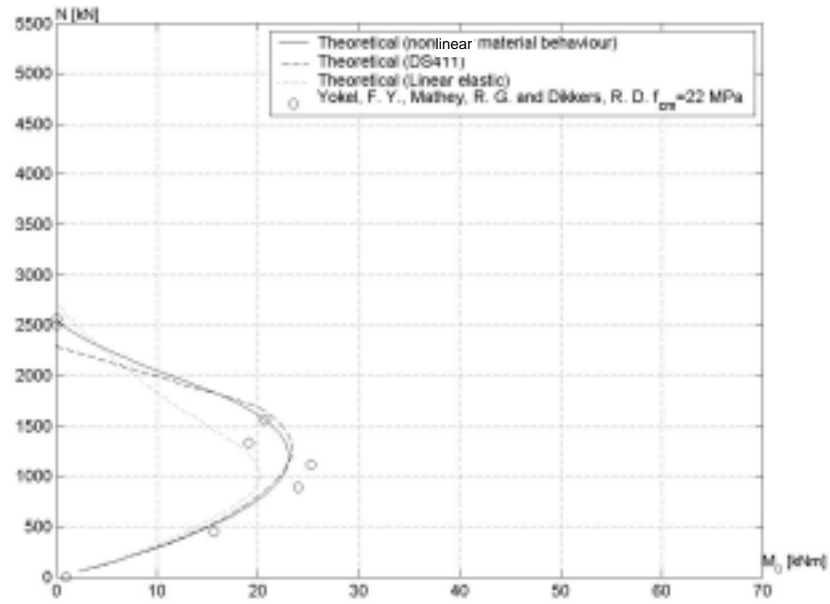
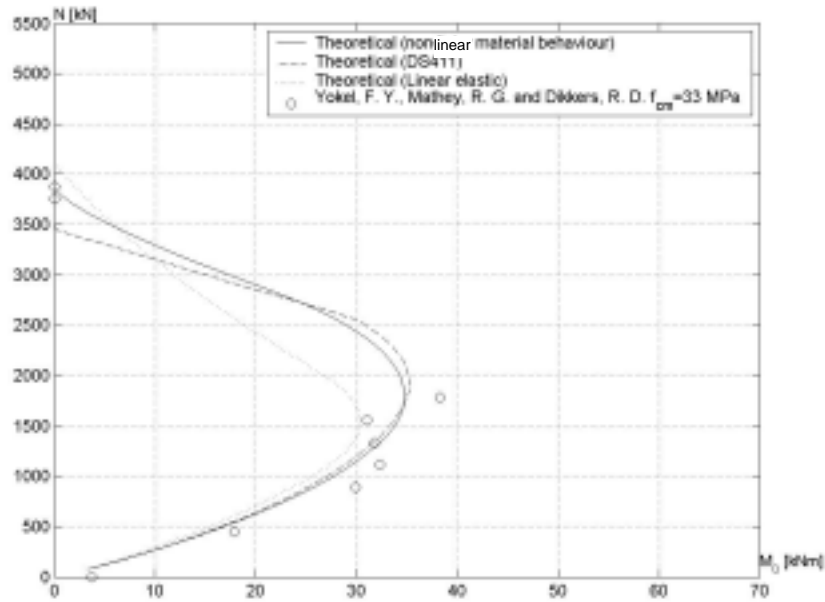**Figure 14.36 Results of tests shown in an interaction diagram**

Figure 14.37 Results of tests shown in an interaction diagram
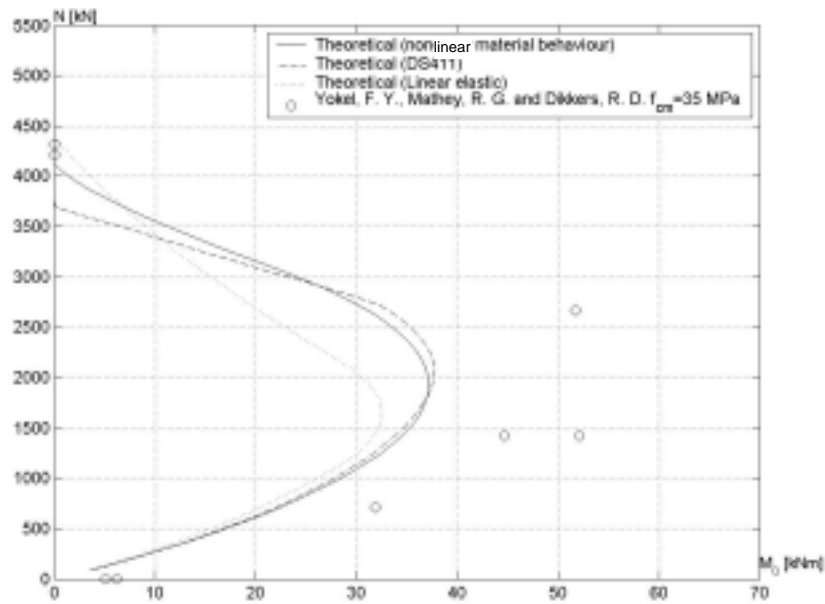

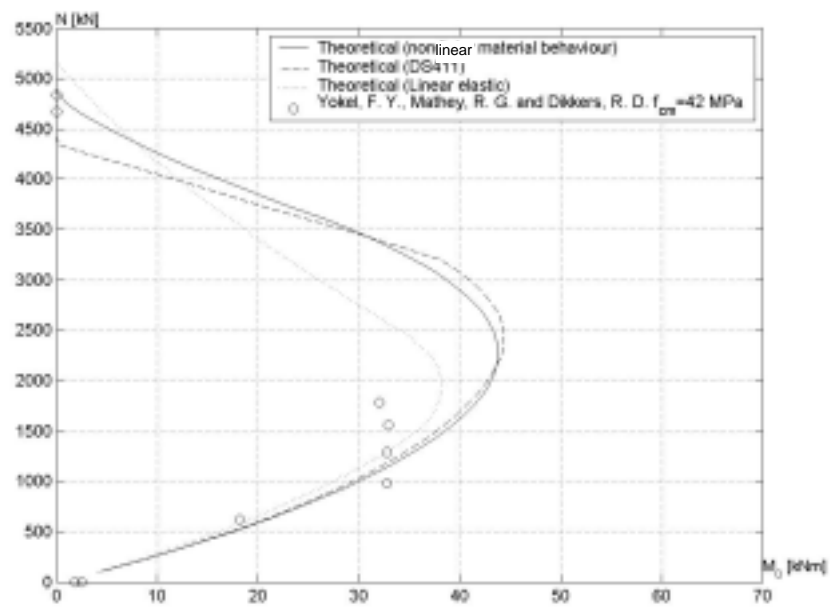**Figure 14.38 Results of tests shown in an interaction diagram**

Figure 14.39 Results of tests shown in an interaction diagram

15 Appendix 2. Experiments, reinforced masonry

Eccentrically and concentrically loaded columns and one-way slabs.

Davey, N. & Thomas, F. G.

Anderson, D. A. & Hoffman, E. S.

15.1 Eccentrically loaded reinforced masonry columns

15.1.1 Davey, N. & Thomas, F. G.

Ref no.	b	h	d/h	100ρ	f_{cm}	f_y	e_i/h	l/h	N_{exp}	$\dfrac{N_{exp}}{N_{theo,par}}$	$\dfrac{N_{exp}}{N_{theo,el}}$	$\dfrac{N_{exp}}{N_{theo,DS}}$
	[mm]	[mm]	[]	[]	[MPa]	[MPa]	[]	[]	[kN]			
40/33B	571,5	685,8	0,8	0,20	11,8	303,4	0,4	4,0	735,8	0,69	0,83	0,72
40/33B	571,5	685,8	0,8	0,20	11,8	303,4	0,8	4,0	264,9	0,95	0,95	0,95
30/33B	457,2	685,8	0,8	0,16	11,8	303,4	0,4	4,0	608,2	0,78	0,91	0,81
30/33B	457,2	685,8	0,8	0,16	11,8	303,4	0,8	4,0	180,5	0,81	0,97	0,97
30/22B	457,2	571,5	0,8	0,19	11,8	303,4	0,5	4,8	294,3	0,68	0,79	0,73
30/22B	457,2	571,5	0,8	0,19	11,8	303,4	0,9	4,8	127,5	0,82	1,02	1,02
40/110/AC	685,8	914,4	0,9	0,18	11,8	303,4	0,3	3,0	3001,9	0,79	0,98	0,80
40/110/BC	685,8	914,4	0,9	0,18	11,8	303,4	0,4	3,0	1667,7	0,83	0,97	0,86
40/90/AC	685,8	914,4	0,9	0,13	11,8	303,4	0,3	3,0	3237,3	0,88	1,08	0,88
40/90/BC	685,8	914,4	0,9	0,13	11,8	303,4	0,4	3,0	1373,4	0,77	0,92	0,77
40/77/AC	571,5	914,4	0,9	0,10	11,8	303,4	0,3	3,0	2599,7	0,85	1,07	0,87
40/77/BC	571,5	914,4	0,9	0,10	11,8	303,4	0,4	3,0	1226,3	0,86	1,04	0,90
40/55/AC	457,2	800,1	0,8	0,18	11,8	303,4	0,3	3,4	1687,3	0,86	1,11	0,90
40/55/BC	457,2	800,1	0,8	0,18	11,8	303,4	0,5	3,4	735,8	0,89	1,06	0,94

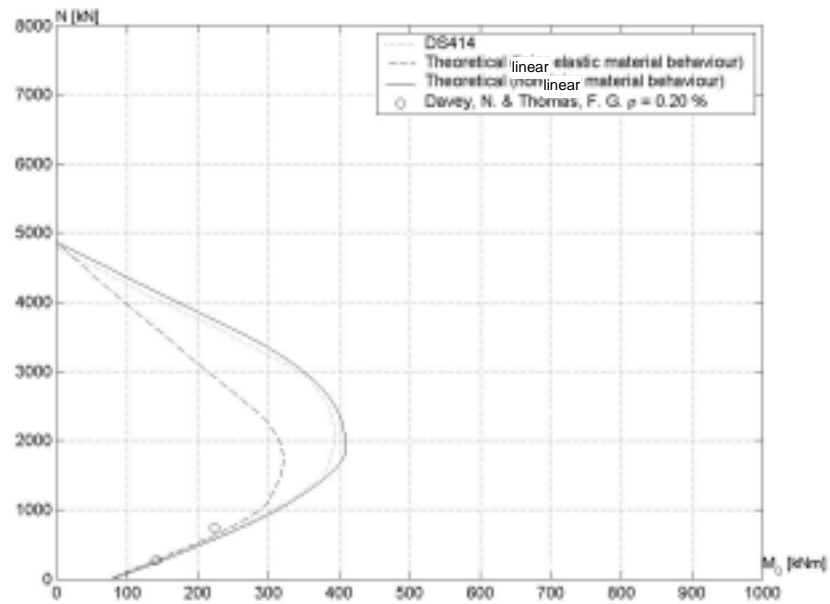**Table 15.1 Data for the calculation of tests taken from [17].**

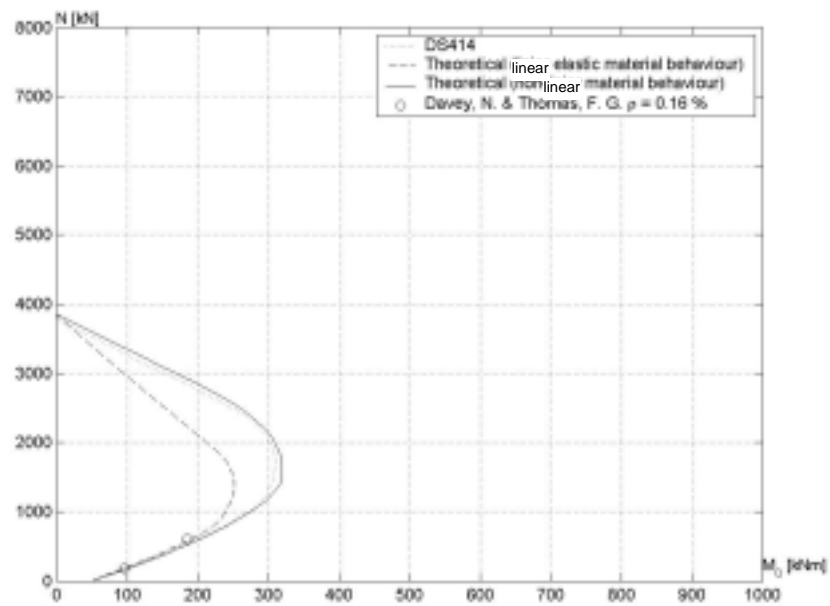**Figure 15.1 Results of tests shown in an interaction diagram**

Figure 15.2 Results of tests shown in an interaction diagram
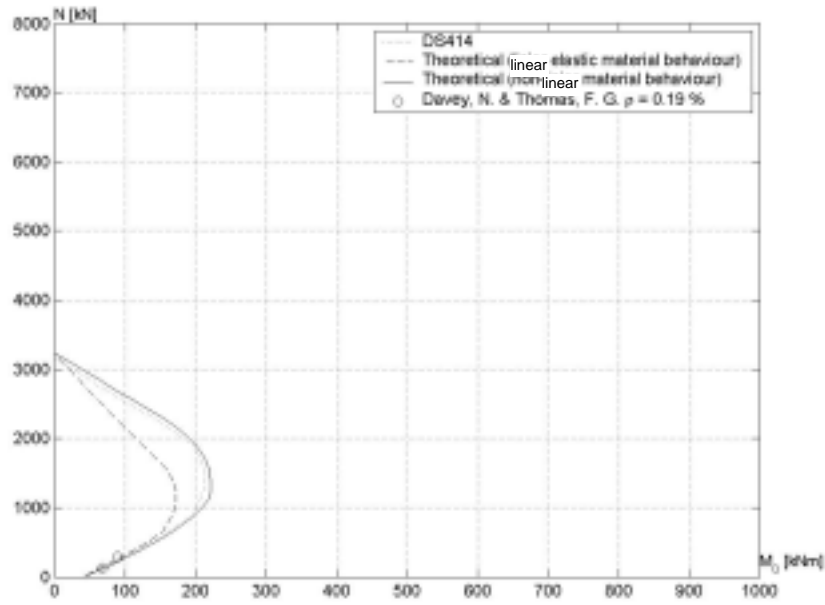
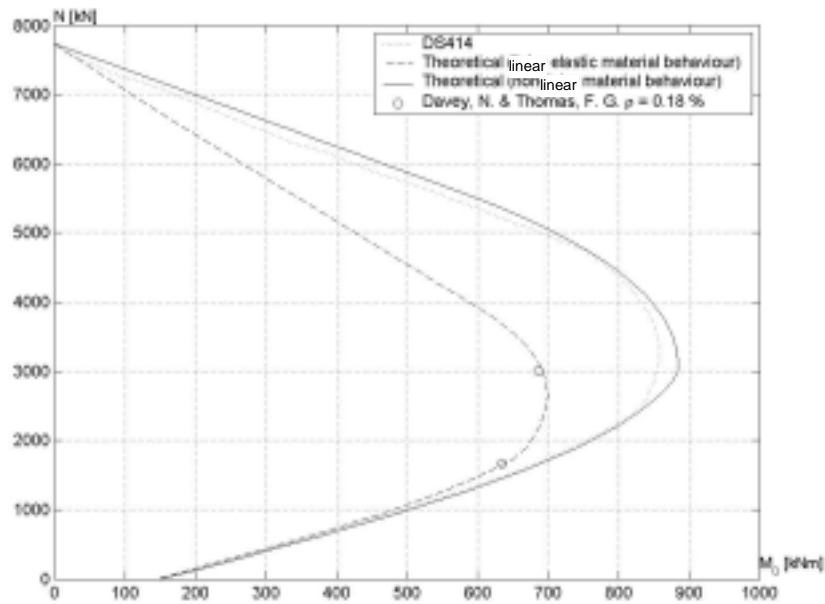**Figure 15.3 Results of tests shown in an interaction diagram**

Figure 15.4 Results of tests shown in an interaction diagram
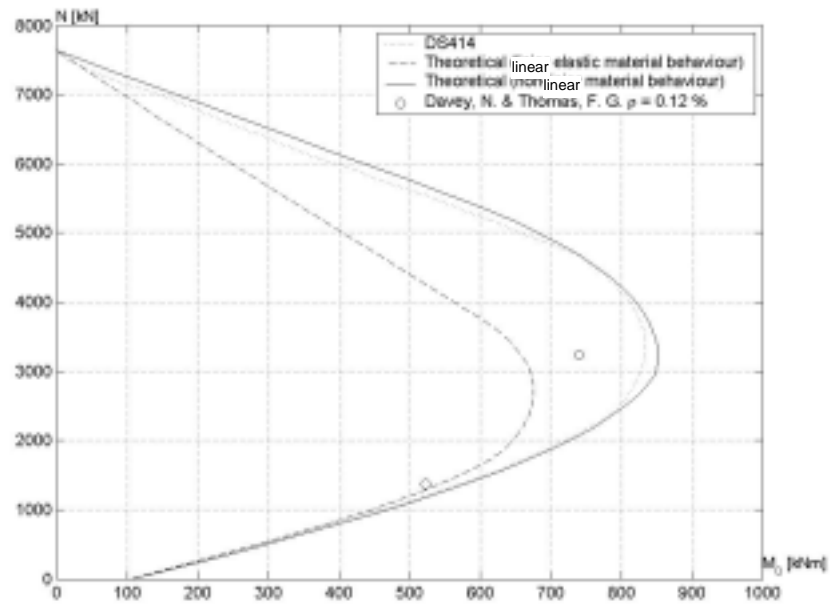
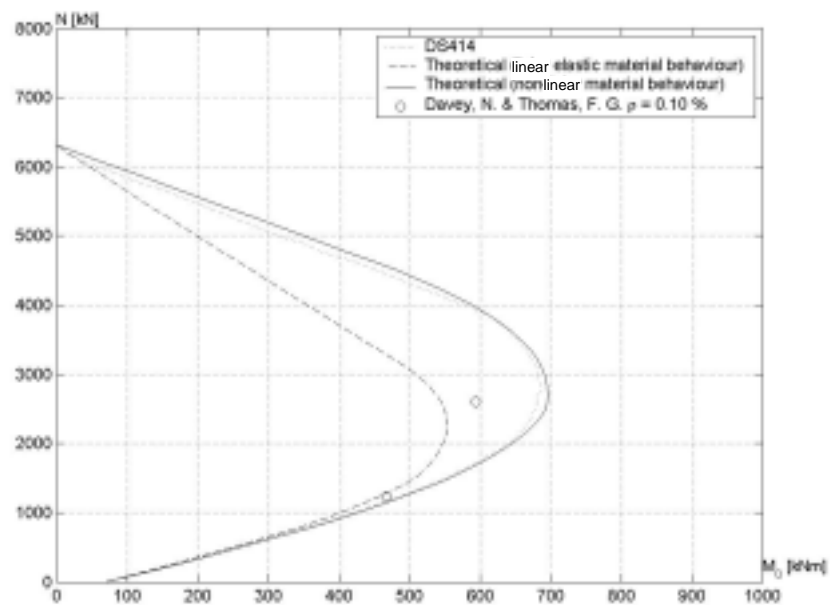**Figure 15.5 Results of tests shown in an interaction diagram**

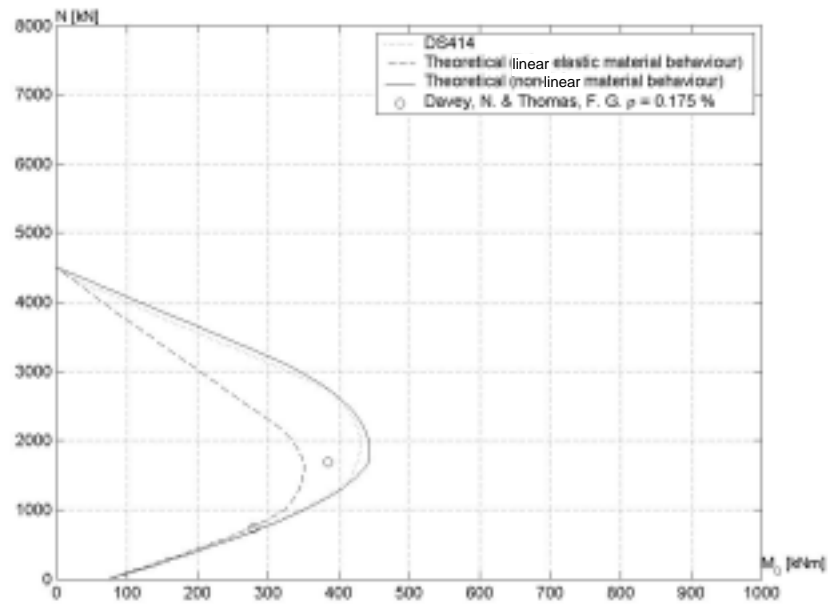**Figure 15.6 Results of tests shown in an interaction diagram**

Figure 15.7 Results of tests shown in an interaction diagram

15.1.2 Anderson, D. A. & Hoffman, E. S.

Ref no.	b	h	d/h	100ρ	f_{cm}	f_y	e_i/h	l/h	N_{exp}	$\frac{N_{exp}}{N_{theo,par}}$	$\frac{N_{exp}}{N_{theo,el}}$	$\frac{N_{exp}}{N_{theo,DS}}$
	[mm]	[mm]	[]	[]	[MPa]	[MPa]	[]	[]	[kN]			
WUGI1	304,8	406,4	0,7	0,6	36,2	275,8	0,1	7,6	4127,7	1,08	1,17	1,07
WUGI2	304,8	406,4	0,7	0,6	36,2	275,8	0,1	7,6	4127,7	1,08	1,17	1,07
WUGI3	304,8	406,4	0,7	0,6	36,2	275,8	0,1	7,6	4096,6	1,08	1,16	1,06
WUGI4	304,8	406,4	0,7	0,6	36,2	275,8	0,1	7,6	3731,9	1,11	1,31	1,11
WUGI5	304,8	406,4	0,7	0,6	36,2	275,8	0,1	7,6	3520,6	1,05	1,23	1,05
WUGI6	304,8	406,4	0,7	0,6	36,2	275,8	0,1	7,6	3525,0	1,05	1,24	1,05
WUGI7	304,8	406,4	0,7	0,6	36,2	275,8	0,2	7,6	2682,1	1,12	1,38	1,12
WUGI8	304,8	406,4	0,7	0,6	36,2	275,8	0,2	7,6	2704,4	1,13	1,39	1,13
WUGI9	304,8	406,4	0,7	0,6	36,2	275,8	0,2	7,6	2442,0	1,02	1,25	1,02
WUGIX	304,8	406,4	0,7	0,6	36,2	275,8	0,3	7,6	1805,9	1,37	1,59	1,29
WUGIY	304,8	406,4	0,7	0,6	36,2	275,8	0,3	7,6	1861,5	1,42	1,64	1,33
WUGIZ	304,8	406,4	0,7	0,6	36,2	275,8	0,3	7,6	1894,8	1,44	1,67	1,35

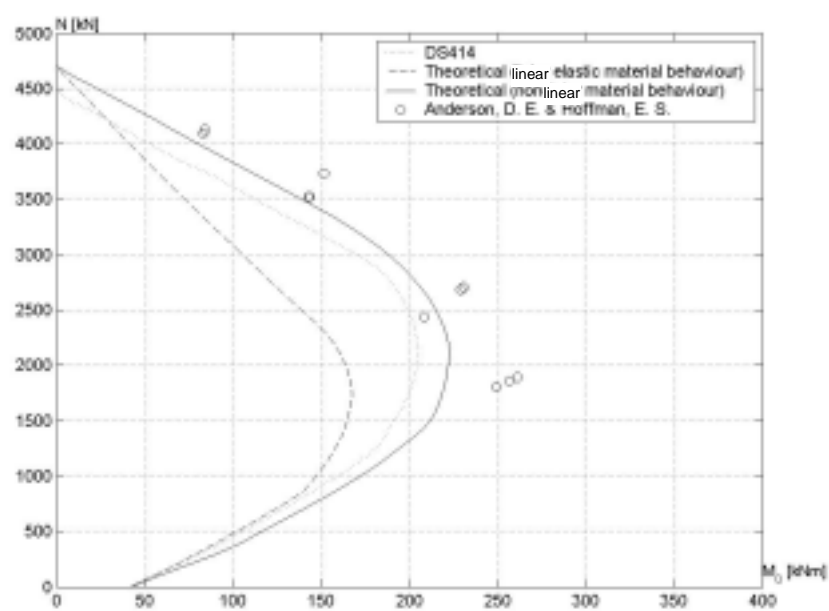**Table 15.2 Data for the calculation of tests taken from [27]**

Figure 15.8 Results of tests shown in an interaction diagram